SOME ELECTRON SPIN RESONANCE EXPERIMENTS ON EXCHANGE INTERACTIONS.

by

E. A. HARRIS

Lincoln College.

BODLEIAN LIBRARY OXFORD
DEPOSITED
THESIS
2. i. 64

A Thesis submitted for the Degree of
Doctor of Philosophy
in the
University of Oxford

Trinity Term, 1963.

ABSTRACT

ABSTRACT

In the work described in this thesis, the exchange interactions between neighbouring magnetic ions in semidilute crystals have been measured from their paramagnetic resonance spectra. The results of these measurements are compared with the magnetic bulk properties of the concentrated crystals. The relationships between these bulk properties and the exchange interactions are considered in chapter 1, where a brief account of the origin of antiferromagnetic exchange is also given.

The experimental measurements have mainly been made using a Q band (λ = 0.85 cm) spectrometer, which is described in chapter 2.

In chapter 3, experiments are described on n.n. pairs of Mn^{++} ions in the face centred cubic MgO crystal lattice. The interaction between two n.n. spins s_1 and s_2 can be divided into two parts, an isotropic and an anisotropic part.

The isotropic exchange interaction is taken to be,

$$\mathcal{H} = J(\underline{s}_1 \cdot \underline{s}_2) - J(\underline{s}_1 \cdot \underline{s}_2)^2 + \ldots$$

The spins are strongly coupled together by this interaction

and act as a single unit with spin $\underline{S} = \underline{s}_1 + \underline{s}_2$, which can take the values 0,1,2,3,4, and 5. For purely first order exchange (j_2 etc = 0), the energy levels for the different S states are spaced according to a Lande interval rule, with S = 0 lowest. In earlier measurements on these pairs, Coles (Thesis 1959) measured the energy splitting between the S = 0 and S = 1 levels, and interpreted it in terms of a first order exchange term, $\frac{J}{k}$ = 38°K, which could not be reconciled with the bulk magnetic properties. In the present work the intervals up to S = 4 have been measured by comparing the temperature variations of intensity for lines from different S states. The measurements of Coles have been confirmed, but it is found that the intervals to not follow a Lande rule, and the present results are interpreted in terms of a first order exchange term, $\frac{J}{k} \approx 15°K$, and a second order term such that $j \approx .05\ J$. This is now in good agreement with bulk magnetic properties which suggest $\frac{J}{k} \approx 11°K$. The difference is consistent with the difference in lattice spacings for the dilute and concentrated crystals. Further evidence for this second order biquadratic exchange in the concentrated

crystals is provided by the anomalous sublattice magnetisation below the transition temperature (Sievers and Tinkham 1963) and by the low temperature transverse susceptibility measured by Jacobs (private communication).

The anisotropy of the exchange interaction is reflected in the anisotropy of the pair resonance lines. The anisotropic exchange is given by,

$$\mathcal{H} = D_c(3s_{1z}s_{2z} - \underline{s}_1\cdot\underline{s}_2) + E_c(s_{1x}s_{2x} - s_{1y}s_{2y}) + \text{higher order terms.}$$

There is also an anisotropic crystal field distortion term acting on each spin separately,

$$\mathcal{H} = D_c(3s_z^2 - \tfrac{1}{3}s(s+1)) + E_c(s_x^2 - s_y^2) + \text{higher order terms.}$$

From measurements of line positions these parameters have been estimated.

$D_c = .054 \pm .0015\ cm^{-1}$ $\quad E_c = .030 \pm .03\ cm^{-1}$

$D_c = -.025 \pm .0015\ cm^{-1}$ $\quad E_c = -.005 \pm .015\ cm^{-1}$

The accuracy of measurement was insufficient to estimate the magnitude of any higher order terms. The value of D_c may be compared with a magnetic dipolar value of $D_c \approx .060\ cm^{-1}$.

Abstract contd.

Measurements that have been made on groups of three exchange-coupled $(IrCl_6)^{2-}$ complexes (triads) are described in chapter 4. The crystals used were K_2PtCl_6 and $(NH_4)_2IrCl_6$, in which Ir was substituted for Pt in a ratio of about 1 : 10. A study of the spectra due to n.n. pairs in these crystals has been described by Griffiths, Owen, Park, and Partridge (1959). No n.n.n. pair spectrum was observed because the n.n.n. anisotropic exchange interaction was too small.

The spectrum from triads consisting of a n.n. pair coupled with a n.n.n. ion has been identified and the n.n.n. isotropic exchange, given by $J_3 g_z \cdot g_z$, has been deduced from the line positions.

$K_2Ir_2PtCl_6$ $\quad J_3 = +0.36 \pm .03\ cm^{-1}$

$(NH_4)_2Ir_2PtCl_6$ $\quad J_3 = +0.33 \pm .03\ cm^{-1}$

The sign and magnitude of these quantities indicate that the ordering is of the third kind. The anomalously high value for $\frac{\theta}{T_N}$ can be explained with these parameters using the spin wave method of Lines (1963).

The spectra from the other types of Triad in which each of the ions is a n.n. to at least one of the others have also been considered. They have been identified

in several places, and it is found that the line positions are given accurately using the anisotropy parameters found for n.n. pairs. By making intensity measurements on the tried lines over a range of temperatures, an independent estimate of J_1 has been obtained, which is in good agreement with that obtained from pair measurements.

LIST OF CONTENTS

		Page
CHAPTER 1.	INTRODUCTION	
1.1	Introduction	1
1.2	Antiferromagnetic Exchange	2
1.3	Properties of concentrated Antiferromagnetic Crystals	7
	The Molecular field Approximation	8
	The Spin Wave Approximation	8
	Bulk Magnetic Properties	9
1.4	Pair Measurements	13
CHAPTER 2.	EXPERIMENTAL TECHNIQUES	
2.1	The spectrometer	14
	The Cavity	14
	The Microwave System	15
	The Detection System	16
	The Magnet	17
2.2	Experimental Measurements	17
	Anisotropy Plots	18
	Measurements of Line Positions	19
	Intensity Measurements	20

CHAPTER 3. MANGANESE PAIRS IN MnO

3.1 Introduction 25

3.2 Energy levels for a n.n. pair

The spin Hamiltonian 25

The Eigenstates 26

The S = 1 Spectrum 30

The S = 2 Spectrum 30

The Spectrum for S > 2 31

Hyperfine Structure 32

3.3 Experimental Work 33

Anisotropy Measurements 34

Intensity Measurements 36

3.4 Discussion of Results

The Anisotropic Interaction 46

Isotropic Exchange 48

The Bulk Magnetic Properties of MnO 50

Sublattice Magnetisation Curve 51

Low Temperature Transverse Susceptibility 52

Antiferromagnetic Resonance 54

High Temperature Susceptibility 54

The Transition Temperature 55

Higher Order Exchange 56

Biquadratic Exchange in Other Crystals 56

3.5 Third Nearest Neighbour Pairs 58

3.6 Possible Impurities in MgO 60

CHAPTER 4. PARAMAGNETIC RESONANCE OF IRIDIUM TRIADS

4.1 Introduction 63

4.2 The Origin of the Exchange Interaction 64

4.3 The N.N. Pair Spectrum 66

4.4 The Theory of Triads 68

The Line Triad 70

The Right Angle Triad 75

The Skew Triad 78

The Equilateral Triad 81

The N.N.N. Triad 82

Other Triads 85

Hyperfine Structure 85

The Intensity of Resonance Lines 88

4.5 Experimental Work

The Crystals 92

Paramagnetic Resonance Experiments 93

Anisotropy Measurements 93

Intensity Measurements 100

Line Widths 102

4.6 Discussion of Results 105

CHAPTER 1.

INTRODUCTION

It has become a well established technique in the investigation of exchange interactions to make measurements on the paramagnetic resonance spectrum of exchange-coupled pairs of paramagnetic ions in otherwise diamagnetic materials (Owen, 1961,1962). The first pair spectrum was identified by Bleaney and Bowers (1952) in crystals of copper acetate, in which isolated pairs of Cu^{2+} ions occur naturally. Usually however the crystal structure does not contain isolated pairs, and it is necessary to create them artificially by using mixed crystals in which there is only a small proportion of paramagnetic ions and suitable diamagnetic ions. The paramagnetic ions distribute themselves at random throughout the crystal lattice, and occur singly, or in groups of two (pairs), three (trinds), or more in a proportion depending on the relative concentrations of the two types of ion. The paramagnetic resonance spectrum from these groups of ions provides a direct method for measuring the exchange interactions between the ions.

In this thesis measurements of this kind on pairs of Mn^{2+} ions in MgO, and on trinds of Ir^{4+} ions in $(NH_4)_2PtCl_6$ and K_2IrCl_6 are described. In each case

all the interactions are found to be antiferromagnetic. These interactions are expected to be similar to those which give rise to the antiferromagnetic bulk properties of MnO, $(NH_4)_2IrCl_6$, and K_2IrCl_6 respectively. The relationship between the present measurements and the bulk properties will be discussed.

In this chapter a brief account is given of the physical background behind these measurements, the origin of antiferromagnetic exchange, and some of the bulk properties of antiferromagnetic materials.

1.2 Antiferromagnetic Exchange

An antiferromagnetic material is one in which neighbouring paramagnetic ions are coupled by an exchange interaction which tends to align their spin vectors in antiparallel directions. An exchange interaction is a quantum mechanical effect which arises when there is overlap of electron orbitals. It was first predicted almost simultaneously by Heisenberg and by Dirac in 1926. The interaction is electrostatic in origin, but as a result of the exclusion principle it is very strongly dependent on the spin direction of the overlapping orbitals. Dirac (1929) showed that for two spins

$s_i = s_j = \frac{1}{2}$, the interaction was formally equivalent to an interatomic potential,

$$V = \frac{J_{ij}}{4}\left(1 + 4\underline{s}_i \cdot \underline{s}_j\right) \qquad (1)$$

J_{ij} is known as the exchange integral, and in terms of the wave functions ψ_a on ion A, and ψ_b on ion B, it may be written,

$$2J_{ij} = \iint \psi_a(1)\,\psi_b(j)\cdot\frac{e^2}{r_{ij}}\cdot\psi_a(j)\,\psi_b(1)\,d\tau_i\,d\tau_j \qquad (2)$$

For spins greater than $\frac{1}{2}$ the interaction is similar to a first approximation, but higher order terms also occur of the form $-j(\underline{s}_i \cdot \underline{s}_j)^2 + k(\underline{s}_i \cdot \underline{s}_j)^3 + \ldots + n(\underline{s}_i \cdot \underline{s}_j)^S$ where $S = s_i + s_j$. When the overlap is small these terms are expected to be much smaller than the first order term (Anderson 1963).

In many substances however magnetic ions are found to interact very strongly with each other even when they are well separated by non-magnetic ions. An explanation of this phenomenon, which is known as superexchange, was first given by Kramers (1934), and his theory has been developed by several authors, in particular Anderson(1950).

The Kramers mechanism assumes that although the ground

state for the intermediate ions is principally diamagnetic, there are small admixtures of excited states which are paramagnetic. Consider as an example MnO. In this the interaction between second nearest neighbour Mn ions acts through an intermediate O ion. In the totally ionic state the configuration is:

$$Mn^{++} \text{ —— } O^{--} \text{ —— } Mn^{++}$$

The separation between the Mn^{++} ions is such that there is no direct overlap of their d orbitals and direct exchange will be quite negligible. There is a finite probability that electrons will transfer from the O^{--} ion on to one or both of the Mn^{++} ions giving a configuration such as:

$$Mn^{+} \text{ —— } O^{-} \text{ —— } Mn^{++}$$

The O^{-} ion is now paramagnetic and direct exchange between it and both Mn ions is possible.

If the totally ionic state is described by a wave function ψ_0, and the possible other states by ψ_i, the total wave function can be written

$$\Psi = b_0 \psi_0 + \sum_i b_i \psi_i \qquad (3)$$

where $b_0^2 + \sum_i b_i^2 = 1$

If the exchange integral corresponding to ψ_i is J_i, then the total exchange interaction can be described by the parameter

$$J = \sum_i b_i^n J_i \qquad (4)$$

The form of the interaction is the same as for direct exchange, and neglecting the constant term this can be written for spins $s_i = s_j = \frac{1}{2}$,

$$\mathcal{H}_{ex} = J\, s_i \cdot s_j \qquad (5)$$

That this model gives order of magnitude agreement with experiment is shown by Griffiths, Owen, Park, and Partridge (1959), for the nearest neighbour exchange in $(NH_4)_2IrCl_6$.

When J is positive, the energy of the interaction is minimised when s_i and s_j are antiparallel, and the interaction is said to be antiferromagnetic. The higher order isotropic exchange terms of the form $-j(s_i \cdot s_j)^n$, $k(s_i \cdot s_j)^3$, etc. which can occur when the spins are greater than $\frac{1}{2}$ are usually small and have been discussed by Anderson (1959, 1963) and Moriya (1960). These will be considered in more detail in chapter 3.

In addition to the isotropic interactions given above,

there are also anisotropic interactions which depend not only on s_i and s_j but also on their alignment relative to the crystal lattice. The simplest form is the dipolar form,

$$\mathcal{H} = D \frac{3(\underline{s}_i \cdot \underline{r})(\underline{s}_j \cdot \underline{r})}{r^2} - (\underline{s}_i \cdot \underline{s}_j) \qquad (6)$$

Magnetic dipolar interaction gives a term of this form with

$$D = - \frac{g^2\beta^2}{r_{ij}^3} \qquad (7)$$

In certain cases there are also contributions from anisotropic exchange, which can arise when there is spin-orbit coupling in addition to isotropic exchange (Van Vleck 1937). It gives a contribution to D of the order,

$$D \quad J\,(g - 2)^2 \qquad (8)$$

(Van Vleck 1951, Moriya 1960)

Higher order anisotropic exchange terms can also occur, but like the higher order isotropic terms they are expected to be small.

1.3 Properties of Concentrated Antiferromagnetic Crystals.

In the experiments described later in this thesis, the interactions between neighbouring magnetic ions in semidilute crystals have been measured. In applying these measurements to the concentrated crystals, it is assumed that the interactions are changed by only a small amount. The materials which have been studied all have a face-centred cubic (f.c.c.) crystal structure, so each ion interacts with 12 nearest neighbours (n.n.) and 12 next nearest neighbours(n.n.n.). The exchange interations tend to align the spins so as to minimise the total exchange energy, but this only manifests itself in a long range ordering at low temperatures when the thermal energy, kT, is less than the exchange energy.

The interaction between two neighbouring spins s_i and s_j can be written in the form,

$$\mathcal{H}_{ij} = J_{ij}\, \underline{s}_i \cdot \underline{s}_j + D_{ij}(3 s_{iz} s_{jz} - \underline{s}_i \cdot \underline{s}_j) + E_{ij}(s_{ix} s_{jx} - s_{iy} s_{jy}) \qquad (9)$$

Higher order terms can also occur, as has already been mentioned.

The behaviour of a concentrated magnetic crystal is described by a Hamiltonian,

$$\mathcal{H} = \sum_{ij} \mathcal{H}_{ij} \qquad (10)$$

At the present time it has not been found possible to treat this Hamiltonian in an exact way, and two types of approximation have been found useful.

The molecular field approximation

This was first developed by Van Vleck (1941,1945). It is essentially a semiclassical theory in which the effect on a spin on its neighbours is represented by an effective field. This is a good approximation at temperatures well above the transition temperature, when the spins have random orientations, and also at very low temperatures when the ordering of the spins is known, but it fails in the region of the transition temperature where there is a certain amount of short range ordering which cannot be properly allowed for. A better approximation is the Bethe-Pierlos-Weiss approximation in which a cluster of neighbouring spins are treated exactly with more remote spins replaced by the molecular field. (Weiss 1948).

The Spin-Wave Approximation

In order to treat the ground states of antiferromagnetic materials, the spin wave approximation is used (Van Kranendonk and Van Vleck, 1958). This is essentially a quantum mechanical theory. It is assumed that the

ground state is not far removed from an ordered basic array, and small deviations of spin are introduced. These deviations do not stay localised on one spin, but are propagated through the crystal lattice in the form of wave packets, or spin waves. If the total deviation from the assumed basic array remains small, then that basic array is stable, and a ground state. The mathematical difficulties in using the theory are very great unless an approximation is made that the mean deviation is small. Thus in practice the spin wave theory is a low temperature approximation.

Bulk Magnetic Properties

The magnetic properties of face centred cubic antiferromagnetic crystals are now briefly discussed.

At high temperatures ($T \gg T_N$), the magnetic susceptibility is well described using molecular field theory. Van Vleck (1941) gives

$$\chi = \frac{C}{T + \theta} \qquad (11)$$

where C is the Curie constant given by

$$C = \frac{Ng^2\beta^2 s(s+1)}{3k} \quad . \qquad (12)$$

θ is known as the Curie-Weiss constant. For a f.c.c.

lattice with isotropic exchange interactions J_1 between the 12 n.n. and J_2 between the 6 n.n.n., θ is given by

$$\theta = (12J_1 + 6J_2)\frac{S(S+1)}{3k} \qquad (13)$$

More refined theories by Opechowski (1937) and also by Li (1951) give expressions of the form

$$\chi = \frac{C}{T}\left(1 + \frac{A}{T} + \frac{B}{T^2} + \ldots\ldots\right) \qquad (14)$$

which reduce to the modified Curie-Weiss law (11) when T is large.

Below the transition temperature, the properties depend on the type of ordering. In the f.c.c. lattice it is not possible for all the spins to be antiparallel to all their neighbours, so the type of ordering that occurs is that for which the exchange energy is minimized. There are several types of ordering which depend on the relative signs and magnitudes of the different interactions. The transition temperature at which the long range ordering sets in cannot be calculated reliably using molecular field theory. The spin wave treatments of Zimen (1953) and Lines (1963) have been found to give much better agreement between theory and experiment, and this will be discussed in the later chapters.

For the ordered states in the crystals discussed

In this thesis, the lattices may be divided into two sublattices of parallel spins which are antiparallel to each other. At zero temperature, the alignment of the spins in the ordered state is very nearly complete, and the magnetisation of the sublattices are given by

$$M_0 = \frac{N}{2} g \beta s . \qquad (15)$$

At higher temperatures deviations become greater and the sublattice magnetisation, M, becomes less until it reaches zero at the transition temperature. It can be expressed as a Brillouin function,

$$\sigma = \frac{M}{M_0} = B\left(\frac{g\beta s}{kT} H_E \right) \qquad (16)$$

where H_E is the effective molecular field. If the exchange interactions are of the form $J\, s_i \cdot s_j$, then H_E is directly proportional to M, and the relative sublattice magnetisation is given by the transcendental equation,

$$\sigma = B\left(\frac{g\beta s}{kT} \lambda \sigma \right) \qquad (17)$$

where λ is a constant, depending on the type of ordering. If there are higher order exchange terms, λ will not be constant but will depend on σ. This variation of the molecular field with temperature affects all the

magnetic properties below the transition temperature.

The low temperature susceptibility is anisotropic. With the magnetic field parallel to the axis of alignment of the spins the susceptibility is zero when T = 0, rising to χ_{T_N} at the transition temperature. With the field perpendicular to the spins, molecular field theory predicts a constant value for $\chi_\perp$ when the exchange is first order, although higher order exchange introduces a variation.

Antiferromagnetic resonance depends not only on H_E, the isotropic exchange field which is the effective field acting on one sublattice due to the interactions with the other, but on H_A, the anisotropy field, which is the difference in effective field between 'easy' and 'hard' directions of magnetisation in the crystal. The condition for resonance is,

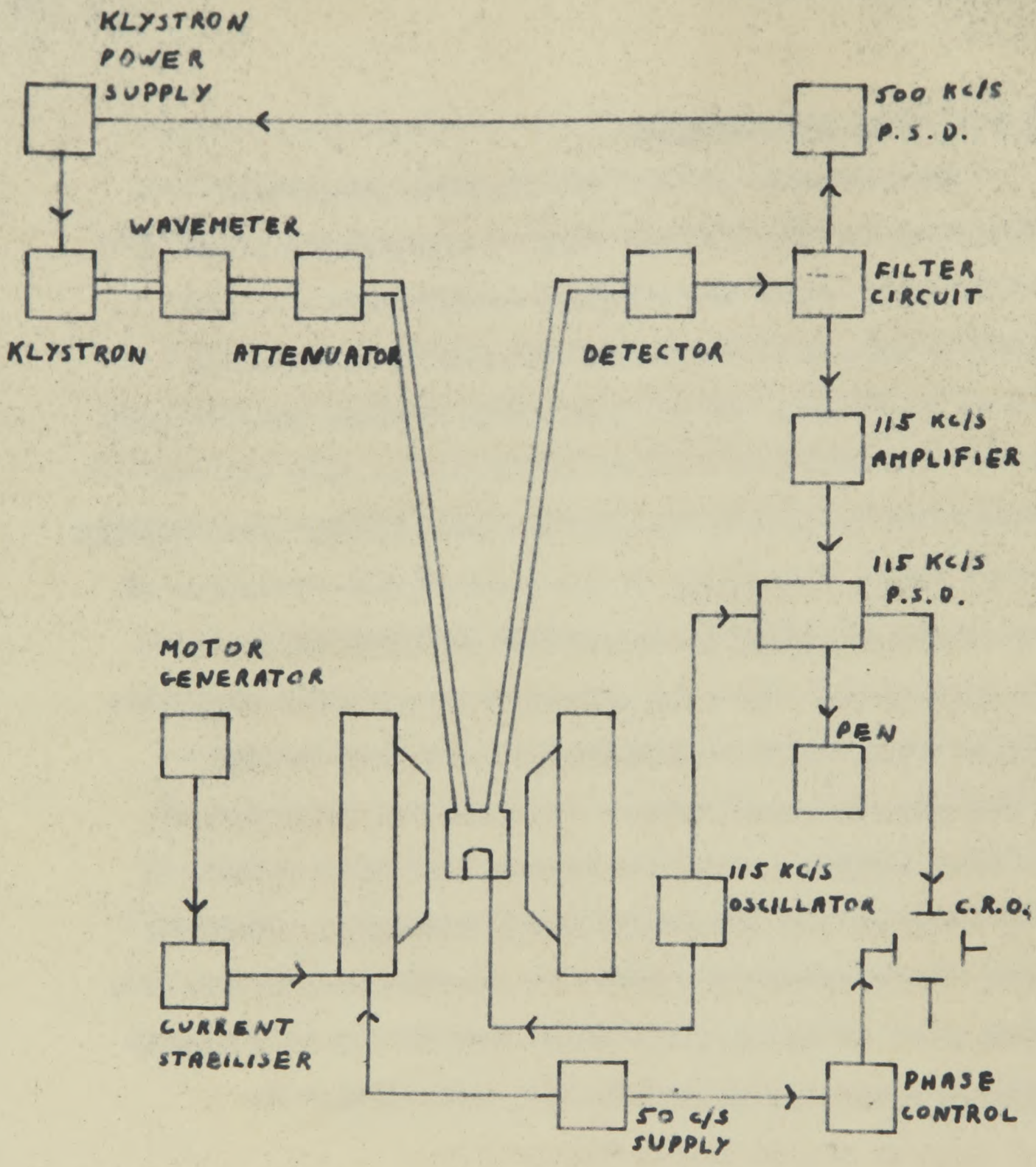
$$h\nu = g\beta \sqrt{(H_A(2H_E + H_A))} \qquad (18)$$

Usually $H_A \ll H_E$, and this can be written,

$$h\nu = g\beta \sqrt{(2H_E H_A)} \ .$$

1.4 Pair Measurements

Measurements of the bulk magnetic properties described in the previous section can provide a lot of information about the exchange interactions. The interpretation of these measurements is necessarily based on quite a lot of approximate theory, and the bulk properties are generally insufficient to give all the parameters necessary to describe the exchange interactions in detail. The study of the paramagnetic resonance of ion pairs in crystals does enable detailed information to be obtained about the interactions in mixed crystals. In applying these measurements to the concentrated crystals, allowance must be made for the variation of lattice spacing, which can have a very great effect on the magnitude of the exchange interactions. Previous pair measurements, and also the present ones do indicate that after allowing for thisthe results can be compared with the bulk properties to give good agreement.



BLOCK DIAGRAM OF APPARATUS

FIG. 1.

CHAPTER 2

EXPERIMENTAL TECHNIQUES

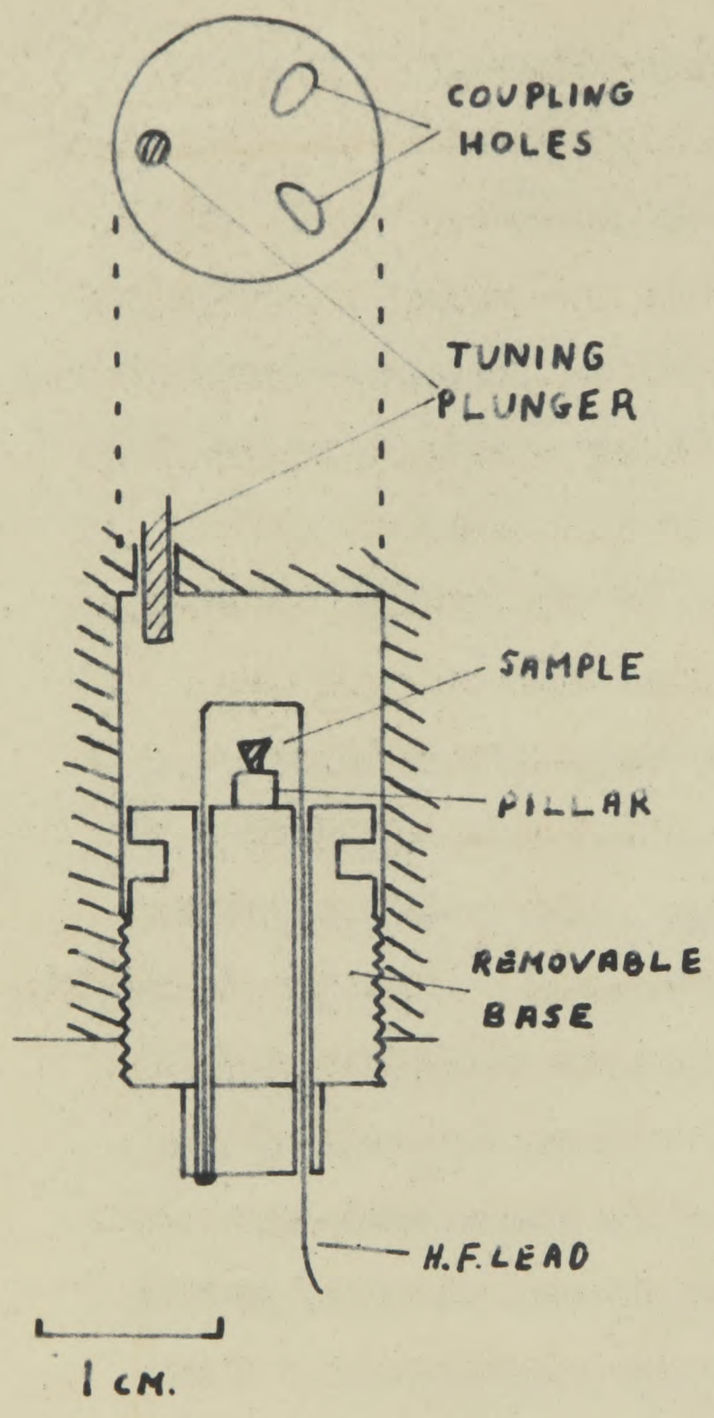
In this chapter a brief description of the C-band (λ = 3.5 cm) spectrometer used in the present experiments is given. The methods of measurement and the precautions taken to ensure accuracy are also described.

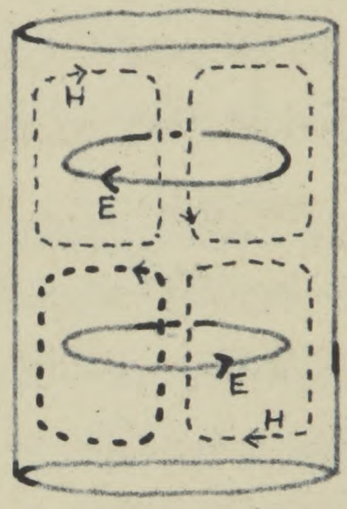
2.1 The Spectrometer

The theoretical sensitivities of different types of spectrometer have been discussed by a number of authors (Feher 1957, Goldsborough and Mandel 1960). In the present experiments a transmission cavity system was used, with a 110 kc/s detection system. This system was chosen mainly for simplicity of operation. A block diagram of the complete apparatus showing the arrangement of the various components is given in fig.1. A double dewar system enables the spectrometer to be used down to liquid helium temperatures.

The Cavity

The cylindrical cavity, which is drawn in fig 2, resonates in the H_{011} mode. This mode was chosen because it can be made to give a higher Q-value than the more usual H_{11} mode, and because the direction of





H_{012} MODE.

FIG. 2. THE CAVITY.

the microwave magnetic field is fixed, and could be arranged so as always to be perpendicular to the applied magnetic field. The base of the cavity screws in and out, and this provides a means for tuning the cavity to the klystron frequency. Fine tuning at low temperatures is provided by a P.T.F.E. tuning plunger operated from outside the cryostat. Power is coupled in and out through two holes in the top of the cavity. These are placed so as to favour the $H_{0,1}$ mode and not the degenerate $E_{1,1}$ mode. The degeneracy is split when a sample is placed in the cavity, and it is possible to tune onto just the $H_{0,1}$ mode. The cavity is silver plated inside, and when empty has a Q value of about 7000.

Samples are mounted where the microwave magnetic field is strongest. This is along the axis of the cavity, about one quarter of the guide wavelength from one end. Large samples are mounted directly on the cavity base, but small ones are supported by a 8 mm dystrene pillar, as shown in fig 8.

The Microwave System

The microwave system is quite conventional. The large stray field from the magnet made it necessary to mount the klystron 8 feet away from the cryostat.

Provision is made to attenuate and monitor the microwaves either side of the cryostat. Thin walled german silver waveguide is used immediately next to the cavity to reduce heat flow. An automatic frequency controlling device, developed by J. Pilbrow, locks the klystron frequency onto the cavity resonance. This works by modulating the reflector voltage with a small amplitude at 500 kc/s and passing the output from the crystal detector into a 500 kc/s phase sensitive detector. The output from this is only zero when the cavity is exactly on tune. This error signal passes through a D.C. amplifier and is fed back to the reflector.

The Detection System

The magnetic field is modulated at 115 kc/s by a loop of wire around the sample inside the cavity. Copper wire was found to vibrate slightly at high fields, thereby modulating the microwaves. Brass wire which is much more rigid was found not to suffer in this way. The oscillator feeding this loop is able to pass currents up to 2 amperes, giving a modulation of about 3 gauss at the sample. The microwaves are detected by a silicon crystal diode. The detected signal is amplified in a 115 kc/s narrow band, high

gain amplifier, and passes through a calibrated attenuator to a phase sensitive detector. The output is fed through a filter circuit with a number of alternative time constants, to reduce the more rapid fluctuations, to a pen recorder. Provision is also made for visual display by modulating the magnetic field with a large amplitude at 50 c/s and displaying the phase sensitive detector output on an oscilloscope with a 50 c/s time base.

The Magnet

The spectrometer is used with a Mullard high field electromagnet, which is water cooled and capable of giving up to 17 kilogauss over a 8 x 2½ inch gap. It is mounted on a turntable. The field is current stabilised, nominally to 1 part in 10^3, and a steady field sweep is obtained electronically.

2.2 Experimental Measurements

Three types of measurements were required in the present investigations.

(i) Anisotropy plots, - to find the variation of the line positions with field direction.

(ii) Accurate measurement of line positions in particular field directions.

(iii) Accurate comparisons of the intensities of different lines at various temperatures.

Anisotropy Plots

The magnet is built so as to rotate in a horizontal plane. The crystal is therefore mounted in the cavity with a known crystal plane horizontal. For the f.c.c. crystals used in the present work the (100) plane is suitable because it contains both the [110] and [100] directions, the principal axes for n.n. and n.n.n. pairs.

The spectrum is drawn out on the pen recorder as the magnet current is increased steadily from zero. A separate pen on the recorder chart acts as a marker, and is operated manually to calibrate the chart in units of magnet current. The field direction is changed by increments of 1° or 2° over a wide range of directions. To observe lines it is necessary to have an appreciable component of the modulating field parallel to the main field, so this limits the range of field directions to about 140°.

From the charts the line position in units of magnet current is plotted against field angle. At low currents the field is very nearly proportional to the current, but at higher currents ($\gtrsim$ 10 amp) the field is found from the magnet calibration curve, which was made from

N.M.R. measurements. This enables the line positions to be given to within ± 50 gauss, which is usually good enough for tentative identification of the lines.

Accurate Measurement of Line Positions

In order to fit the spectrum to parameters in the Spin Hamiltonian, the positions of lines for certain field directions, at crossing points or along axes of symmetry, are required as accurately as possible. In the present experiments the lines were all comparatively wide (~100 gauss), and the principal error in measuring a line position arises in estimating the mid-point. Proton resonance was used in low fields, up to about 7 kilogauss, and above that, Li^7 resonance. For intense lines the measurements are straightforward. Using a 50 c/s field sweep, the electron and nuclear resonance lines can be observed simultaneously on a double beam oscilloscope. The n.m.r. frequency is then measured on a Rohde and Schwarz frequency meter. For weak lines, including most pair lines, which cannot be observed on the oscilloscope, the pen marker is used to mark known n.m.r. frequencies on the recorder chart. Using a very slow steady field sweep, and a small 50 c/s sweep, the n.m.r. oscillator is set successively to different harmonics of 100 kc/s, and the marker pen

is operated as the nuclear resonance crosses the oscilloscope screen.

A measurement of microwave frequency is also required. This can be measured using a wavemeter, but it is more accurate to measure the field at which the sharp line from D.P.P.H. occurs, at g = 2.003. In the present experiments the former method was quite accurate enough, but both were used.

Intensity Measurements

Absolute measurements of intensity at several temperatures would be very difficult to carry out, and would not give reliable results. The intensity of a line depends to a large extent on factors such as the distribution of microwave magnetic field within the cavity, the Q of the cavity, and the coupling between the cavity and the waveguides, all of which are likely to change by an unknown amount as the temperature is varied. The easiest experimental procedure is to compare the intensities of two lines, the behaviour of one of which is known. This also can prove difficult. It is necessary to find a comparison substance with a line well separated from any others in either sample. It must be possible to observe this line over the same temperature range, and under the same conditions as the

line under comparison, which means that it must not saturate at low temperatures, or broaden too much at high temperatures. The two samples are mounted in the cavity together, and it must be assumed that any variations in the modulation field, or in the microwave field, with temperature affect both samples equally. This is quite a genuine difficulty, because when the temperature is changed, the cavity must be retuned, and this is bound to affect the distribution of microwave field inside the cavity. It is clearly a great advantage to be able to carry out the intensity comparisons using two lines from the same specimen. This was found possible in Mn^{++} : ZnF (Brown, Gales, Owen and Stephenson, 1961), in which the temperature variation of lines from Mn pairs were compared with that of an Iron impurity. In the present work on Mn pairs in MgO comparisons have been made between transitions from spin states with different energies, in order to find the energy splittings between the states. This situation is ideal for intensity measurements, because not only do the lines come from within the same sample, but they have the same shape and width, and only saturate under the same conditions.

Any non linearity in the amplification and recording system directly affects intensity measurements, so this was checked in a separate experiment. In this the non-linearity was plotted on a correction curve, which was applied to all subsequent measurements.

The line shape drawn out by the pen is proportional to the differential of the absorption. The total intensity of a line is the integrated absorption, so in order to obtain the intensity of a line, it must be integrated twice over its whole width. For lines of the same shape and width, the intensity will be proportional to the peak to peak height of the differential.

For the Mn pairs in MgO described in chapter 3, the peak to peak height was found to be proportional to the integrated intensity, but for the Iridium pairs and triads described in chapter 4, broadening occured at higher temperatures, and it was necessary to integrate the pen recordings.

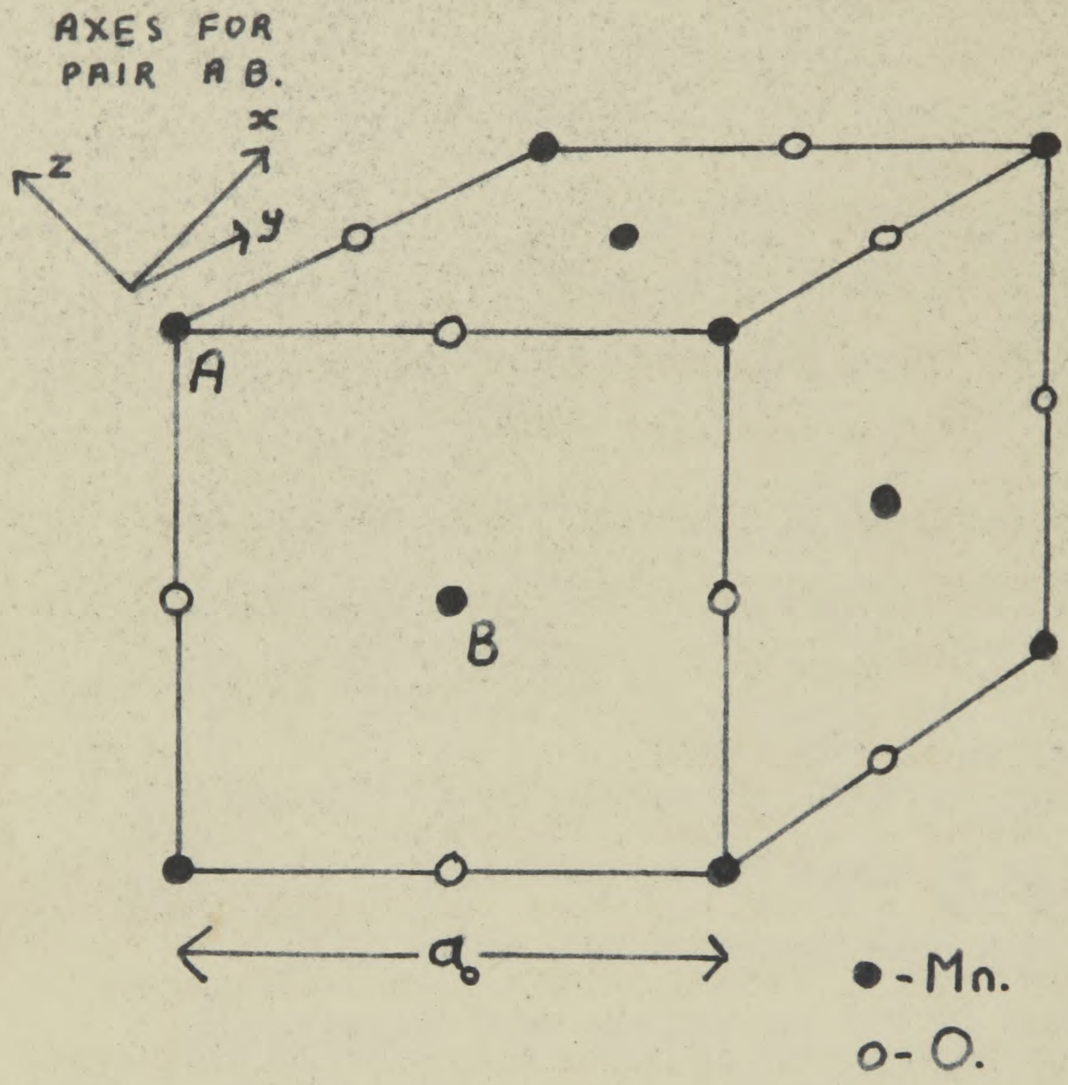
CHAPTER 5

PARAMAGNON PAIRS IN MnO

5.1 Introduction

Paramagnetic resonance measurements on the exchange interactions between pairs of Mn^{++} ions in MgO have been made in an earlier series of experiments (Coles 1959, Coles et al. 1960). Resonance lines from both n.n. and n.n.n. pairs were observed, and estimates made of the isotropic and anisotropic exchange parameters. The isotropic exchange interactions, J_1 and J_2, were both found to be about 80°K., much larger than those estimated from bulk measurements, about 11°K.

In order to try to explain this discrepancy, a more detailed study of the pair spectrum has been made, and is described in this chapter. In these experiments only the spectrum from n.n. pairs has been studied. The results suggest that in addition to the usual bilinear term for the isotropic exchange, $J(\underline{s}_1 \cdot \underline{s}_2)$, there is an appreciable biquadratic term, $j(\underline{s}_1 \cdot \underline{s}_2)^2$. Such a term certainly helps to explain the earlier discrepancy, and is considered when discussing the bulk magnetic properties of MnO.



STRUCTURE OF MnO

FIG. 3..

The crystal used in the experiments was provided by Prof. Wurtz, and was grown from a melt of MgO with about 6% Mn_2O_3, but from the colour of the crystal, and from the intensity of the magnetic resonance lines it is estimated that the crystal contains about 1 % Mn.

Both MnO and MgO have a f.c.c. crystal structure, see fig 5. A n.n. pair has an axis along a face diagonal [110], and a n.n.n. pair along a cube edge [100]. The exchange interactions act by superexchange through the intermediate O^{--} ions as was discussed in chapter 1. The lattice parameters are,

MgO : $a_0 = 4.203$ Å

MnO : $a_0 = 4.4448$ Å (Wyckoff, 1960)

This rather large difference means that in the mixed crystal the spacing between the ions of a Mn pair will be appreciably different from that in pure MnO.

Dr. W. Marshall (private communication) estimates that a 5% difference in lattice spacing could change the exchange by about 30%, so this must be included when applying the results of pair measurements to the bulk properties of MnO. There will also be a certain amount of lattice distortion around the pairs, which will be reflected in the anisotropy parameters of the spin Hamiltonian.

2.2 Energy levels for a n.n. pair

The spin Hamiltonian

The Hamiltonian for a pair may be written

$$\mathcal{H}_{12} = \mathcal{H}_1 + \mathcal{H}_2 + \mathcal{H}_{ex} \qquad (1)$$

where $\mathcal{H}_1$ and $\mathcal{H}_2$ define the crystal field acting on each spin s_1 and s_2 separately, and $\mathcal{H}_{ex}$ defines the interaction between them. The spectrum due to isolated ions of Mn^{++} in MgO has been analysed by Low (1957). The crystal field has cubic symmetry given by,

$$\mathcal{H}_{cub} = \frac{a}{6}\left[s_{x'}^4 + s_{y'}^4 + s_{z'}^4 + \tfrac{1}{5} s(s+1)(3s^2+3s-1) \right] \qquad (2)$$

where $a = 18.65 \times 10^{-4}$ cm^{-1}. The axes x' y' z' are the cube edges in the crystal lattice. For the remaining terms axes will be taken with z along the [110] direction joining the ions of the pair, y along the [001] direction normal to this, and x along the $[1\bar{1}0]$ direction normal to both of these, see fig 3.

There is an interaction with the Manganese nuclear spin, $I = \frac{5}{2}$, giving a hyperfine term,

$$\mathcal{H}_{hf} = A\, \underline{I} \cdot \underline{S} \qquad (3)$$

where $A = -81.0 \times 10^{-4}$ cm^{-1}.

The distortion of the crystal field due to a second

spin will lead to further terms.

$$\mathcal{H}_{cf} = D_c\left[S_z^2 - \tfrac{1}{3}S(S+1)\right] + E_c\left[S_x^2 - S_y^2\right]$$
$$+ F_c\left[35S_z^4 - 30S(S+1)S_z^2 + 25S_z^2 + 3S^2(S+1)^2 - 6S(S+1)\right]$$
$$+ \text{other higher order terms} \qquad (4)$$

We now have,

$$\mathcal{H}_1 = \mathcal{H}_{cub} + \mathcal{H}_{hf} + \mathcal{H}_{cf} \qquad (5)$$

The interaction between two spins is taken to be of the form,

$$\mathcal{H}_{ex} = J(\underline{s}_1 \cdot \underline{s}_2) - J(\underline{s}_1 \cdot \underline{s}_2)^2 + D_c(3s_{1z}s_{2z} - \underline{s}_1 \cdot \underline{s}_2)$$
$$+ E_c(s_{1x}s_{2x} - s_{1y}s_{2y}) \qquad (6)$$

Other higher order terms may occur, but are neglected. D_c and E_c represent the anisotropy of the interaction. It is expected that D_c will be mainly due to the magnetic dipolar interaction,

$$D = -\frac{\mu^2\beta^2}{r^3} \qquad (7)$$

Anisotropic exchange will contribute to both D_c and E_c.

<u>The Hamiltonian</u>.

The total Hamiltonian, which is the sum of all the terms listed above, is dominated by the first order

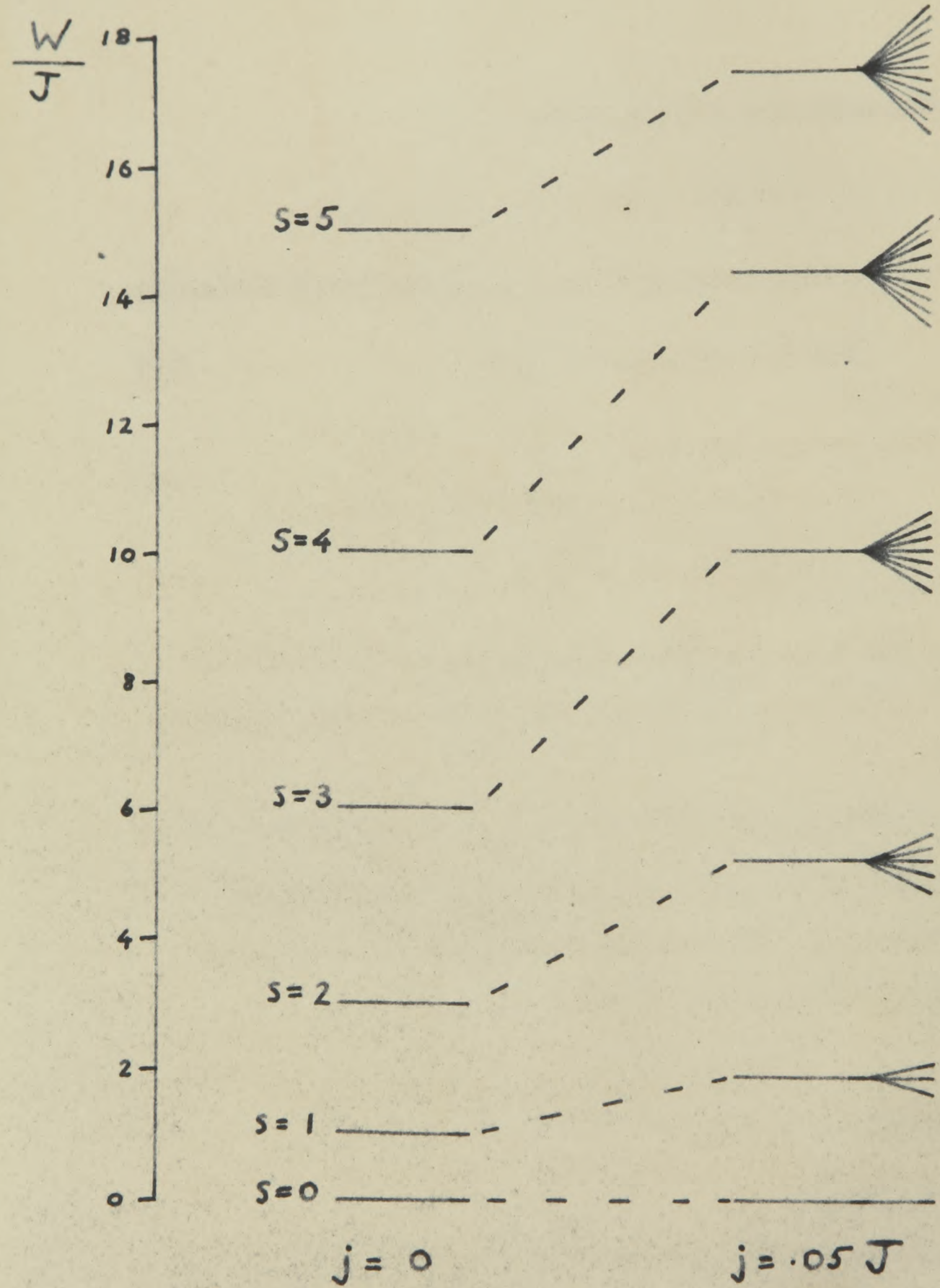


FIG. 4. ENERGY LEVEL SCHEME FOR A MN - MN PAIR.

isotropic exchange interaction,

$$\mathcal{H} = J\,(\underline{s}_1 \cdot \underline{s}_2) \qquad (8)$$

Defining a total spin, $\underline{S} = \underline{s}_1 + \underline{s}_2$, this may be written,

$$\mathcal{H} = \frac{J}{2}\,(\underline{S}^2 - \underline{s}_1^2 - \underline{s}_2^2) \qquad (9)$$

This gives energy levels,

$$W_S = \frac{J}{2}\{\, S(S+1) - s_1(s_1+1) - s_2(s_2+1)\}$$

$$= \frac{J}{2}\{\, S(S+1) - \frac{35}{2}\,\} \qquad (10)$$

where S can take the values 0, 1, 2, 3, 4, 5, so the energy levels are spaced according to a Landé interval rule, i.e.

$$\Delta W_{S,S-1} = J\,S. \qquad (11)$$

Higher order exchange terms will modify this interval rule. The second isotropic term, $-j(\underline{s}_1\cdot\underline{s}_2)^2$ changes the levels by amounts,

$$-\frac{j}{4}\,\{\, S(S+1) - s_1(s_1+1) - s_2(s_2+1)\,\}^2 \qquad (12)$$

giving a modified interval rule,

$$\Delta W_{S,S-1} = JS - jS(S^2 - s_1(s_1+1) - s_2(s_2+1)) \qquad (13)$$

The energy level schemes when $\frac{j}{J} = 0$, and $\frac{j}{J} = .05$ are compared in fig 4.

$$|5\rangle_5 = |\tfrac{5}{2}, \tfrac{5}{2}\rangle$$

$$|4\rangle_5 = (1/\sqrt{2})(|\tfrac{3}{2}, \tfrac{5}{2}\rangle + |\tfrac{5}{2}, \tfrac{3}{2}\rangle)$$

$$|3\rangle_5 = \tfrac{1}{3}(\sqrt{2}|\tfrac{1}{2}, \tfrac{5}{2}\rangle + \sqrt{2}|\tfrac{5}{2}, \tfrac{1}{2}\rangle + (5)^{\frac{1}{2}}|\tfrac{3}{2}, \tfrac{3}{2}\rangle)$$

$$|2\rangle_5 = (1/2\sqrt{3})(|-\tfrac{1}{2}, \tfrac{5}{2}\rangle + |\tfrac{5}{2}, -\tfrac{1}{2}\rangle + (5)^{\frac{1}{2}}|\tfrac{1}{2}, \tfrac{3}{2}\rangle + (5)^{\frac{1}{2}}|\tfrac{3}{2}, \tfrac{1}{2}\rangle)$$

$$|1\rangle_5 = [1/2(21)^{\frac{1}{2}}][\sqrt{2}(|-\tfrac{3}{2}, \tfrac{5}{2}\rangle + |\tfrac{5}{2}, -\tfrac{3}{2}\rangle) + 2(5)^{\frac{1}{2}}(|-\tfrac{1}{2}, \tfrac{3}{2}\rangle + |\tfrac{3}{2}, -\tfrac{1}{2}\rangle) + 2(10)^{\frac{1}{2}}|\tfrac{1}{2}, \tfrac{1}{2}\rangle]$$

$$|0\rangle_5 = [1/6(7)^{\frac{1}{2}}][(|-\tfrac{5}{2}, \tfrac{5}{2}\rangle + |\tfrac{5}{2}, -\tfrac{5}{2}\rangle) + 5(|-\tfrac{3}{2}, \tfrac{3}{2}\rangle + |\tfrac{3}{2}, -\tfrac{3}{2}\rangle) + 10(|-\tfrac{1}{2}, \tfrac{1}{2}\rangle + |\tfrac{1}{2}, -\tfrac{1}{2}\rangle)]$$

$$|4\rangle_4 = (1/\sqrt{2})(|\tfrac{3}{2}, \tfrac{5}{2}\rangle - |\tfrac{5}{2}, \tfrac{3}{2}\rangle)$$

$$|3\rangle_4 = (1/\sqrt{2})(|\tfrac{1}{2}, \tfrac{5}{2}\rangle - |\tfrac{5}{2}, \tfrac{1}{2}\rangle)$$

$$|2\rangle_4 = [1/2(7)^{\frac{1}{2}}][3(|-\tfrac{1}{2}, \tfrac{5}{2}\rangle - |\tfrac{5}{2}, -\tfrac{1}{2}\rangle) + (5)^{\frac{1}{2}}(|\tfrac{1}{2}, \tfrac{3}{2}\rangle - |\tfrac{3}{2}, \tfrac{1}{2}\rangle)]$$

$$|1\rangle_4 = [1/(7)^{\frac{1}{2}}][(|-\tfrac{3}{2}, \tfrac{5}{2}\rangle - |\tfrac{5}{2}, -\tfrac{3}{2}\rangle) + (\tfrac{5}{2})^{\frac{1}{2}}(|-\tfrac{1}{2}, \tfrac{3}{2}\rangle - |\tfrac{3}{2}, -\tfrac{1}{2}\rangle)]$$

$$|0\rangle_4 = [1/2(7)^{\frac{1}{2}}][(|-\tfrac{5}{2}, \tfrac{5}{2}\rangle - |\tfrac{5}{2}, -\tfrac{5}{2}\rangle) + 3(|-\tfrac{3}{2}, \tfrac{3}{2}\rangle - |\tfrac{3}{2}, -\tfrac{3}{2}\rangle) + 2(|-\tfrac{1}{2}, \tfrac{1}{2}\rangle - |\tfrac{1}{2}, -\tfrac{1}{2}\rangle)]$$

$$|3\rangle_3 = \tfrac{1}{3}[2|\tfrac{3}{2}, \tfrac{3}{2}\rangle - (\tfrac{5}{2})^{\frac{1}{2}}(|\tfrac{1}{2}, \tfrac{5}{2}\rangle + |\tfrac{5}{2}, \tfrac{1}{2}\rangle)]$$

$$|2\rangle_3 = (1/2\sqrt{3})[|\tfrac{1}{2}, \tfrac{3}{2}\rangle + |\tfrac{3}{2}, \tfrac{1}{2}\rangle - (5)^{\frac{1}{2}}(|-\tfrac{1}{2}, \tfrac{5}{2}\rangle + |\tfrac{5}{2}, -\tfrac{1}{2}\rangle)]$$

$$|1\rangle_3 = [1/(30)^{\frac{1}{2}}][(8)^{\frac{1}{2}}|\tfrac{1}{2}, \tfrac{1}{2}\rangle - (|-\tfrac{1}{2}, \tfrac{3}{2}\rangle + |\tfrac{3}{2}, -\tfrac{1}{2}\rangle) - (10)^{\frac{1}{2}}(|-\tfrac{3}{2}, \tfrac{5}{2}\rangle + |\tfrac{5}{2}, -\tfrac{3}{2}\rangle)]$$

$$|0\rangle_3 = [1/6(5)^{\frac{1}{2}}][4(|-\tfrac{1}{2}, \tfrac{1}{2}\rangle + |\tfrac{1}{2}, -\tfrac{1}{2}\rangle) - 7(|-\tfrac{3}{2}, \tfrac{3}{2}\rangle + |\tfrac{3}{2}, -\tfrac{3}{2}\rangle) - 5(|-\tfrac{5}{2}, \tfrac{5}{2}\rangle + |\tfrac{5}{2}, -\tfrac{5}{2}\rangle)]$$

$$|2\rangle_2 = [1/2(7)^{\frac{1}{2}}][3(|\tfrac{1}{2}, \tfrac{3}{2}\rangle - |\tfrac{3}{2}, \tfrac{1}{2}\rangle) - (5)^{\frac{1}{2}}(|-\tfrac{1}{2}, \tfrac{5}{2}\rangle - |\tfrac{5}{2}, -\tfrac{1}{2}\rangle)]$$

$$|1\rangle_2 = [1/2(7)^{\frac{1}{2}}][2(|-\tfrac{1}{2}, \tfrac{3}{2}\rangle - |\tfrac{3}{2}, -\tfrac{1}{2}\rangle) - (10)^{\frac{1}{2}}(|-\tfrac{3}{2}, \tfrac{5}{2}\rangle - |\tfrac{5}{2}, -\tfrac{3}{2}\rangle)]$$

$$|0\rangle_2 = [1/2(21)^{\frac{1}{2}}][4(|-\tfrac{1}{2}, \tfrac{1}{2}\rangle - |\tfrac{1}{2}, -\tfrac{1}{2}\rangle) - (|-\tfrac{3}{2}, \tfrac{3}{2}\rangle - |\tfrac{3}{2}, -\tfrac{3}{2}\rangle) - 5(|-\tfrac{5}{2}, \tfrac{5}{2}\rangle - |\tfrac{5}{2}, -\tfrac{5}{2}\rangle)]$$

$$|1\rangle_1 = [1/(105)^{\frac{1}{2}}][(27)^{\frac{1}{2}}|\tfrac{1}{2}, \tfrac{1}{2}\rangle + (15)^{\frac{1}{2}}(|-\tfrac{3}{2}, \tfrac{5}{2}\rangle + |\tfrac{5}{2}, -\tfrac{3}{2}\rangle) - (24)^{\frac{1}{2}}(|-\tfrac{1}{2}, \tfrac{3}{2}\rangle + |\tfrac{3}{2}, -\tfrac{1}{2}\rangle)]$$

$$|0\rangle_1 = [1/(70)^{\frac{1}{2}}][|-\tfrac{1}{2}, \tfrac{1}{2}\rangle + |\tfrac{1}{2}, -\tfrac{1}{2}\rangle - 3(|-\tfrac{3}{2}, \tfrac{3}{2}\rangle + |\tfrac{3}{2}, -\tfrac{3}{2}\rangle) + 5(|-\tfrac{5}{2}, \tfrac{5}{2}\rangle + |\tfrac{5}{2}, -\tfrac{5}{2}\rangle)]$$

$$|0\rangle_0 = [1/(6)^{\frac{1}{2}}][(|-\tfrac{5}{2}, \tfrac{5}{2}\rangle - |\tfrac{5}{2}, -\tfrac{5}{2}\rangle) - (|-\tfrac{3}{2}, \tfrac{3}{2}\rangle - |\tfrac{3}{2}, -\tfrac{3}{2}\rangle) + (|-\tfrac{1}{2}, \tfrac{1}{2}\rangle - |\tfrac{1}{2}, -\tfrac{1}{2}\rangle)]$$

TABLE I SUBSTATES FOR $S_1 = S_2 = \frac{5}{2}$, WRITTEN IN THE FORM $|M\rangle_S = \sum_i a|m_1, m_2\rangle$. TO OBTAIN $|-M\rangle_S$, THE SIGNS OF m_1 AND m_2 ARE REVERSED.

Each of these states consists of 2S+1 substates which may be represented by the magnetic quantum numbers,

$M_S = -S , -S+1 , \ldots\ldots\ldots , S-1 , S .$

Alternatively the states may be represented in terms of the magnetic quantum numbers, m_1, m_2, for the two spins, s_1, s_2, respectively, the relation between these representations being of the form,

$$(M)_S = a(m_1 m_2) + b(m_1-1, m_2+1) + \ldots \quad (14)$$

where $a^2 + b^2 + \ldots = 1$, and $m_1 + m_2 = M$

The coefficients a, b, . . . can be found from the relation,

$$\mathcal{H}\Psi = W\Psi \quad (15)$$

The full scheme of states for $s_1 = s_2 = \frac{5}{2}$, coupled by an isotropic interaction is given in Table I.

The effect of the anisotropic terms in the spin Hamiltonian will be to mix the states slightly, and to split the energy levels by small amounts. The matrix elements between substates with different S values will be unimportant, moving the energy levels by amounts of the order $\frac{D^2}{J}$, which is very small because $J \gg D$. This means that the substates within a given S state manifold can be considered apart from the other substates. The spin Hamiltonian can be

simplified, and expressed in terms of $\underline{S} = \underline{S}_1 + \underline{S}_2$.

The spectra in the present work have been interpreted using the spin Hamiltonian,

$$\mathcal{H} = g\beta \underline{H}\cdot\underline{S} + D_s(S_z - \tfrac{1}{3}S(S+1)) + E_s(S_x^2 - S_y^2)$$
$$+ F_s(35S_z^4 - 30S(S+1)S_z^2 + 25S_z^2 + 3S^2(S+1)^2 - 6S(S+1)) \quad (16)$$

The cubic field term is omitted because it is expected to be small compared with the experimental errors, assuming it is similar to that for the isolated ion. The hyperfine term has been omitted because it does not affect the line positions. It will be discussed later. The parameters D_s , E_s , F_s , are related directly to D_c , E_c , F_c , D_c , E_c , by comparing equivalent matrix elements using the two representations. These relationships are given by,

$$D_s = a_s D_c^{\frac{1}{2}} + \beta_s D_c \quad (17)$$

$$E_s = a_s E_c + \beta_s E_c \quad (18)$$

$$F_s = \gamma_s F_c \quad (19)$$

where, $$a_s = \tfrac{2}{3}\left(\frac{S(S+1) + 4s(s+1)}{(2S-1)(2S+3)}\right) \quad (20)$$

$$\beta_s = \frac{3S(S+1) - 3 - 4s(s+1)}{(2S-1)(2S+3)} \quad (21)$$

$$\gamma_s = \frac{35S^2(S+1)^2 - 10S(S+1) + 12S - 12S(S+1)s(s+1) + 4s^2(s+1)^2 + 44s(s+1)}{4(2S+3)(2S+5)(2S-3)(2S-1)} \quad (22)$$

M	1	-1	2	0	-2
1	$G+D-\frac{24F}{7}$	$3E$	0	0	0
-1	$3E$	$-G+D-\frac{24F}{7}$	0	0	0
2	0	0	$2G+4D-\frac{12F}{7}$	$E\sqrt{6}$	0
0	0	0	$E\sqrt{6}$	0	$E\sqrt{6}$
-2	0	0	0	$E\sqrt{6}$	$-2G+4D-\frac{12F}{7}$

FIG. 5. $S = 2$ ENERGY MATRIX

$H // z$, $G = g\beta H$.

Derivations of equns 20-22 have been given by Windsor (1963). For the present case with $s = \frac{5}{2}$ they give the following values,

S	1	2	3	4	5
a_s	$\frac{27}{10}$	$\frac{41}{30}$	$\frac{47}{90}$	$\frac{5}{14}$	$\frac{5}{10}$
β_s	$-\frac{22}{5}$	$-\frac{20}{21}$	$-\frac{8}{45}$	$\frac{2}{7}$	$\frac{4}{5}$
γ_s	0	$\frac{10}{7}$	$-\frac{1}{5}$	$-\frac{1}{7}$	$\frac{1}{21}$

The S = 1 Spectrum

This was studied by Coles et al (1960) who found the following anisotropy parameters,

$$D_1 = .776 \pm .01 \text{ cm}^{-1}$$
$$E_1 = .149 \pm .005 \text{ cm}^{-1}$$

The S = 2 Spectrum

Operating with the Hamiltonian (18) on the substates of the S = 2 manifold, taking H parallel to z, we get the energy matrix given in fig 5, where $\theta = g\beta H$.

The energy levels are found by solving the equation obtained by equating the associated secular determinant to zero. This is straightforward when H // z, because the determinant factorises easily, but for other field

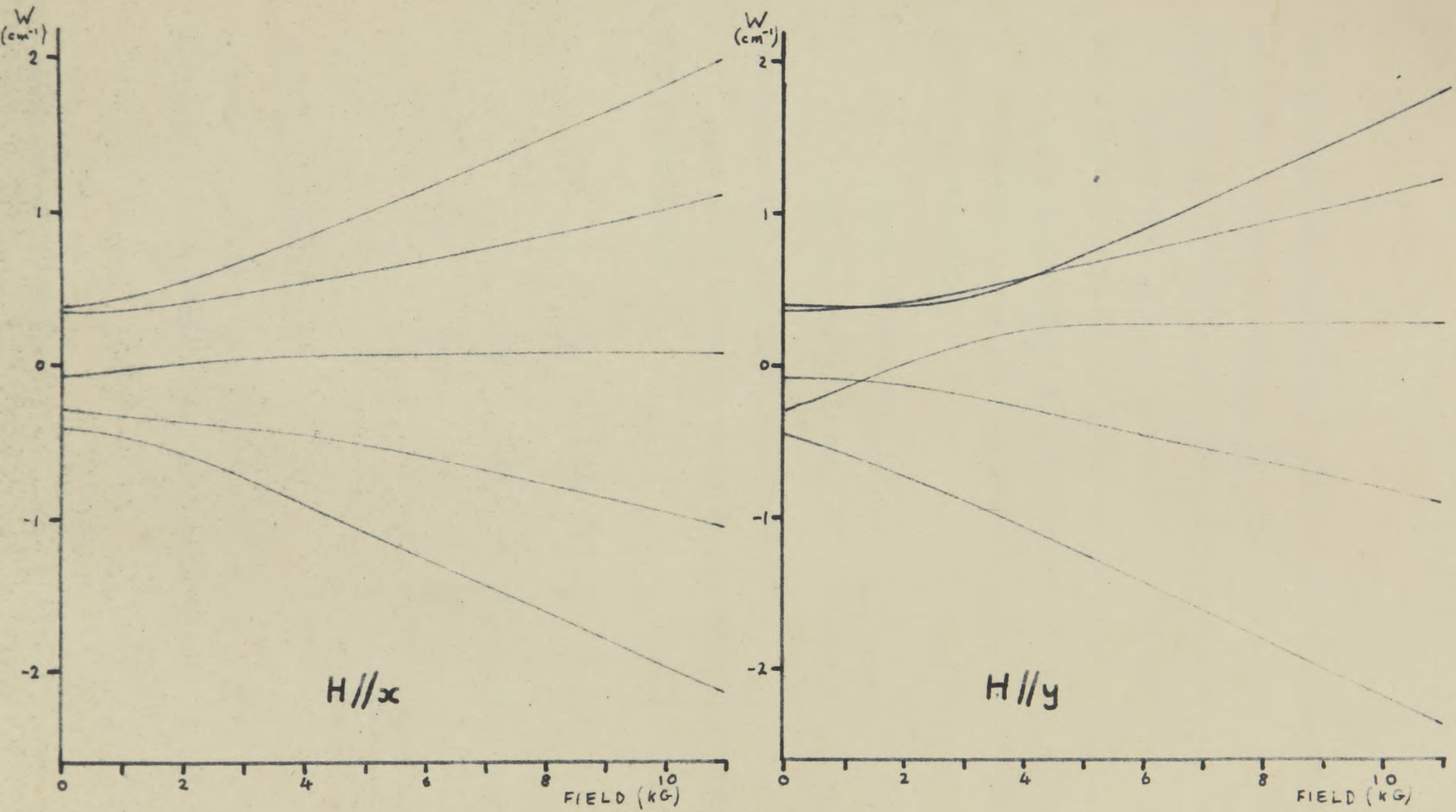


FIG. 6A. MN:MgO, S = 2 ENERGY LEVELS ASSUMING, $D_2 = .182\ cm^{-1}$, $E_2 = .035\ cm^{-1}$, $g = 2$

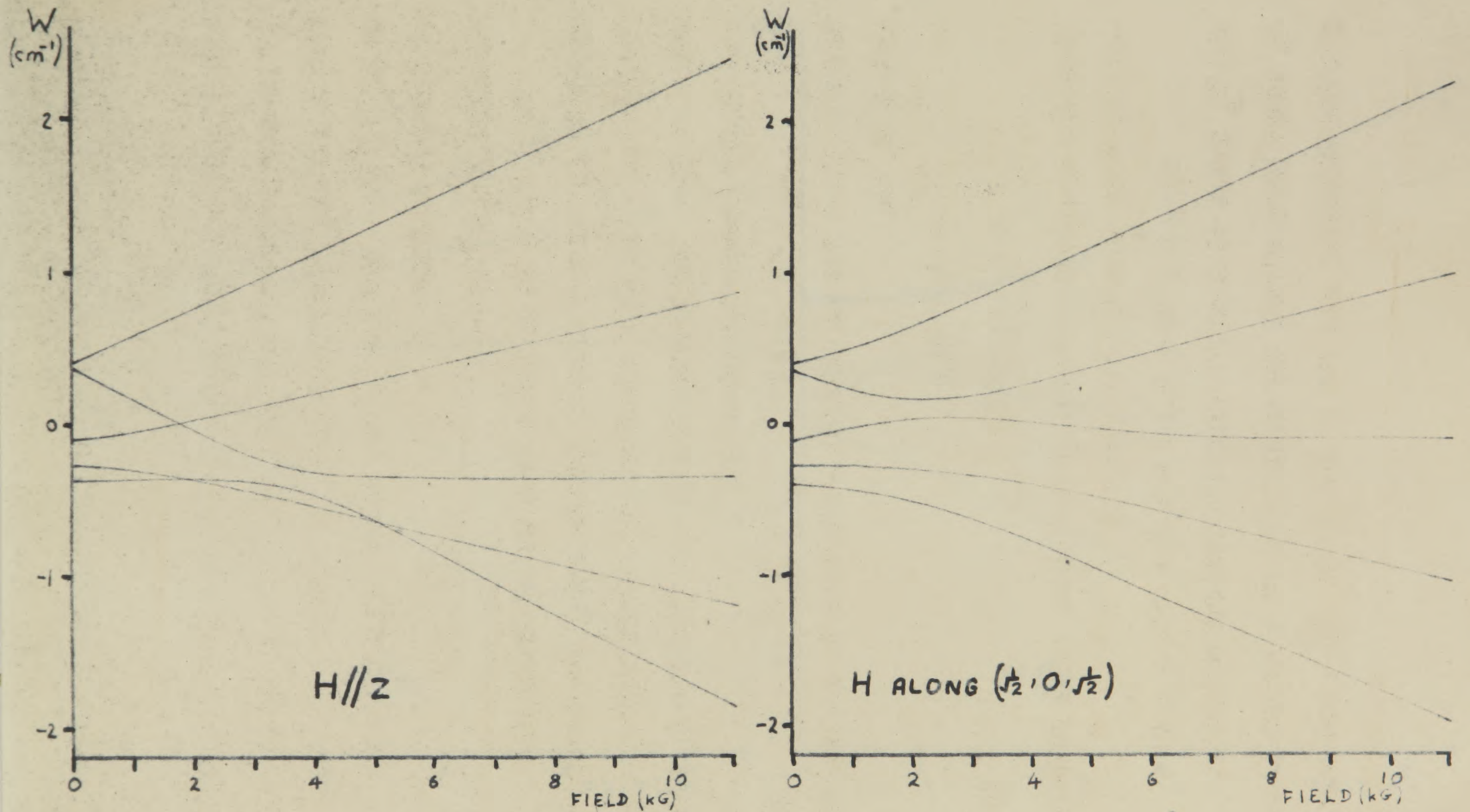


FIG. 6B. MN:MGO, S=2 ENERY LEVELS. ASSUMING: $D_2 = \cdot 182\ cm^{-1}$, $E_2 = \cdot 035\ cm^{-1}$, $g = 2$.

directions it is more difficult. For this reason a computer programme was made to calculate the energy levels for any field direction, and for all S values up to S = 5. S=2 levels are shown for some field directions in fig6.

Spectrum for $g_\parallel > g_\perp$.

When $H \parallel z$ it is quite easy to calculate the spectrum for high S states without using the computer programme. The only off-diagonal matrix elements are those in H_3. Neglecting these, and also the P_3 terms the energy levels are given by,

$$W_M = GS_z + D_3M^3 \qquad (23)$$

The condition for an allowed transition to occur, with $\Delta M = \pm 1$, is,

$$h\nu = W_M - W_{M-1}$$

$$= G + D_3(3M^2-1) \qquad (24)$$

Thus the spectrum consists of 2S lines, split from the main line at $h\nu = G$, by amounts,

$$3S - 1 \ , \ 3S - 3 \ , \ \ldots \ 3 - 3S \ , \ 1 - 3S \ .$$

The P_3 terms will alter these splittings slightly. H_3 terms only affect the splittings as a second order perturbation, by amounts of the order $\frac{E^2}{G}$, and except

at very low fields, this second order perturbation is a good enough approximation

Hyperfine Structure

The hyperfine term in the Hamiltonian is,

$$\mathcal{H} = A (\underline{g}_1 \cdot \underline{I}_1 + \underline{g}_2 \cdot \underline{I}_2) \qquad (25)$$

where for manganese, $I_1 = I_2 = \frac{5}{2}$. This may be written,

$$\mathcal{H} = \frac{A}{2}(\underline{g}_1+\underline{g}_2)\cdot(\underline{I}_1+\underline{I}_2) + \frac{A}{2}(\underline{g}_1-\underline{g}_2)\cdot(\underline{I}_1-\underline{I}_2) \qquad (26)$$

The second term gives off-diagonal matrix elements, which affect the energy levels by the order of $\frac{A^2}{\gamma}$, which is negligible. The first term moves the energy levels by an amount,

$$\Delta W = \frac{A}{2} M (I_1 + I_2) \qquad (27)$$

and for the observed transitions, $\Delta M = 1$, $\Delta I = 0$, so the resonance lines will be moved by an amount,

$$\Delta = \frac{A}{2} (I_1 + I_2). \qquad (28)$$

$I_1 + I_2$ can take eleven different values, from -5 to +5, so the resonance lines will have an eleven line hyperfine structure. The components will have intensities in the ratio, 1:5:5:4:5:6:5:4:5:5:1, corresponding to the number of different ways in which each value of $I_1 + I_2$ can be formed. The spacing between the lines

will be $\frac{A}{g} \approx 40$ gauss, half the spacing of the main line hyperfine structure. The presence of this structure provides good evidence for the identification of pair lines.

3.3 Experimental Work

The present series of experiments was carried out using a wavelength of 0.85 cm (Q band). The earlier series used a wavelength of 1.23 cm (K band) and some of the measurements made then have also been found useful. The measurements have been of two types.

(i) The measurement of the positions of the pair lines, and their variation with field direction.

(ii) The variation of the relative intensities of the lines from different S states with temperature.

The paramagnetic resonance spectrum is dominated by the very intense isotropic line with a 6 component hyperfine structure due to isolated Mn^{++} ions which occurs at $g = 2$. There is also a weak isotropic line at $g = 4$, which can be ascribed to forbidden transitions from isolated ions, with a small transition probability, possibly due to weak interactions with remote neighbours. The width of this half-field line is consistent with that

expected from Mn^{++} ions, but the hyperfine structure cannot be resolved.

The pair spectrum consists of a large number of much weaker anisotropic lines centred on the main line. Many of these show the eleven component hyperfine structure expected for pair lines (see fig 11). The concentration of these lines is very great near to the main line, the overall width of each line is large, about 400 gauss, and some of their positions change very quickly with field direction. In addition to the n.n. pair lines, there are also lines due to n.n.n. pairs, which lie closer to the main line because the n.n.n. interaction is less anisotropic than the n.n. interaction. These factors make it very difficult to identify lines near to the main line, and even more difficult to estimate their intensities because they overlap to such a large extent. For this reason all the measurements were made on lines whose splittings from the main line was quite large.

Anisotropy Measurments

The spectrum was drawn out on a pen recorder as the magnetic field was swept from zero up to the main line (12.5 kG at Q band, 8 kG at K band). The

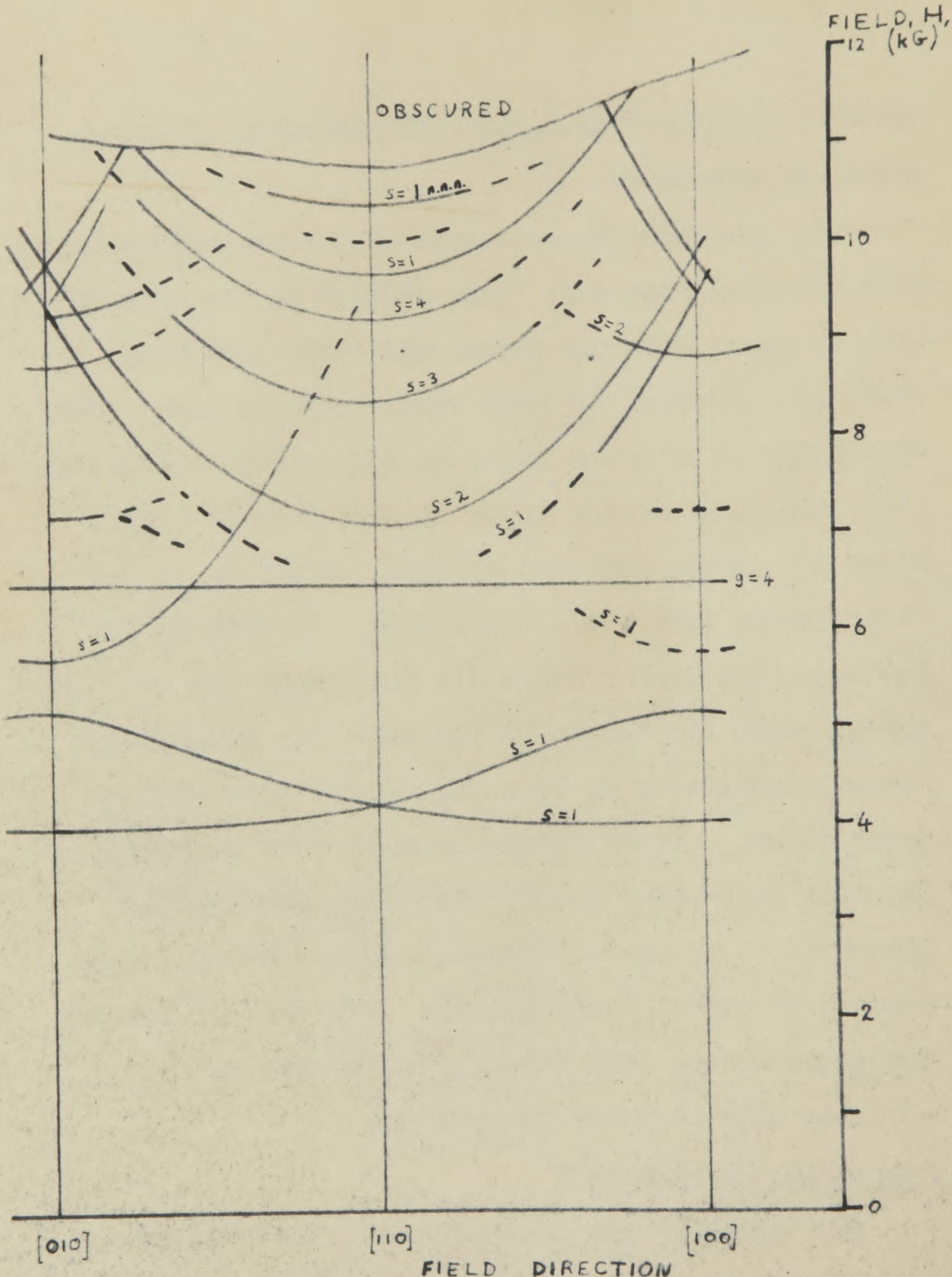


FIG. 7. MN:MgO, OBSERVED PAIR SPECTRUM.

Q BAND, 77°K, (001) PLANE

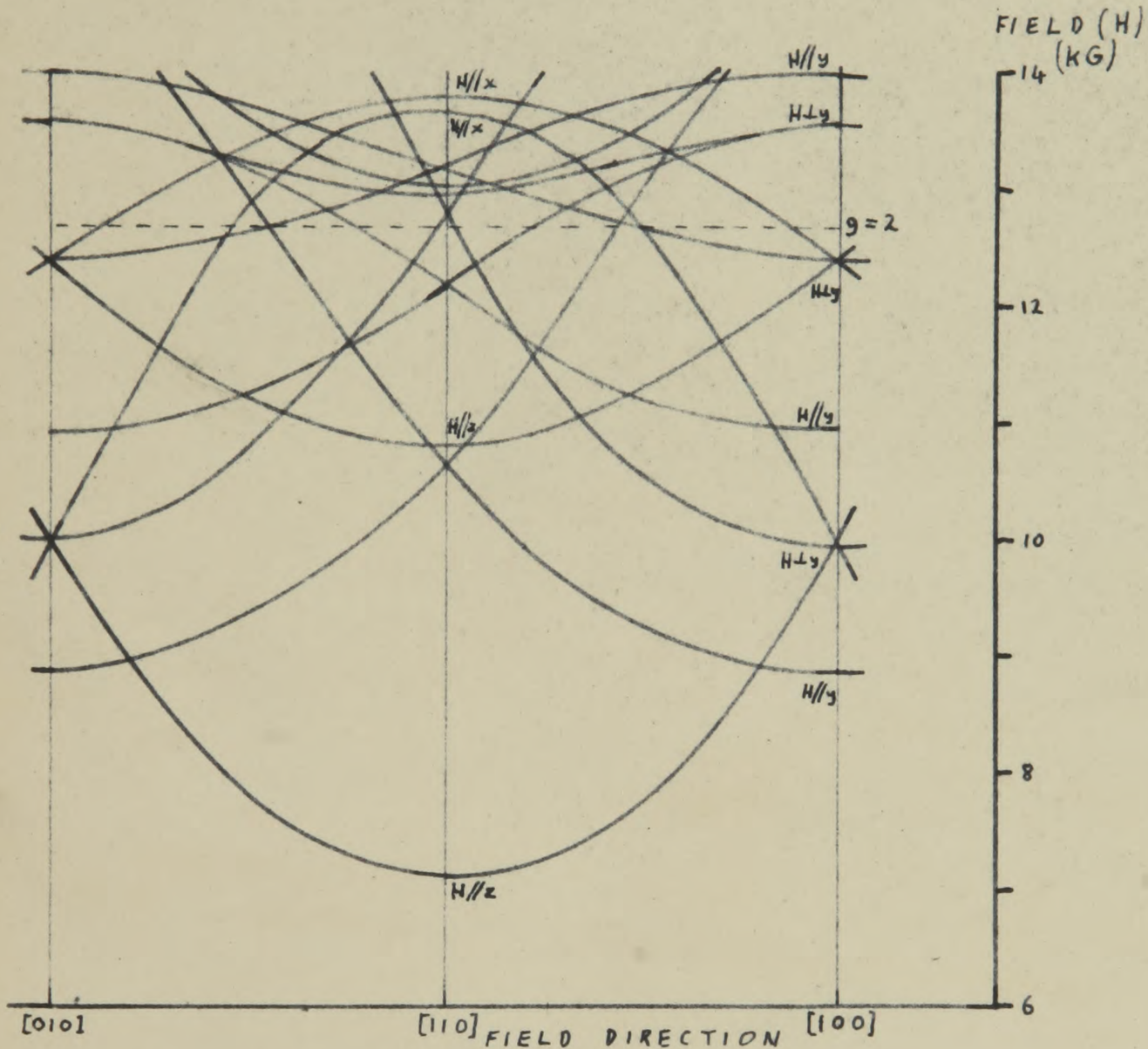


FIG. 8. $Mn:MgO$, $S = 2$ PAIR SPECTRUM

PREDICTED FOR ROTATION IN A (001) PLANE,

ASSUMING: $\nu = 1{\cdot}18\ cm^{-1}$, $D_2 = 0{\cdot}182\ cm^{-1}$, $E_2 = 0{\cdot}035\ cm^{-1}$, $g = 2$.

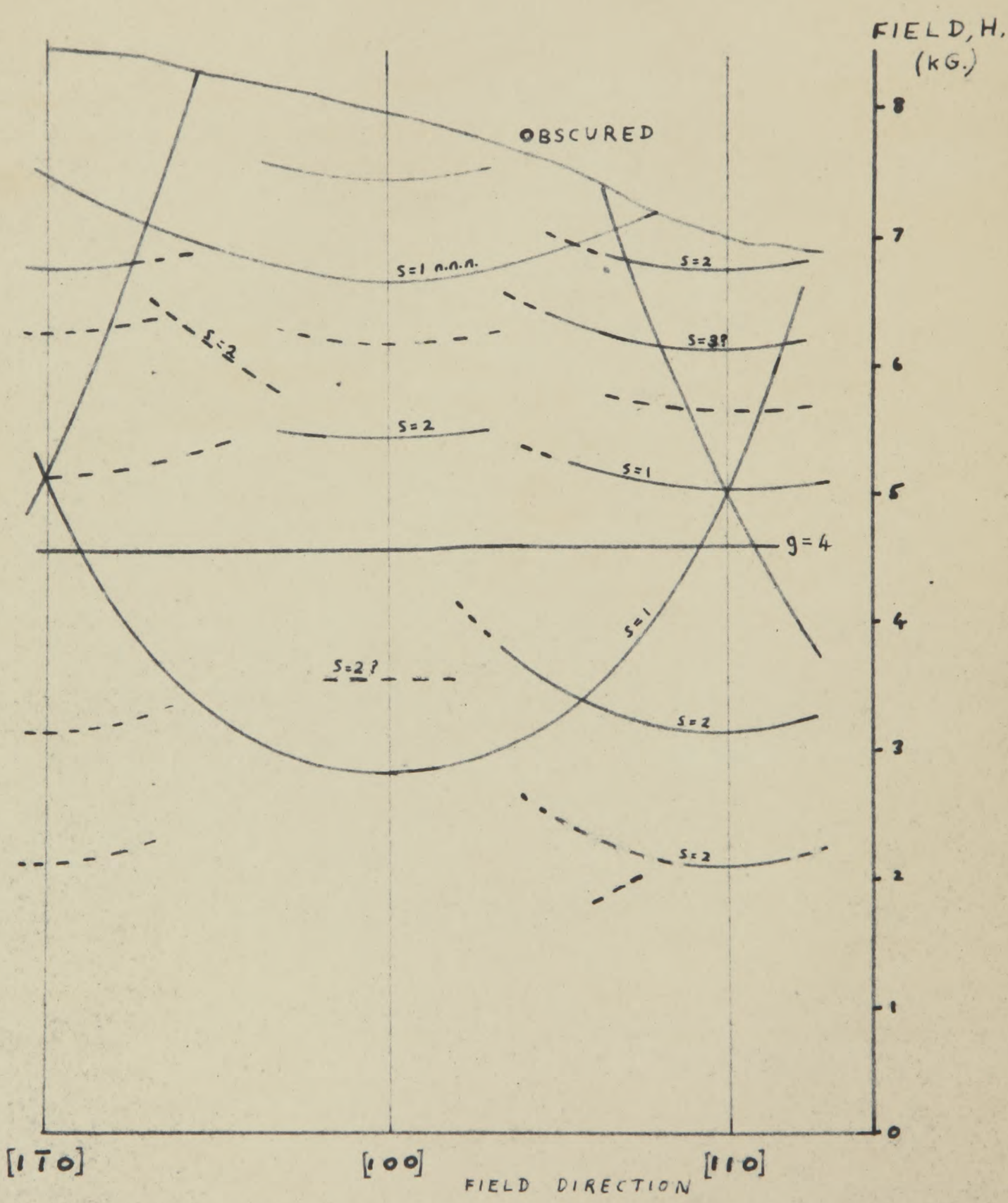


FIG. 9. MN:MGO, OBSERVED PAIR SPECTRUM.

K BAND, 77°K, (001) PLANE

(FROM CHARTS OF B.A. COLES)

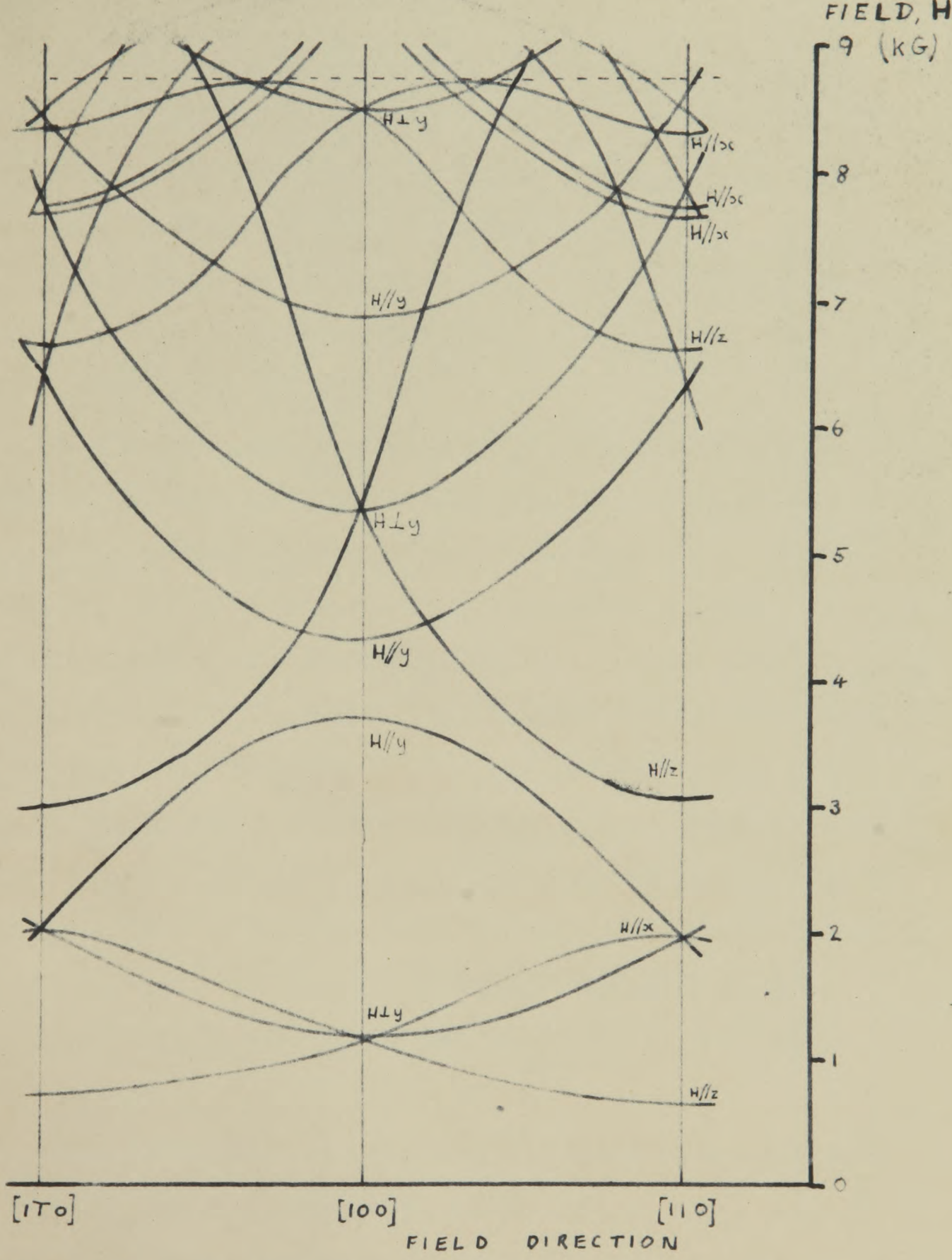


FIG.10. MN:MgO, S=2 PAIR SPECTRUM.

PREDICTED FOR ROTATION IN A (001) PLANE,

(ASSUMING: $D = 0.916\ cm^{-1}$, $D_2 = 0.182\ cm^{-1}$, $E_2 = 0.035\ cm^{-1}$, $g = 2$.

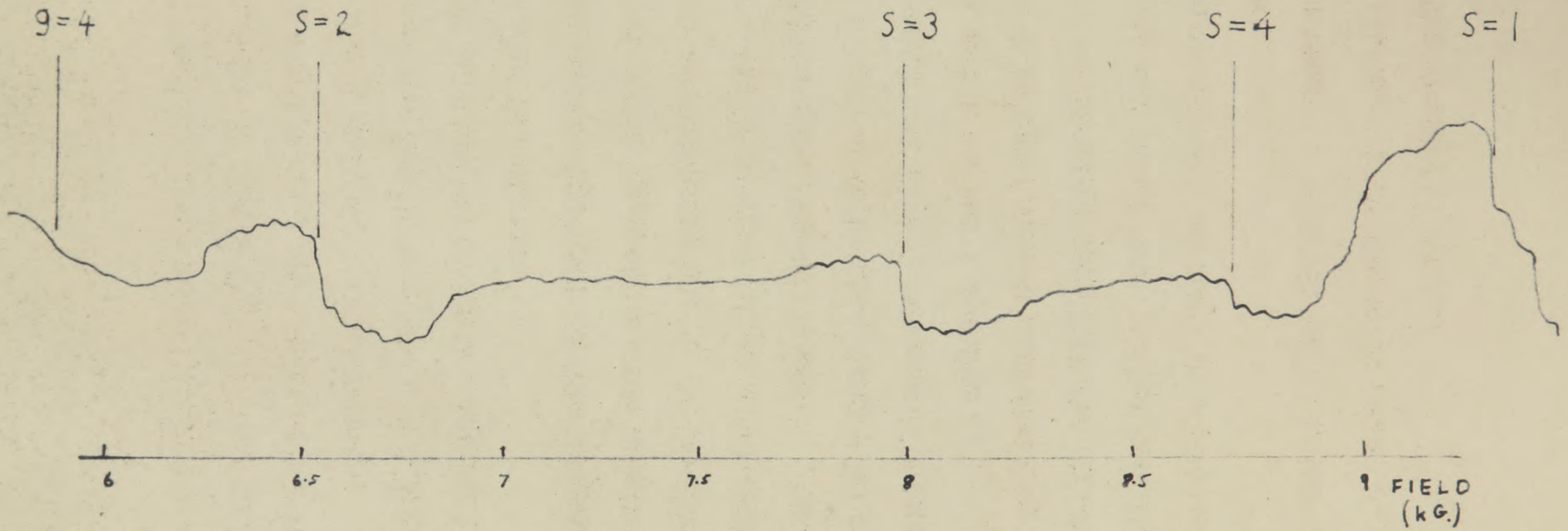


FIG. 11. MN:MgO, PART OF THE PAIR SPECTRUM AT Q BAND.

THIS PEN RECORDING WAS MADE AT 77° K, WITH THE MAGNETIC FIELD IN A [110] DIRECTION. IT SHOWS S=2,3,4 LINES WITH MN PAIR H.F.S.

magnetic field was rotated about the crystal in a (100) plane at intervals of about 5°. The anisotropy diagrams made from these recordings at X band and K band at 77°K are shown in fig 7 and fig 9 respectively.

The parameters describing the S = 1 spectrum were known from the earlier experiments, and so the S = 1 lines were easily identified.

It was expected that most of the transitions from higher S states would be grouped much closer to the main line, and consequently harder to observe. The splitting from the main line is greatest with the magnetic field parallel to the z axis. Lines were observed at X band with turning values in this direction which were identified as the outermost transitions from the S = 2, 3, and 4 states (see fig 11). They were identified in this way because they had the eleven line pair hyperfine structure, they did not fit into the S = 1 spectrum, and their intensities had different temperature dependences, as will be considered in the next section.

At a frequency ν = 1.165 cm^{-1}, these line positions and their splittings from the main line, Δ, were found to be as in the following table.

S	Observed line Position (kG)	Δ (cm^{-1})
2	6.660	0.542
3	7.990	0.418
4	8.735	0.349

These splittings are almost independent of E_s, as was pointed out earlier, the contribution from E_2 to Δ_2 being given by,

$$\Delta_2 = \frac{6E^2}{20+4D-\frac{16}{7}F} - \frac{2E^2}{20} \approx -0.004\ cm^{-1} \qquad (29)$$

Similarly, $\Delta_3 \approx \Delta_4 \approx -0.001\ cm^{-1}$

After applying these corrections, values for D_c, D_c, and F_c can be found from the relations,

$$\Delta_2 = 0.546 = 3D_2 + 60F_2 = \frac{123}{14} D_c - \frac{60}{21} D_c + \frac{900}{7} F_c$$

$$\Delta_3 = 0.419 = 5D_3 + 600F_3 = \frac{47}{6} D_c - \frac{5}{9} D_c - 200F_c$$

$$\Delta_4 = 0.350 = 7D_4 + 2100F_4 = \frac{15}{2} D_c + 5D_c - 300F_c$$

To this we may also add the relation,

$$D_1 = 0.776 = \frac{111}{10} D_c - \frac{32}{5} D_c$$

From these equations, the best values for the parameters are,

$$D_0 = 0.054 \pm .0015 \quad cm^{-1}$$

$$D_2 = 0.055 \pm .0015 \quad cm^{-1}$$

$$F_2 = 0.00003 \pm .00010 \quad cm^{-1}$$

Since theseffect of F_2 is negligible, these measurements also give,

$$D_2 = \frac{\Delta^2}{5} = 0.182 \pm .003 \quad cm^{-1}$$

$$D_3 = \frac{\Delta^3}{5} = 0.084 \pm .001 \quad cm^{-1}$$

$$D_4 = \frac{\Delta^4}{7} = 0.050 \pm .001 \quad cm^{-1}$$

No other lines from the S = 3 or S = 4 states could be identified, but the S = 2 lines were observed at several places, both at K band and at Q band. These line positions were fitted to the parameters,

$$D_2 = 0.182 \pm .005 \quad cm^{-1}$$

$$B_2 = 0.035 \pm .010 \quad cm^{-1}$$

$$F_2 = 0.000 \pm .001 \quad cm^{-1}$$

The theoretical spectra with these parameters are shown in figs 8 and 10. Measurements of line positions were carried out at several places, and these are listed in the following table.

Crystal direction	Observed position (gauss)	Pair direction	States	Calculated position (gauss)
K band, $\nu = 0.816\ cm^{-1}$				
110	3040	$\frac{1}{2}\ \frac{1}{\sqrt{2}}\ \frac{1}{2}$	2, -1	3040
110	5130	0 0 1	2, 1	3060
110	6700	0 0 1	0, 1	6850
100	8460	$\frac{1}{\sqrt{2}}\ 0\ \frac{1}{\sqrt{2}}$	2, 1	8380
Q band, $\nu = 1.165\ cm^{-1}$				
110	6660	0 0 1	2, 1	6660
$\nu = 1.188\ cm^{-1}$				
100	9760	$\frac{1}{\sqrt{2}}\ 0\ \frac{1}{\sqrt{2}}$	2, 1	9700
100	8730	0 1 0	-1,-2	8700

Intensity Measurements

The intensity of a resonance line is proportional to the difference in population of the energy levels concerned. The population of a given level with energy E_i is proportional to,

$$\frac{g^{-E/kT}}{Z}$$

where Z is the total partition function for the system,

$$Z = \sum_i g^{-E_i/kT} \qquad (30)$$

If the energy levels are spaced according to a Lande interval rule, i.e. $j = 0$,

$$Z = 1 + 3g^{-J/kT} + 5g^{-3J/kT} + 7g^{-6J/kT} + 9g^{-10J/kT} + 11\,g^{-15J/kT} \qquad (31)$$

For a transition occuring between two energy levels with energies, E, and $E + h\nu$, the intensity will be,

$$I \propto \frac{g^{-E/kT} - g^{-(E+h\nu)/kT}}{Z}$$

$$\propto (1 - g^{-h\nu/kT}) \cdot \frac{g^{-E/kT}}{Z} \qquad (32)$$

The ratio of the intensities of two lines from the same scheme of energy levels is given by,

$$\frac{I_1}{I_2} = \frac{P_1}{P_2} \cdot g^{(E_2 - E_1)/kT} \qquad (33)$$

where P_1 and P_2 are the transition probabilities for the two lines.

In the previous series of experiments, the temperature variation of the intensity of S = 1 lines was found by comparison with lines from other crystals, $Na_3Ir_2PtCl_6 \cdot 6H_2O$, and $Ni_2Zn(NH_4)_2(SO_4)_2 \cdot 6H_2O$. Comparisons were also made of the S = 1 lines against an S = 2 line.

In the present experiments, the S = 1 lines have again been compared with a line from another substance, this time a pair line in $(NH_4)_3Ir_2PtCl_6$. Comparisons have also been made between lines from S = 1, 2, 3, and 4 states.

The choice of a suitable comparison substance has been discussed in chapter 2. The most important factors are that the comparison line should be clear of any others, that its temperature variation should be known well, that it should not saturate or broaden too much in the range of temperature used. It is convenient if the comparison line is chosen so as to lie near to the other line, and that its width should be of the same order of magnitude. The $(NH_4)_3Ir_2PtCl_6$ pair lines fulfill all these conditions. Their temperature variation is given by,

$$I \propto (1 - e^{-h/kT}) \cdot \frac{e^{-J'/kT}}{1 + 3e^{-J'/kT}} \qquad (34)$$

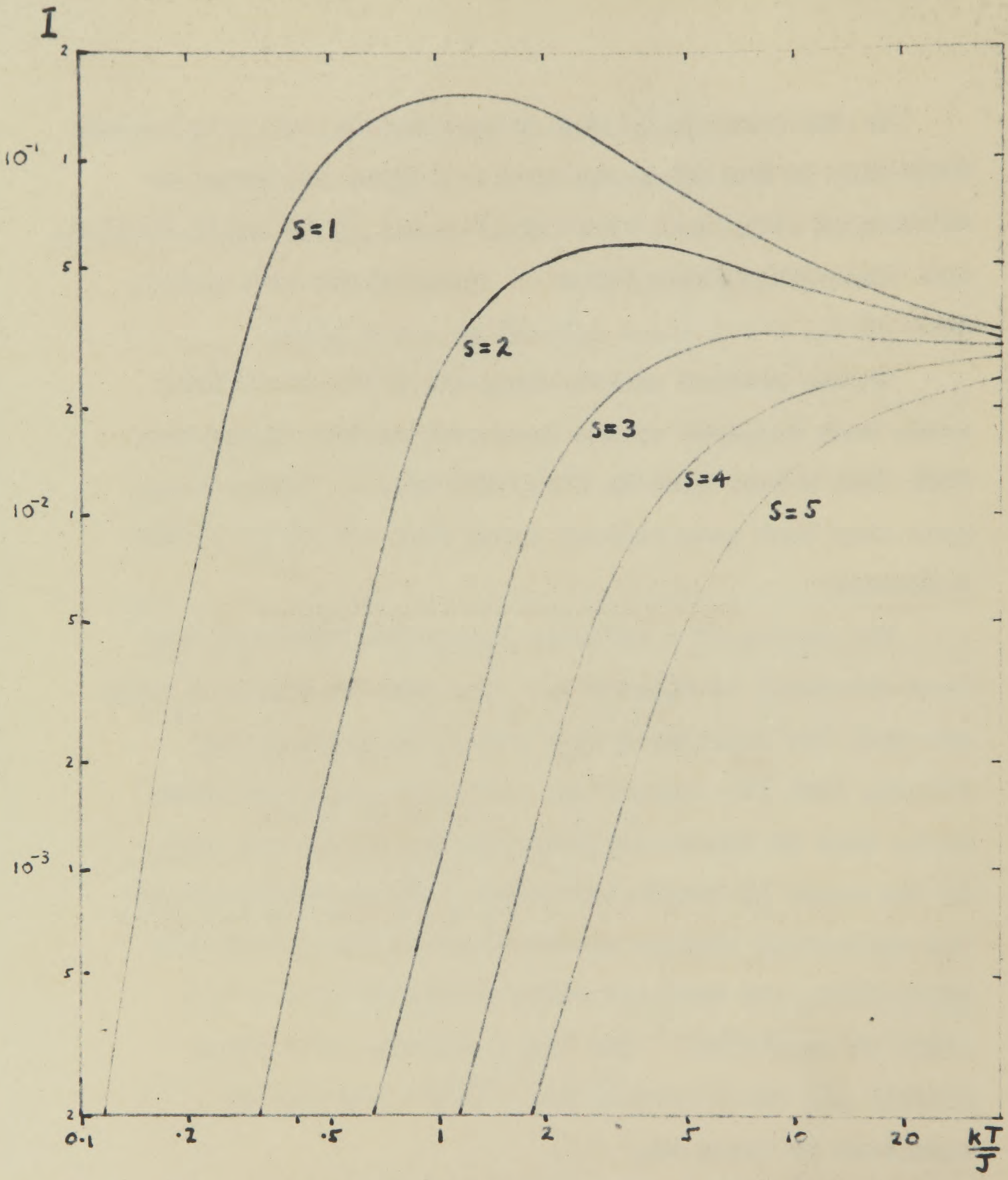


FIG. 12. RELATIVE INTENSITIES OF TRANSITIONS FROM DIFFERENT S STATES, ASSUMING LANDÉ INTERVALS.

In this expression, $\frac{J'}{k} = 7.5 \pm 1$ °K, (see chapter 4). This large error in $\frac{J'}{k}$ introduces a possible error of only about 3 % in the determination of $\frac{J}{k}$ for Mn, which is well within the error expected from other sources.

Comparisons of the intensities of the two lines were made at three temperatures, 20 °K, 14 °K, and 4.2°K, and with the crystal in two different positions.

Temperature (°K)	Observed ratio, I_{Ir} / I_{Mn}.	
	1st expt.	2nd expt.
20	0.109 ± 5%	1.47 ± 4%
14	0.145 ± 5%	2.20 ± 5%
4.2	-	50.0 ± 50%

For the comparison Ir pair line, the change of intensity with temperature is,

$$\frac{I_{20}}{I_{14}} = 1.06 \pm 5\%$$

$$\frac{I_{20}}{I_{4.2}} = 1.94 \pm 10\%$$

If these results are fitted to the curves given in fig 13, for states spaced with Lande intervals, a value

for J can be deduced. Higher order exchange terms change the intervals, but at temperatures below about 20°K, the shape of the S = 1 curve is practically unchanged. The J value deduced from the Lande interval curves, however, is really a measure of the energy splitting between the S = 0 and S = 1 levels, W_{01}.

The above measurements give,

1st expt. $\frac{I_{21}}{I_{10}} = 1.40 \pm 6\%$ $W_{01} = 33 \pm 2$ °K

2nd expt. $\frac{I_{21}}{I_{10}} = 1.54 \pm 9\%$ $W_{01} = 30 \pm 2$ °K

$\frac{I_{21}}{I_{10}} = 65 \pm 60\%$ $W_{01} = 26 \pm 4$ °K

Mean value: $W_{01} = 28.5 \pm 2$°K.

This result is in good agreement with the earlier measurements of Coles.

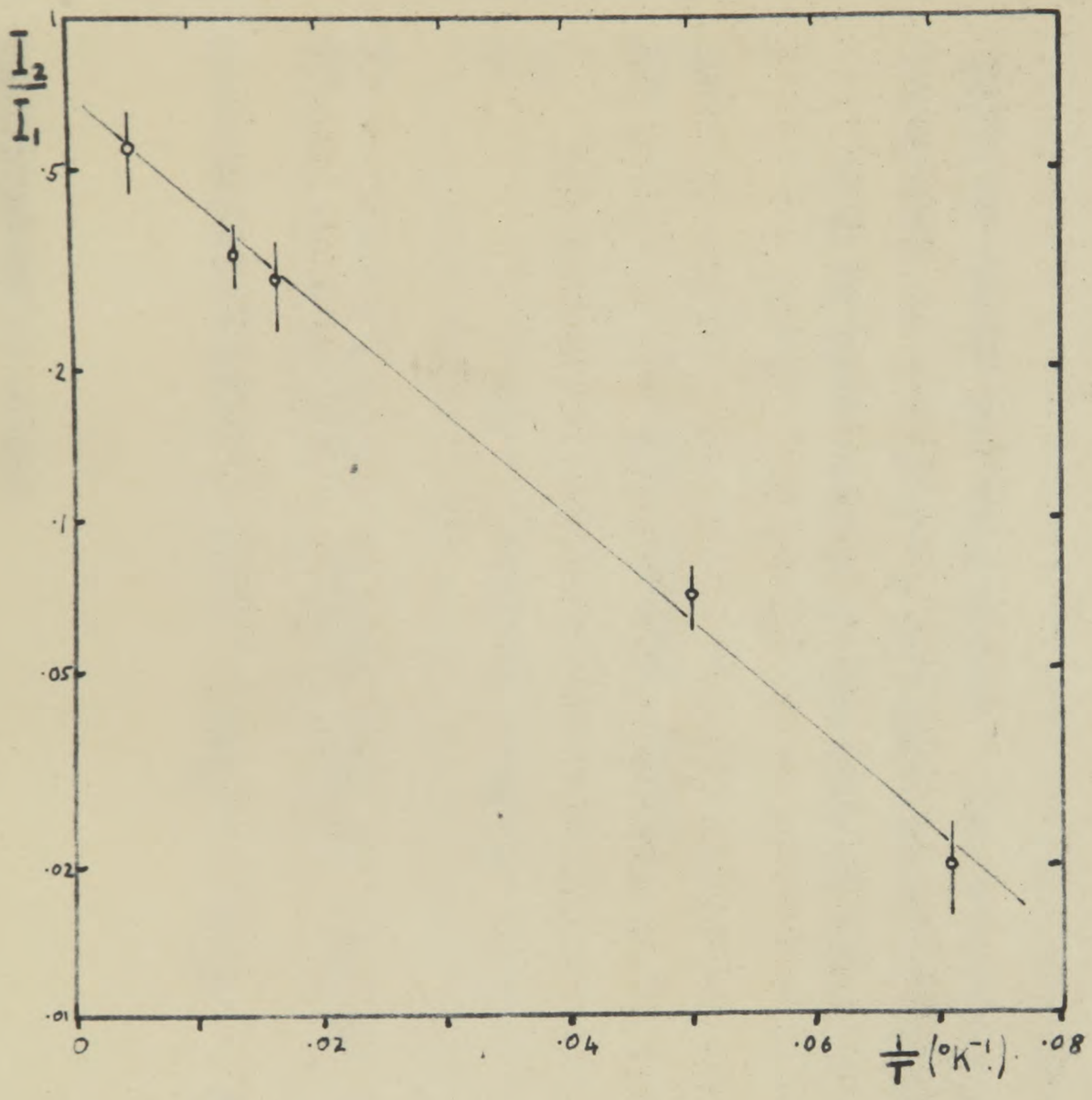
Comparisons of the relative intensities of the lines from S = 1, 2, 3, and 4 states were made at 200°, 77°, 63°, 20°, and 14°K. The results of these measurements are given in the table which follows.

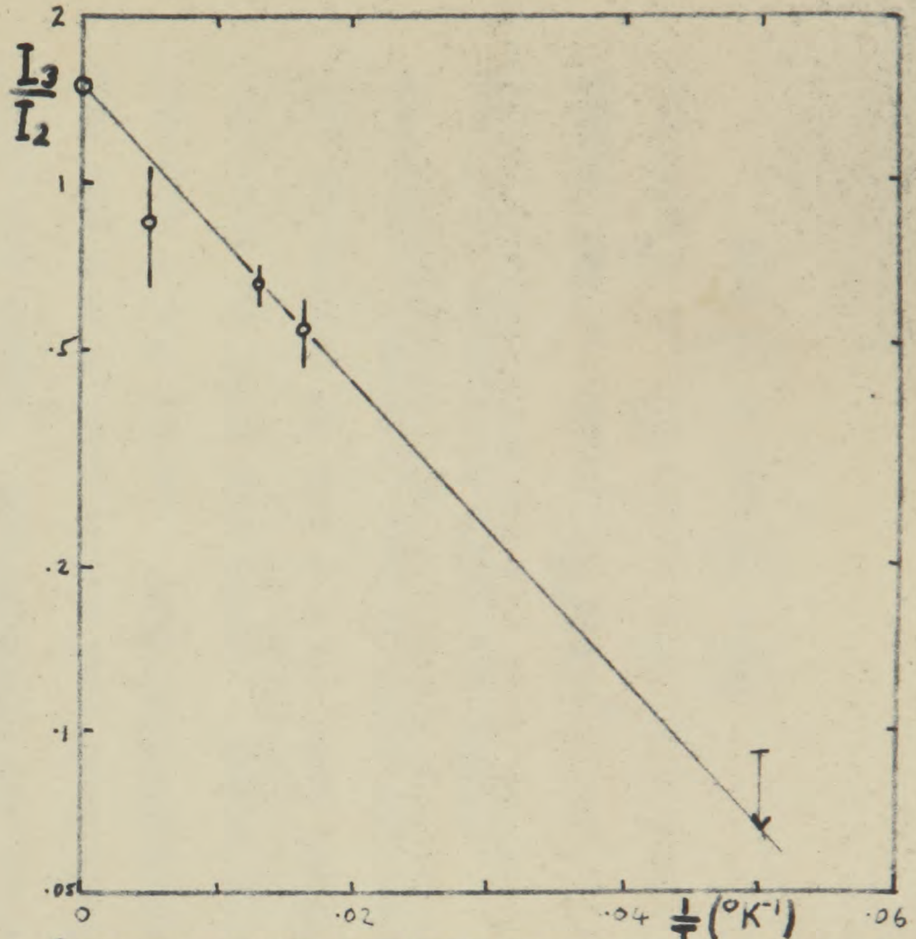
Temperature:	300°K	77°K	63°K	30°K	14°K
$\frac{I_2}{I_1}$	.55 ±.1	.34±.03	.30±.06	.07±.01	.02±.004
$\frac{I_3}{I_0}$	.85±.2	.65±.05	.54±.07	<.03	-
$\frac{I_2}{I_3}$	.70 ±.2	.54±.05	.43±.07	-	-

Each of these ratios is the mean of about 10 pen recordings of each line. The line shapes were integrated twice to obtain the intensities. The measurements at 300°K had a large scatter on them because the noise level was high. The scatter was particularly great for the δ = 4 line which lay very close to a much more intense δ = 1 line. The most reliable numbers were obtained at 77°K and 63°K. Below this temperature the intensity of the δ = 4 line rapidly became indistinguishable, and at 30°K the δ=3 line could only just be separated from the noise.

Since $\frac{I_1}{I_0} = \frac{P_1}{P_0} e^{-\Delta E/kT}$,

$$\log \frac{I_1'}{I_0'} = \log \frac{P_1'}{P_0'} - \frac{\Delta E}{kT} \qquad (35)$$





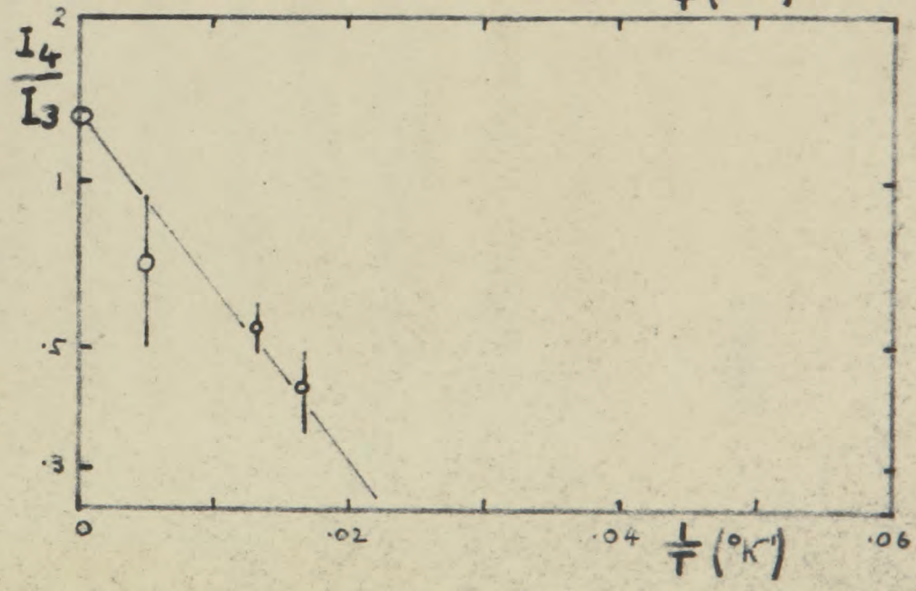


FIG. 13. EXPERIMENTAL INTENSITY VARIATIONS FOR S = 1, 2, 3, 4, LINES.

In fig 13, $\log_e \frac{I_2}{I_1}$, $\log_e \frac{I_3}{I_2}$, and $\log_e \frac{I_4}{I_3}$, are plotted against $\frac{1}{T}$. When $\frac{1}{T} = 0$,

$$\left(\frac{I_a}{I_b}\right)_o = \frac{P_a}{P_b} \qquad (36)$$

The transition probabilities were calculated for the S = 2, 3, and 4 lines, and were found to be proportional to 2, 3, and 4, respectively, so the intercepts when $\frac{1}{T} = 0$ for the $\frac{I_3}{I_2}$ and the $\frac{I_4}{I_3}$ lines are known to be 1.5 and 1.33 respectively. The gradients of these lines give the energy splitting between the states. These are found to be,

$$\frac{W_{23}}{k} = 49 \pm 4 \text{ °K.}$$

$$\frac{W_{34}}{k} = 64 \pm 6 \text{ °K.}$$

$$\frac{W_{45}}{k} = 70 \pm 12 \text{ °K.}$$

Although the experimental errors are quite large, the measurements indicate that the simple Lande interval rule is not obeyed. A much better fit may be obtained assuming a second order exchange term, so that,

$$\mathcal{H} = J(\underline{s}_1 \cdot \underline{s}_2) - j(\underline{s}_1 \cdot \underline{s}_2)^2 \qquad (37)$$

Values for $\frac{j}{J}$ from .02 to .09 are covered by the experimental errors, but the best agreement is obtained with the ratio,

$$\frac{j}{J} = .06$$

giving the parameters,

$$\frac{J}{k} = 15 \text{ °K.}$$

$$\frac{j}{k} = 0.75 \text{ °K.}$$

The measured intervals are compared with theory in the table below.

Measured Interval	Experimental Energy (°K)	Theoretical Interval	Calculated $\frac{J}{k}=15°, \frac{j}{k}=.75°K$
W_{10}	28.5 ± 2	$J + 16.5j$	27.4
$\frac{1}{2}xW_{21}$	24.5 ± 2	$J + 13.5j$	25.1
$\frac{1}{2}xW_{32}$	21.0 ± 2	$J + 6.5j$	21.4
$\frac{1}{2}xW_{43}$	17.5 ± 2	$J + 1.5j$	16.1

5. A Discussion of results

The Anisotropic Interaction

The anisotropic interaction parameters have been determined as follows,

S	1	2	3	4
$D_0(cm^{-1})$	0.776	0.192	0.634	0.060
$E_0(cm^{-1})$	0.149	0.035	-	-

These may be interpreted in the form,

$D_0 = .054 \pm .0025\ cm^{-1}$ $E_0 = 0.030 \pm .020\ cm^{-1}$

$D_c = -.035 \pm .0015\ cm^{-1}$ $E_c = -0.006 \pm .015\ cm^{-1}$.

The value for D_c may be compared with a point dipole value of $0.000\ cm^{-1}$, corresponding to a lattice spacing midway between that in MnO and MgO. The small difference could be due to anisotropic exchange. The large experimental error in E_0 makes it impossible to deduce whether the E term arises principally from anisotropic exchange or from crystal field distortion. The measurements suggest that it is more probably the

former, although only a small anisotropic exchange is expected theoretically. The expression $(g - 2)^2 J$ gives about 0.001 cm^{-1} for anisotropic exchange.

An effect which could alter the interpretation of these parameters might arise as a result of a balance between elastic and exchange forces. Since the isotropic exchange interaction is a rapidly varying function of ionic separation, there is a repulsive force acting between the ions of a pair, which will give rise to a small distortion until it is balanced by elastic forces.

If K is an elastic constant, and if the ion separation, a_0, is changed by an amount Δa,

$$K \frac{\Delta a}{a_0} = -\frac{\partial J}{\partial a} (\underline{s}_1 \cdot \underline{s}_2) \qquad (38)$$

Putting $J = J_0 a^{-n}$, and $\underline{s}_1 + \underline{s}_2 = \underline{S}$

$$K \frac{\Delta a}{a_0} = \frac{nJ}{a_0} \cdot \frac{1}{2}\{ S(S+1) - \frac{3n}{2} \} \qquad (39)$$

Putting in the elastic constant for MgO, and assuming $n = 10$, then the change in Δa between the $S = 1$ and $S = 4$ states is,

$$\frac{\Delta a_4 - \Delta a_1}{a_0} \approx 6 \times 10^{-3}$$

The magnetic dipolar term, D_c, is proportional to a^{-3}, so over this range the variation of D_c is likely to be,

$$\frac{\Delta D}{D_c} = 2\ \%\ .$$

The possible error in the present estimate of De would be rather greater than this, possibly about 3%, which would make it agree rather more closely with the point dipole value.

Isotropic Exchange

The energy splittings between the different spin states have been determined as follows, (in °K.),

	W_0:	$\frac{1}{2} W_{ab}$	$\frac{1}{2} W_{ac}$	$\frac{1}{2} W_{ad}$
Present Measurements	28.5 ±2	24.5 ± 2	21.0 ± 2	17.5±3
Earlier Measurements (Coles, 1953)	26.0 ±3	24.5 ±1	-	-

These quantities have been interpreted as due to a first order isotropic exchange, $\frac{J}{k} = 15°K$, and a second order exchange, $j = .05J$.

The presence of a comparatively large biquadratic isotropic exchange does not seem to be inconsistent with

current theories of superexchange (Anderson 1950, 1963, Moriya, 1960). These theories predict $\frac{J}{j} \approx .01$, although in a private communication, Anderson has suggested that values up to $\frac{J}{j} = 0.1$ could be possible.

Another mechanism for an effective biquadratic exchange is due to the elastic distortion mentioned earlier (Kittel, 1960, Penn and Redfield, 1962). Using the same notation as before, the total energy of an ion is the sum of the exchange energy and the elastic energy.

$$E = Jg_1 \cdot g_2 - \frac{K}{2a_0}(\Delta a)^2 \qquad (40)$$

$$\text{but} \quad (g_1 \cdot g_2)\frac{\partial J}{\partial a} = -\frac{K}{a_0}\Delta a \qquad (41)$$

$$\therefore E = Jg_1 \cdot g_2 - \frac{a_0}{2K}\left(\frac{\partial J}{\partial a}\right)^2 (g_1 \cdot g_2)^2 \qquad (42)$$

$$= Jg_1 \cdot g_2 - \frac{a_0^2 J'^2}{2Ka_0}(g_1 \cdot g_2)^2 \qquad (43)$$

Using the elastic constant and lattice parameters for MgO, a value $\frac{J}{j} = .05$ would require $n \approx 50$. This is much larger than seems likely, so it appears that the second order exchange arises through Anderson's mechanism, with possibly a small contribution from the elastic effect. A combination of the two effects would also give rise to a third order term.

The Bulk Magnetic Properties of MnO

According to Anderson, the first order term of the isotropic exchange is proportional to (overlap)^2, whereas the second order term is proportional to (overlap)^8. In the concentrated MnO crystal, the lattice parameters are greater than for MgO, so the overlap may be expected to be less. This means that if J is reduced by a factor a in going from the pair to the concentrated crystal, then j may be expected to be reduced by a factor a^2, and $\frac{j}{J}$ will be reduced by a factor a.

The bulk magnetic properties of MnO appear to be consistent with parameters,

$$\frac{J}{k} = 11°K. \qquad \frac{j}{J} = .02$$

In general the magnetic properties depend on the n.n.n. exchange interaction as well as the n.n. one. The measurements of Oclea (1960) on the S = 1 states for both types of pair indicated that the two exchange interactions were very nearly equal. In the absence of any more direct evidence for the magnitudes of J_2 and j_2, and in view of the similarity in the mechanisms for the n.n and n.n.n. interactions, it seems reasonable

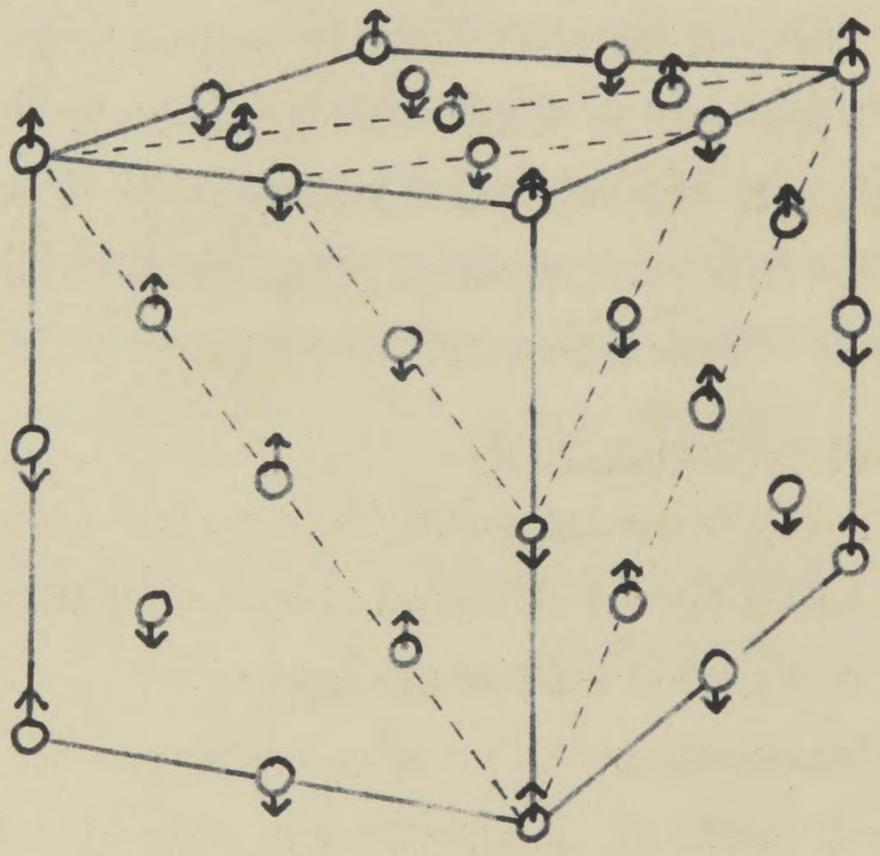


FIG. 14. SPIN ORDERING OF Mn^{++} IONS IN MnO. (TYPE 2 ORDER)

to assume that $J_1 \approx J_2$ and $j_1 \approx j_2$.

The magnetic properties below the transition temperature depend on the type of ordering. In MnO, neutron diffraction experiments by Shull, Strauser, and Wollan (1951) have shown that there is a type 2 order, in which the spins lie in antiparallel sheets in (111) planes. Each spin has all its 6 n.n.n. spins antiparallel, and its 12 n.n. spins are divided with 6 parallel and 6 antiparallel. This arrangement is shown in fig 14.

Sublattice Magnetisation curve

The most direct evidence for biquadratic exchange in MnO is provided by the observed anomalous variation with temperature of the sublattice magnetisation (fig 15a). This can be deduced from the neutron diffraction measurements of Shull et al (1951), and also from the thermal expansion measurements of Foex (1949). Further evidence for the anomalous sublattice magnetisation is provided by the recent antiferromagnetic resonance measurements of Sievers and Tinkham (1963).

The shape of this curve can be explained by assuming a biquadratic exchange with $\frac{j}{J} \approx .02$ (Rodbell, Jacobs, Owen and Harris 1963).

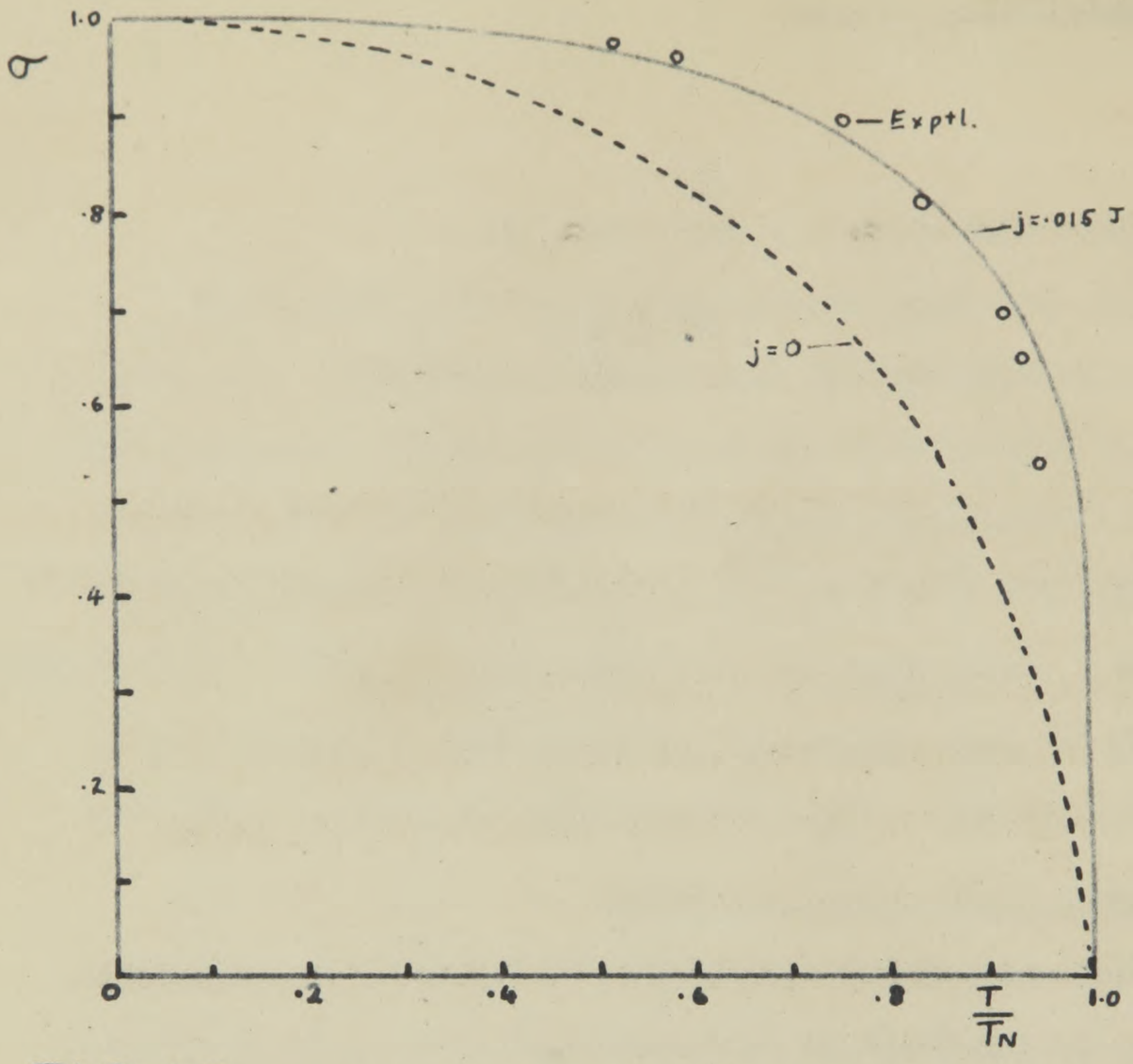


FIG. 15A SUBLATTICE MAGNETIZATION CURVE FOR MnO, COMPARING THEORETICAL CURVE WHEN j = ·015 J WITH RESULTS OF SIEVERS AND TINKHAM (1963)

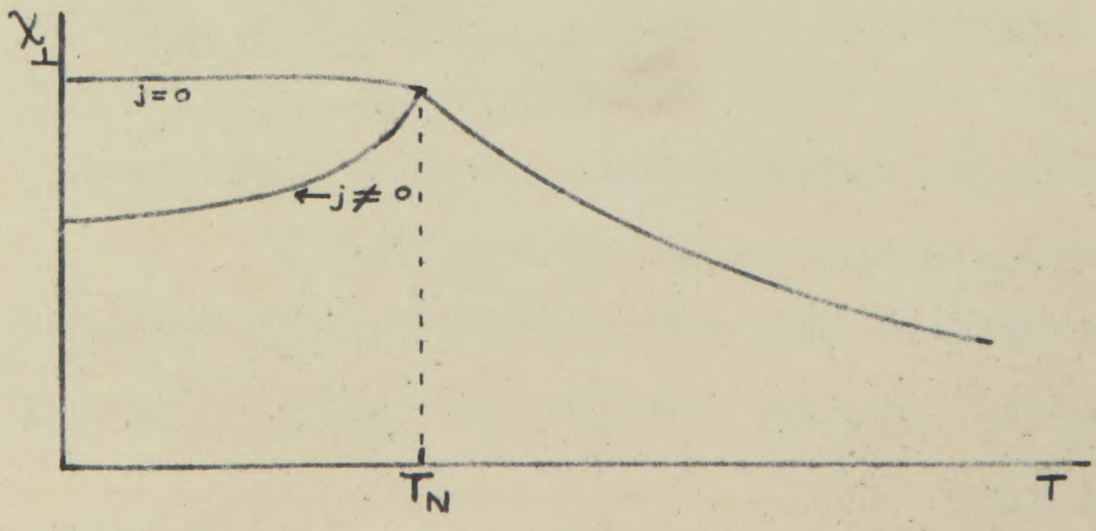


FIG. 15B. THE EFFECT OF A j TERM ON $\chi_\perp$.

(SEE TEXT)

The magnetisation, σ , is given by,

$$\frac{T}{T_N} = F(\sigma)\left(1 + 2\alpha^2\sigma^2 \cdot \frac{2j_1 + j_2}{J_2}\right) \qquad (44)$$

where $F(\sigma)$ generates the usual Brillouin derived curve, equn 1.17. This curve is plotted out in fig 16a.

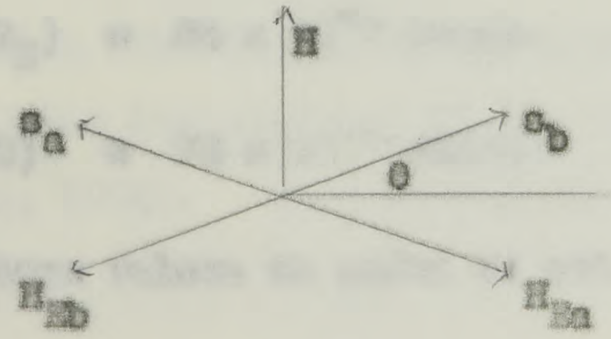
Low Temperature Transverse susceptibility

A biquadratic exchange interaction also predicts an anomaly in the transverse susceptibility, which has been confirmed experimentally.

The effective field, H_E, acting on one sublattice due to the other can be written,

$$g\beta H_E = 6\alpha(J_1 + J_2 + 2\alpha^2\sigma^2 j_1 + 2\alpha^2\sigma^2 j_2) \qquad (45)$$

When a field is applied perpendicular to H_E, the magnetisations turn through an angle θ, such that, $\sin\theta = \frac{H}{H_E}$.



Total Magnetisation, $M = Ng\beta\sigma\sin\theta$ (46)

$$M = \frac{Ng\beta_B - H}{2H_E} \qquad (47)$$

This gives, $\chi_\perp = \frac{M}{H}$

$$= \frac{Ng^2\beta^2}{12(J_1+J_2)} \cdot \left[1 + \frac{2z^2\sigma^2(j_1+j_2)}{J_1+J_2}\right]^{-1} \qquad (48)$$

Although this theory is probably only reliable when $T \gg T_N$, it seems reasonable to suppose that as $T \to T_N$, and $\sigma \to 0$, $\chi_\perp$ will rise by an amount given approximately by,

$$\frac{\chi(T_N)}{\chi_\perp(0)} = 1 + 2z^2\left(\frac{j_1+j_2}{J_1+J_2}\right) \qquad (49)$$

(See fig 15b)

Recent measurements on the transverse susceptibility at low temperatures and at high magnetic fields by Jacobs (private communication), give,

$$\chi(T_N) = 84 \times 10^{-6} \text{ emu/g.}$$

$$\chi(0) = 74 \times 10^{-6} \text{ emu/g.}$$

Substituting these values in equns 48 and 49, we get,

$$\frac{J}{k} = 11.0°K, \qquad \frac{j}{J} = .011$$

assuming that $j_1 = j_2$ and $J_1 = J_2$.

The other bulk properties give no direct evidence for biquadratic exchange, but appear to be in agreement.

Antiferromagnetic Resonance

The condition for antiferromagnetic resonance is approximately,

$$h = g\beta \sqrt{(2H_E H_A)} \qquad (50)$$

Using the anisotropy parameters measured in the present experiments to give the anisotropy field, H_A, and allowing for 3rd and more distant neighbours as dipolar interactions (Lines and ter Haar, 1962), this gives,

$$\frac{J + 12.5j}{k} = 14.5\ ^\circ K.$$

assuming $J_1 = J_2$ and $j_1 = j_2$. With $\frac{j}{J} = .02$, this means $J = 11.6^\circ K$.

High Temperature Susceptibility

In the region 100° to 300°K, the susceptibility obeys a Curie-Weiss law with $\theta = 610^\circ K$, (Bizette, Squire and Tsai, 1938). On molecular field theory this is given by,

$$\theta = (12J_1 + 6J_2)\frac{S(S+1)}{3k} \qquad (51)$$

Putting $J_1 = J_2 = J$, this gives,

$$\frac{J}{k} = 11.6\ ^\circ K.$$

in good agreement with other results.

More recent measurements by Benedicks, Heidelberg and Luxem,(1961) in the temperature range 600 - 1200 °K suggest a rather lower value for θ. This can probably be explained as a result of thermal vibrations which make J apparently increase steadily with temperature (J.Owen, private communication).

The Transition Temperature

The observed transition temperature for MnO is,

$$T_N = 116\ ^\circ K.$$

Molecular field theory is notoriously unreliable in the region of the transition temperature, particularly when applied to the f.c.c. lattice. The observed ratio, $\frac{\theta}{T_N} = 5.25$, has been shown by Lines (1963), using a spin wave method, to be in agreement with the previous result of Coles (1959), $J_1 = J_2$. The effect of second order exchange is hard to estimate, but agreement seems likely if $j_1 \approx j_2$.

Higher Order exchange

Higher order exchange, including terms of the form

$$k(\underline{s}_1 \cdot \underline{s}_2)^3 \ , \ -l(\underline{s}_1 \cdot \underline{s}_2)^4 \ , \ m(\underline{s}_1 \cdot \underline{s}_2)^5$$

are possible on purely symmetry considerations. In view of the surprisingly large value for j, it seems possible that these higher order terms might not be negligible.

The measurements available hardly justify an estimate of the magnitude of the third order exchange, $k(\underline{s}_1 \cdot \underline{s}_2)^3$, but it may be pointed out that if it is assumed,

$$\frac{k}{j} = \frac{1}{3} = .33 \ ,$$

then the pair measurements can be fitted even better than before. Such a third order term would have practically no effect on the bulk properties since it may be assumed to be greatly diminished on changing the lattice parameters. However the ratio $\frac{j(\text{pair})}{j(\text{MnO})}$ would now be much closer to the expected value of $\left[\frac{J(\text{pair})}{J(\text{MnO})}\right]^2 \approx 2$

Biquadratic exchange in other crystals

Measurements on the sublattice magnetisation of NiO (Sievers and Tinkham, 1963) has shown very similar

behaviour to that of MnO. The observed magnetisation curve can be fitted to equn 44 with $\frac{j}{J} \approx .046$. An anomaly in the transverse susceptibility has also been observed by Singer (1956) which is in good agreement with this value. The value of J in NiO is much larger than in MnO, and on the theory of Anderson, the somewhat larger value for $\frac{j}{J}$ is expected as a result of this. In MnF_2, however, where J is much smaller than in MnO, the sublattice magnetisation follows a good Brillouin curve, suggesting that $\frac{j}{J}$ is very small.

Evidence for biquadratic exchange has also been found by Liu, Behrendt, Legvold, and Good, (1960) in Dysprosium, and by Rimai, Statz, Weber, dollars, and Koster (1960) in ruby.

It therefore seems that there is considerable evidence for higher order terms in the exchange interactions between magnetic ions in crystals, and these have important effects on certain magnetic properties. In particular, by posulating a second order exchange in the Mn - O - Mn interaction, all experimental measurements seem to be consistent.

5 . 5 Third Nearest Neighbour Pairs

Any exchange interaction for third nearest neighbour pairs must act through at least two intermediate ions, and so J_3 must be expected to be very much smaller than J_1 and J_2 . The anisotropic interaction expected from the magnetic dipoles should have a value of about,

$$D_0 = .015 \text{ cm}^{-1} .$$

We assume a pair Hamiltonian of the form,

$$\mathcal{H} = g\beta \mathbf{H}\cdot(\mathbf{s}_1+\mathbf{s}_2) + J_3\mathbf{s}_1\cdot\mathbf{s}_2 + D_0(3s_{1z}s_{2z} - \mathbf{s}_1\cdot\mathbf{s}_2) \quad (52)$$

where z is along the direction joining the ions of the pair. There are two cases when the splittings can be found easily.

(1) If $J_3 = D_0$, the Hamiltonian becomes,

$$\mathcal{H} = g\beta \mathbf{H}\cdot(\mathbf{s}_1 + \mathbf{s}_2) + 3D_0 s_{1z}s_{2z} \quad (53)$$

The allowed transition with the maximum splitting from the main line will be that from $|\tfrac{1}{2},-\tfrac{1}{2}\rangle$ to $|\tfrac{5}{2},-\tfrac{5}{2}\rangle$, which has the splitting,

$$\Delta_{max} = 7.5\, D_0 \approx .098 \text{ cm}^{-1}$$

(ii) If $J_3 \gg D_e$, the theory will be the same as for the n.n. pairs, and the maximum splitting from the main line will be with H // z , from an S = 1 state.

$$\Delta_{max} = 3g_e D_e \quad .144 \text{ cm}^{-1}$$

Experiments have been carried out in an attempt to identify the spectrum from the 3rd n.n. pairs. Rotating the magnetic field in the (100) plane, a group of lines were observed close to the main line with turning values 90° away from the [100] direction, as expected. This is the nearest approach in the (100) plane to the [111] direction along which the 3rd n.n. pairs have their axis. The lines were observed at temperatures as low as 1.9°K, consistent with a very small J. However the large amount of overlapping of the lines, and the power absorption from the wings of the main line made intensity measurements impossible.

The splittings, Δ, of the principal lines from the main line were measured as follows.

Δ = .148 ($\pm$.003) cm^{-1}

.133

.123

.118

.087

.078

After applying corrections to allow for the direction of the magnetic field not being quite in the z direction, these splittings do not appear to fit the Hamiltonian in either of the simple cases given earlier. In view of the uncertainty in the observed splittings, principally due to the difficulty in estimating the centres of overlapping lines, it appears pointless to attempt an exact fit with suitable intermediate values for J_3 and D_c. Should such a fit be possible, it is certain that the probable error on the parameters would be very great. Two deductions can be made however.

(i) J_3 is not great compared with D_c.

(ii) D_c is of the order of magnitude expected from a magnetic dipolar interaction, but possibly slightly larger.

3.6 Possible Impurities in MgO

Before ending this discussion on Mn in MgO, It seems important to mention some of the possible impurities which might occur in the crystals. It is very difficult to grow single crystals of pure MgO, and Orton (1959) made a detailed survey of iron group impurities in

several supposedly pure crystals. None of these were found to contain less than about 1 part in 10^5 paramagnetic impurities. Paramagnetic resonance spectra were identified from the following ions.

V^{2+}, Cr^{3+}, Mn^{2+}, Fe^{3+}, Fe^{2+}, Co^{2+}, Ni^{2+} and Ti^{3+}.

The line widths were generally small, some being as little as 1 gauss wide. It may be supposed that in the mixed crystals used in the present experiments similar impurities occur. However in the presence of ~ 1% paramagnetic Mn^{2+} ions the dipolar broadening will be quite large and make most of the impurity spectra disappear. No systematic search for impurities has been carried out in the present work. The chief concern is whether impurity lines could be confused with pair lines. For the n.n. spectrum this is certainly not so. The eleven component hyperfine structure unambiguously identifies the lines as pair lines. Those lines interpreted as due to 3rd n.n. pairs show traces of a poorly resolved hyperfine structure of about the right spacing, but they overlap too much to be certain about this. Their identification is justified mainly by the turning value found along

a [211] direction. None of the impurities found by Orton had this direction as an axis of symmetry.

CHAPTER 4

PARAMAGNETIC RESONANCE OF IRIDIUM TRIADS

4.1 Introduction

The first pair measurements on exchange interactions in diluted antiferromagnetic salts were made by Griffiths, Owen, Park, and Partridge (1959), on the antiferromagnetic salts K_2IrCl_6 and $(NH_4)_2IrCl_6$, in which about 98% of the paramagnetic Iridium ions were replaced by diamagnetic Platinum ion. The paramagnetic resonance spectra from pairs of exchange coupled nearest neighbour ions were studied, and parameters describing the isotropic and anisotropic exchange were deduced. No resonance was detected that could be attributed to next nearest neighbour pairs, indicating that any anisotropic exchange for such pairs is very small, and all transitions were obscured by the main line. In order to understand the antiferromagnetic ordering in a face centred cubic lattice, it is important to know the sign and magnitude of the n.n.n. isotropic exchange interaction. The main purpose of the experiments described in this chapter has been to measure this interaction from groups

of three exchange-coupled ions, (triads).

Preliminary experiments were performed by B.A.Coles and by B.F.Hamm, and a short account of some of the present results has been published, (Harris, Lines and Owen, 1963)

4.8 The Origin of the Exchange Interaction

In K_2IrCl_6 and $(NH_4)_2IrCl_6$ crystals, Ir^{4+} ions lie on a f.c.c. lattice. Each of these ions is surrounded by a regular octahedron of six Cl^- ions, and this constitutes the $(IrCl_6)^{2-}$ complex. The configuration of the Ir^{4+} ion is $5d^5$. In the octahedral molecular field the 5 degenerate d orbitals are split into a ground state d^5 triplet and a highly excited d^5 doublet. At normal temperatures only the triplet states are appreciably populated. The five d electrons occupy these six states, leaving an electron hole with effective spin $s = \frac{1}{2}$.

The paramagnetic resonance spectrum due to isolated $(IrCl_6)^{2-}$ complexes in $(NH_4)_2Ir_xPtCl_6$ has been studied using crystals in which Ir : Pt 1 : 500 by Griffiths, and Owen (1954) and by Cipollini, Owen, Thornley and Windsor (1963). An intense line was found at g = 1.736

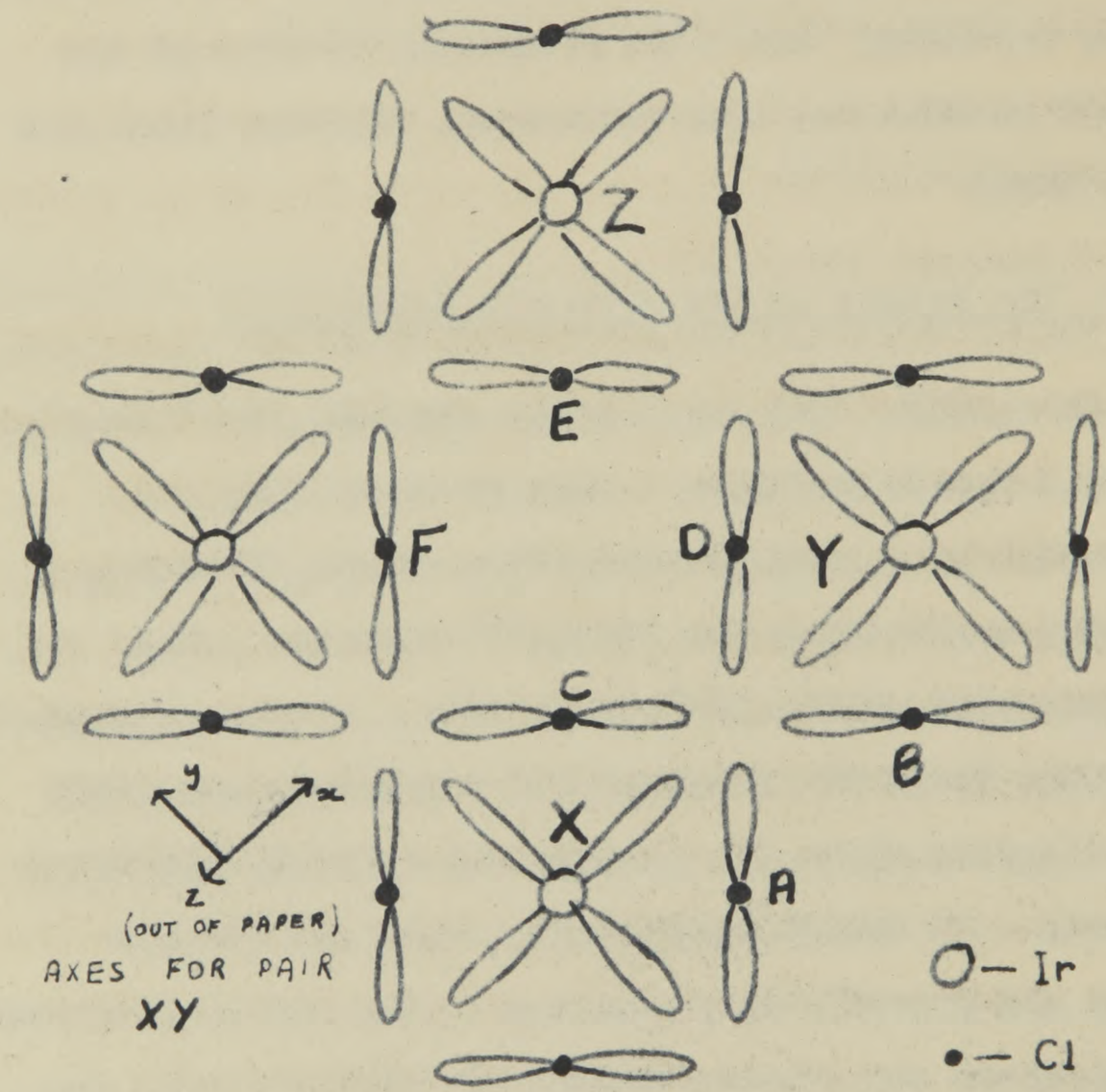


FIG. 16. SECTION IN A (100) PLANE FOR A F.C.C. ($IrCl_6$) CRYSTAL.

SHOWING RELATIVE POSITIONS OF Ir AND Cl NUCLEI, AND POSSIBLE ELECTRON ORBITALS.

with a hyperfine structure corresponding to interactions between the electron hole and both the Ir and Cl nuclei. Analysis of this hyperfine structure showed that the electron hole can be regarded as being about 70% in a d orbit around the Ir ion, and about 5% in p_π orbits around each of the Cl ions.

In the crystals the arrangements of the atoms and electron orbitals is as shown in fig 16. The mechanism of the interaction between neighbouring Ir ions is superexchange acting through the Cl ions. Referring to fig 16, for the n.n. pair XY there is overlap of the p_π orbits between A and B and between C and D. This π bonding is similar to that between the two Cl atoms in a Cl_2 molecule. For a n.n.n. such as XZ there are two paths for the interaction. There will be a certain direct overlap of the orbitals around C and E. This will be much smaller than for n.n. because the CE separation is greater than the AB separation, and because the lobes of the p_π orbitals are in unfavourable directions for overlap. There will also be an interaction acting through 3 Cl ions, such as CDE or CFE. It seems reasonable to suppose that this will be an order of magnitude less than the n.n. interaction, although it is hard to make a reliable estimate.

4.3 The N.N. Pair Spectrum

The interaction between two n.n. spins, $s_1 = s_2 = \frac{1}{2}$ can be described by a spin Hamiltonian,

$$\mathcal{H} = J_1 \underline{s}_1 \cdot \underline{s}_2 + D_1(3s_{1z}s_{2z} - \underline{s}_1 \cdot \underline{s}_2) + E_1(s_{1x}s_{2x} - s_{1y}s_{2y}) \quad (1)$$

J_1 is the n.n. isotropic exchange interaction and D_1 and E_1 describe the anisotropy of the interaction. x, y, z are axes of symmetry for the pair, z being along the [100] direction normal to the plane containing the four Cl ions through which the interactions take place, x is along the line joining the two Ir ions, and y is perpendicular to this. These axes are drawn in fig 18 for the pair XY. The values of these parameters were measured by Griffiths et al (1956) and are given below.

	$K_2Ir_2PtCl_8$	$(NH_4)_2Ir_2PtCl_8$
$\frac{J_1}{k}$	+11.5 ± 1°K	+7.5 ± 1°K
J_1	+ 8.0 ± .8 cm^{-1}	+5.2 ± .8 cm^{-1}
D_1	+ 0.45 ± .01 cm^{-1}	+0.42 ± .01 cm^{-1}
E_1	- 0.18 ± .01 cm^{-1}	-0.22 ± .01 cm^{-1}

The relative signs of D_o and E_o were not given by Griffiths et al, but have since been determined by Coles (1959) and have been labelled accordingly.

D_o and E_o are much greater than would be expected from magnetic dipolar interaction, and may attributed almost entirely to anisotropic exchange.

The Hamiltonian gives rise to four energy levels. In this case, since $J_1 \gg D_o, E_o$, these levels form a singlet with total spin $\underline{S} = \underline{s}_1 + \underline{s}_2 = 0$, corresponding to s_1 and s_2 antiparallel, and a triplet, with $\underline{S} = 1$ corresponding to s_1 and s_2 parallel. The energy separation between the singlet and the triplet is J_1, and since it is positive the triplet level is highest. The D_o and E_o terms split the triplet levels, their centre of gravity remaining unchanged.

In a magnetic field H, we can consider the triplet levels with reference to the Hamiltonian,

$$\mathcal{H} = g\beta\underline{H}\cdot\underline{S} + D_p(S_z^2 - \tfrac{1}{3}S(S+1)) + E_p(S_x^2 - S_y^2) \qquad (2)$$

where $D_p = \frac{3}{2} D_o$, $E_p = \frac{1}{2} E_o$, $g = 1.79$.

With $H \parallel z$ this gives energy levels,

$$W = -\frac{2}{3} D_p , \qquad W = +\frac{1}{6} D_p \pm (G^2 + E_p^2)^{\frac{1}{2}} \qquad (3)$$

where $G = g\beta H$

Transitions between these levels give rise to the observed pair spectrum.

In the earlier experiments D_p and E_p were found from the line positions in this spectrum. J_1 was found from the variation of line intensity with temperature, the intensity being proportional to the difference in population of the two levels concerned, which under the experimental conditions is expected to obey a Boltzmann law. Neglecting the splittings of the triplet levels, this can be written,

$$I \propto (1 - e^{-\frac{h\nu}{kT}}) \frac{e^{-\frac{J_1}{kT}}}{1 + 3e^{-\frac{J_1}{kT}}} \qquad (4)$$

4.4 The Theory of Triads

There are several types of triad which occur. They may be divided into two groups.

(i) n.n. Triads, in which each of the ions in the triad is a n.n. to at least one of the other two ions.

(ii) n.n.n. Triads, which consist of a n.n. pair and one n.n.n. ion.

The Hamiltonians describing these triads can each be written as the sum of the Hamiltonians for each individual interaction. For a n.n. interaction between

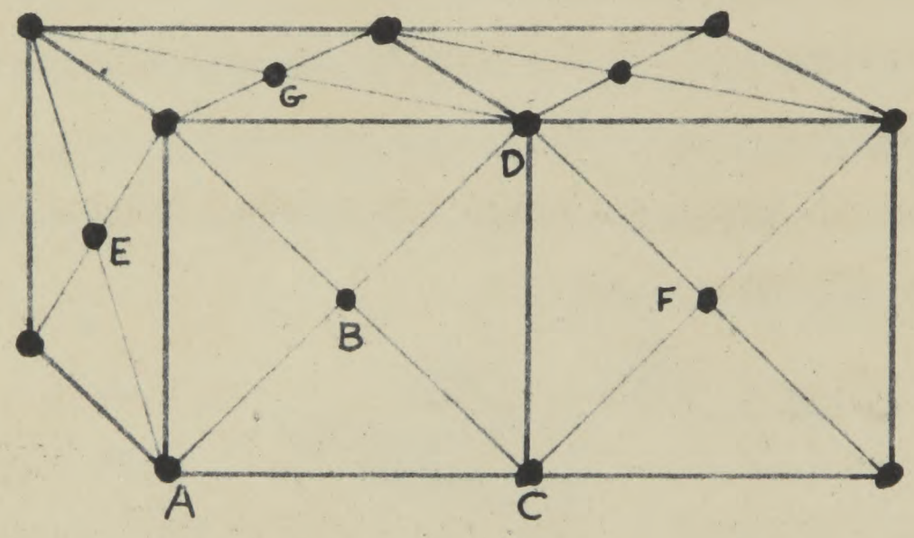


FIG. 17. TYPES OF TRIAD. (SEE TEXT)

spins s_1 and s_2, the Hamiltonian will be the same as that for an isolated pair, equn.1, and will be abbreviated $\mathcal{H}_{12}$. A n.n.n. interaction between spins s_1 and s_2 will be taken as,

$$\mathcal{H} = J_3 \underline{s}_1 \cdot \underline{s}_2 \qquad (5)$$

J_3 is small compared with J_1 and any anisotropic exchange is neglected.

The various types of triad are listed below, with reference to fig 17.

Name of Triad		e.g.	Hamiltonian
n.n.	Line Triad	A B D	$H_{12} + H_{23}$
	Right angle Triad	A B C	$H_{12} + H_{23} + J_3 \underline{s}_1 \cdot \underline{s}_2$
	Skew Triad	A B G	$H_{12} + H_{23}$
	Equilateral Triad	A B E	$H_{12} + H_{23} + H_{31}$
n.n.n.	135°	A B F	$H_{12} + J_3 \underline{s}_2 \cdot \underline{s}_3$
	90°	E A C	

The energy levels for these triads are now derived. The theory of the line triad is first given in some detail and much of it is applicable to the other n.n. triads.

The Line Triad.

For the Line, Skew, and Right angle triads, the largest terms in the Hamiltonian are the n.n. isotropic exchange terms,

$$\mathcal{H} = J_1(\underline{s}_1 \cdot \underline{s}_2 + \underline{s}_2 \cdot \underline{s}_3) \qquad (6)$$

The energy levels from this are two doublets at $W = 0$, and $W = -J_1$, corresponding to a total spin, $\underline{S} = \underline{s}_1 + \underline{s}_2 + \underline{s}_3 = \frac{1}{2}$, and a quadruplet at $W = +\frac{J_1}{2}$, corresponding to $S = \frac{3}{2}$. Introduction of the anisotropic terms splits the $S = \frac{3}{2}$ levels. Transitions between these levels form the experimentally observed triad spectra. Transitions between the $S = \frac{1}{2}$ doublet levels will all fall under the main line. The effect of the D_o and E_o terms is found using the full Hamiltonian. For the line triad this is,

$$\mathcal{H} = J_1(\underline{s}_1 \cdot \underline{s}_2 + \underline{s}_2 \cdot \underline{s}_3) + D_o(3s_{1z}s_{2z} - \underline{s}_1 \cdot \underline{s}_2 + 3s_{2z}s_{3z} - \underline{s}_2 \cdot \underline{s}_3)$$
$$+ E_o(s_{1x}s_{2x} - s_{1y}s_{2y}) + E_o(s_{2x}s_{3x} - s_{2y}s_{3y}) \qquad (7)$$

Putting $s_+ = s_x + is_y$, $s_- = s_x - is_y$,

$$\mathcal{H} = (J_1 + 2D_o)(s_{1z}s_{2z} + s_{2z}s_{3z}) + \tfrac{1}{2}(J_1 - D_o)(s_{1+}s_{2-} + s_{1-}s_{2+} + s_{2+}s_{3-} + s_{2-}s_{3+})$$
$$+ \tfrac{1}{2}E_o(s_1^2 + s_2^2 + s_1^2 - s_2^2 - + s_2^2 s_3^2 + + s_2^2 - s_3^2 -) \qquad (8)$$

$\lvert m_1\, m_2\, m_3\rangle$	$\lvert \frac{1}{2}\ \frac{1}{2}\ \frac{1}{2}\rangle$	$\lvert \frac{1}{2}\ \frac{1}{2}\ -\frac{1}{2}\rangle$	$\lvert \frac{1}{2}\ -\frac{1}{2}\ \frac{1}{2}\rangle$	$\lvert -\frac{1}{2}\ \frac{1}{2}\ \frac{1}{2}\rangle$	$\lvert \frac{1}{2}\ -\frac{1}{2}\ -\frac{1}{2}\rangle$	$\lvert -\frac{1}{2}\ \frac{1}{2}\ -\frac{1}{2}\rangle$	$\lvert -\frac{1}{2}\ -\frac{1}{2}\ \frac{1}{2}\rangle$	$\lvert -\frac{1}{2}\ -\frac{1}{2}\ -\frac{1}{2}\rangle$
$\lvert \frac{1}{2}\ \frac{1}{2}\ \frac{1}{2}\rangle$	$\frac{1}{2}(J+2D)$	0	0	0	$\frac{E}{2}$	0	$\frac{E}{2}$	0
$\lvert \frac{1}{2}\ \frac{1}{2}\ -\frac{1}{2}\rangle$	0	0	$\frac{1}{2}(J-D)$	0	0	0	0	$\frac{E}{2}$
$\lvert \frac{1}{2}\ -\frac{1}{2}\ \frac{1}{2}\rangle$	0	$\frac{1}{2}(J-D)$	$-\frac{1}{2}(J+2D)$	$\frac{1}{2}(J-D)$	0	0	0	0
$\lvert -\frac{1}{2}\ \frac{1}{2}\ \frac{1}{2}\rangle$	0	0	$\frac{1}{2}(J-D)$	0	0	0	0	$\frac{E}{2}$
$\lvert \frac{1}{2}\ -\frac{1}{2}\ -\frac{1}{2}\rangle$	$\frac{E}{2}$	0	0	0	0	$\frac{1}{2}(J-D)$	0	0
$\lvert \frac{1}{2}\ \frac{1}{2}\ -\frac{1}{2}\rangle$	0	0	0	0	$\frac{1}{2}(J-D)$	$-\frac{1}{2}(J+2D)$	$\frac{1}{2}(J-D)$	0
$\lvert -\frac{1}{2}\ -\frac{1}{2}\ \frac{1}{2}\rangle$	$\frac{E}{2}$	0	0	0	0	$\frac{1}{2}(J-D)$	0	0
$\lvert -\frac{1}{2}\ -\frac{1}{2}\ -\frac{1}{2}\rangle$	0	$\frac{E}{2}$	0	$\frac{E}{2}$	0	0	0	$\frac{1}{2}(J+2D)$

FIG. 18. LINE TRIAD ENERGY MATRIX.

This Hamiltonian is used to operate on the substates given by the different combinations of the magnetic quantum numbers for the individual ions, m_1, m_2, $m_3 = \pm \frac{1}{2}$ using the operations,

$$\begin{aligned} s_z|m\rangle &= m|m\rangle \\ s_+|m\rangle &= (s(s+1)-m(m+1))^{\frac{1}{2}}|m+1\rangle \\ s_-|m\rangle &= (s(s+1)-m(m-1))^{\frac{1}{2}}|m-1\rangle \end{aligned} \qquad (9)$$

This gives the energy matrix shown in fig 18. The energy levels are found by subtracting W from each diagonal element and equating the determinant so formed to zero. If the terms in E_0 are neglected this can be solved exactly, giving the roots,

$$W = 0 \qquad (10)$$

$$W = \frac{J_1}{2} + D_0 \qquad (11)$$

$$W = -\frac{J_1}{4} - \frac{D_0}{2} + \tfrac{1}{2}(9J_1^2 - 12D_0J_1 + 12D_0^2)^{\frac{1}{2}}$$

Since $J_1 \gg D_0$, these last roots are approximately,

$$W = \frac{J_1}{2} - D_0 + \frac{D_0^2}{3J_1 - 2D_0} \qquad (12)$$

$$W = -J_1 - \frac{D_0^2}{3J_1 - 2D_0} \qquad (13)$$

The quantum states corresponding to these energy levels can be represented by their total spin S, and

TABLE II

STATES FOR A N.N. TRIAD.

STATE	$\lvert M\rangle_S$	$\sum_i a_i \lvert m_1, m_2, m_3\rangle$
$\lvert a\rangle$	$\lvert\frac{3}{2}\rangle_{\frac{3}{2}}$	$\lvert\frac{1}{2}, \frac{1}{2}, \frac{1}{2}\rangle$
$\lvert b\rangle$	$\lvert\frac{1}{2}\rangle_{\frac{3}{2}}$	$\frac{1}{\sqrt{3}}\left(\lvert\frac{1}{2}, \frac{1}{2}, -\frac{1}{2}\rangle + \lvert\frac{1}{2}, -\frac{1}{2}, \frac{1}{2}\rangle + \lvert-\frac{1}{2}\ \frac{1}{2}\ \frac{1}{2}\rangle\right)$
$\lvert c\rangle$	$\lvert-\frac{1}{2}\rangle_{\frac{3}{2}}$	$\frac{1}{\sqrt{3}}\left(\lvert\frac{1}{2}, -\frac{1}{2}, -\frac{1}{2}\rangle + \lvert-\frac{1}{2}, \frac{1}{2}, -\frac{1}{2}\rangle + \lvert-\frac{1}{2}, -\frac{1}{2}, \frac{1}{2}\rangle\right)$
$\lvert d\rangle$	$\lvert-\frac{3}{2}\rangle_{\frac{3}{2}}$	$\lvert-\frac{1}{2}, -\frac{1}{2}, -\frac{1}{2}\rangle$
$\lvert e\rangle$	$\lvert\frac{1}{2}\rangle_{\frac{1}{2}}$	$\frac{1}{\sqrt{2}}\left(\lvert\frac{1}{2}, \frac{1}{2}, -\frac{1}{2}\rangle - \lvert-\frac{1}{2}, \frac{1}{2}, \frac{1}{2}\rangle\right)$
$\lvert f\rangle$	$\lvert-\frac{1}{2}\rangle_{\frac{1}{2}}$	$\frac{1}{\sqrt{2}}\left(\lvert-\frac{1}{2}, -\frac{1}{2}, \frac{1}{2}\rangle - \lvert\frac{1}{2}, -\frac{1}{2}, -\frac{1}{2}\rangle\right)$
$\lvert g\rangle$	$\lvert\frac{1}{2}\rangle_{\frac{1}{2}}$	$\frac{1}{\sqrt{6}}\left(2\lvert\frac{1}{2}, -\frac{1}{2}, \frac{1}{2}\rangle - \lvert\frac{1}{2}, \frac{1}{2}, -\frac{1}{2}\rangle - \lvert-\frac{1}{2}, \frac{1}{2}, \frac{1}{2}\rangle\right)$
$\lvert h\rangle$	$\lvert-\frac{1}{2}\rangle_{\frac{1}{2}}$	$\frac{1}{\sqrt{6}}\left(2\lvert-\frac{1}{2}, \frac{1}{2}, -\frac{1}{2}\rangle - \lvert-\frac{1}{2}, -\frac{1}{2}, \frac{1}{2}\rangle - \lvert\frac{1}{2}, -\frac{1}{2}, -\frac{1}{2}\rangle\right)$

their total magnetic quantum number, M. These states, written M_S can then be expressed as a linear combination of substates in the $m_1\ m_2\ m_3$ representation, where $M = m_1 + m_2 + m_3$. The relations between these two representations can be found in the same way as for pairs (see chapter 3) and are given in Table II.

We can now consider the term in E_o in the Hamiltonian, equn 7. This term will not appreciably alter the states as given above, but it will affect the splitting of the $S = \frac{3}{2}$ quadruplet. Operating with the Hamiltonian on the quadruplet states, using the $m_1\ m_2\ m_3$ representation we get the energy matrix,

$$\begin{array}{c} \\ |a\rangle \\ |c\rangle \\ |b\rangle \\ |d\rangle \end{array} \begin{array}{c} \begin{array}{cccc} |a\rangle & |c\rangle & |b\rangle & |d\rangle \end{array} \\ \begin{pmatrix} \frac{J'}{2}+D_o & \frac{E_o}{\sqrt{3}} & 0 & 0 \\ \frac{E_o}{\sqrt{3}} & \frac{J'}{2}-D_o & 0 & 0 \\ 0 & 0 & \frac{J'}{2}-D_o & \frac{E_o}{\sqrt{3}} \\ 0 & 0 & \frac{E_o}{\sqrt{3}} & \frac{J'}{2}+D_o \end{pmatrix} \end{array}$$

This gives energy levels at,

$$W = \frac{J'}{2} \pm (D_o^2 + \frac{E_o^2}{3})^{\frac{1}{2}} \qquad (14)$$

The total zero field splitting Δ, will include the small term, $-D_o^2/(3J_1 - 2D_o)$, obtained in equation 12, which arises through mixing between the $S = \frac{1}{2}$ and $S = \frac{3}{2}$ states.

$$\Delta = 2(D_o^2 + \frac{E_o^2}{3})^{\frac{1}{2}} - \frac{D_o^2}{3J_1 - 2D_o} \qquad (15)$$

The next step is to consider the effect of a magnetic field on the $S = \frac{3}{2}$ levels. For this the easiest approach is to use the H_S representation. The triad can then be described by a Hamiltonian,

$$\mathcal{H} = g\beta\underline{H}.\underline{S} + D_1(S_z^2 - \tfrac{1}{3}S(S+1)) + E_1(S_x^2 - S_y^2) \qquad (16)$$

Taking $H \parallel z$, and expressing S_x and S_y in terms of the operators S_+ and S_- this becomes,

$$\mathcal{H} = GS_z + D_1(S_z^2 - \tfrac{5}{4}) + \frac{E_1}{2}(S_+^2 + S_-^2) \qquad (17)$$

where $G = g\beta H$.

By operating with this on the four $S = \frac{3}{2}$ states, we obtain the elements of the energy matrix,

$$\begin{array}{c} \\ |\tfrac{3}{2}\rangle \\ |-\tfrac{1}{2}\rangle \\ |\tfrac{1}{2}\rangle \\ |-\tfrac{3}{2}\rangle \end{array} \begin{pmatrix} \frac{3}{2}G + D_1 & \sqrt{3}E_1 & 0 & 0 \\ \sqrt{3}E_1 & -\frac{1}{2}G - D_1 & 0 & 0 \\ 0 & 0 & \frac{1}{2}G - D_1 & \sqrt{3}E_1 \\ 0 & 0 & \sqrt{3}E_1 & -\frac{3}{2}G + D_1 \end{pmatrix}$$

The energy levels from this matrix are,

$$W = +\frac{Q}{2} \pm ((D_1+3)^2 + 3E_1^2)^{\frac{1}{2}} \qquad (18)$$

$$W = -\frac{Q}{2} \pm ((D_1-3)^2 + 3E_1^2)^{\frac{1}{2}} \qquad (19)$$

The energy levels for $H // x$, or $H // y$ can be obtained directly from these by rotating the axes. The transformations for this are (see Bowers and Owen, 1955),

$$H // x, \quad D_1 \rightarrow \tfrac{1}{2}(3E_1 - D_1) \quad , \quad E_1 \rightarrow -\tfrac{1}{2}(D_1 + E_1)$$

$$H // y, \quad D_1 \rightarrow \tfrac{1}{2}(3E_1 + D_1) \quad , \quad E_1 \rightarrow \tfrac{1}{2}(D_1 - E_1)$$

The parameters D_1 and E_1 are related directly to D_o and E_o. By comparing equivalent matrix elements in the two representations it follows directly that,

$$E_1 = \frac{E_o}{3} \qquad (20)$$

The zero field splitting Δ, must also be the same in both representations.i.e.,

$$2(D_1^2+3E_1^2)^{\frac{1}{2}} = 2(D_o^2+\frac{E_o^2}{3}) - \frac{D_o^2}{3J_1 - 2D_o}$$

$$\therefore D_1 = D_o\left(1 - \frac{D_o^2 + E_o^2/3}{6J_1 - 4D_o}\right) \qquad (21)$$

Substituting the values for D_o and E_o found from pair

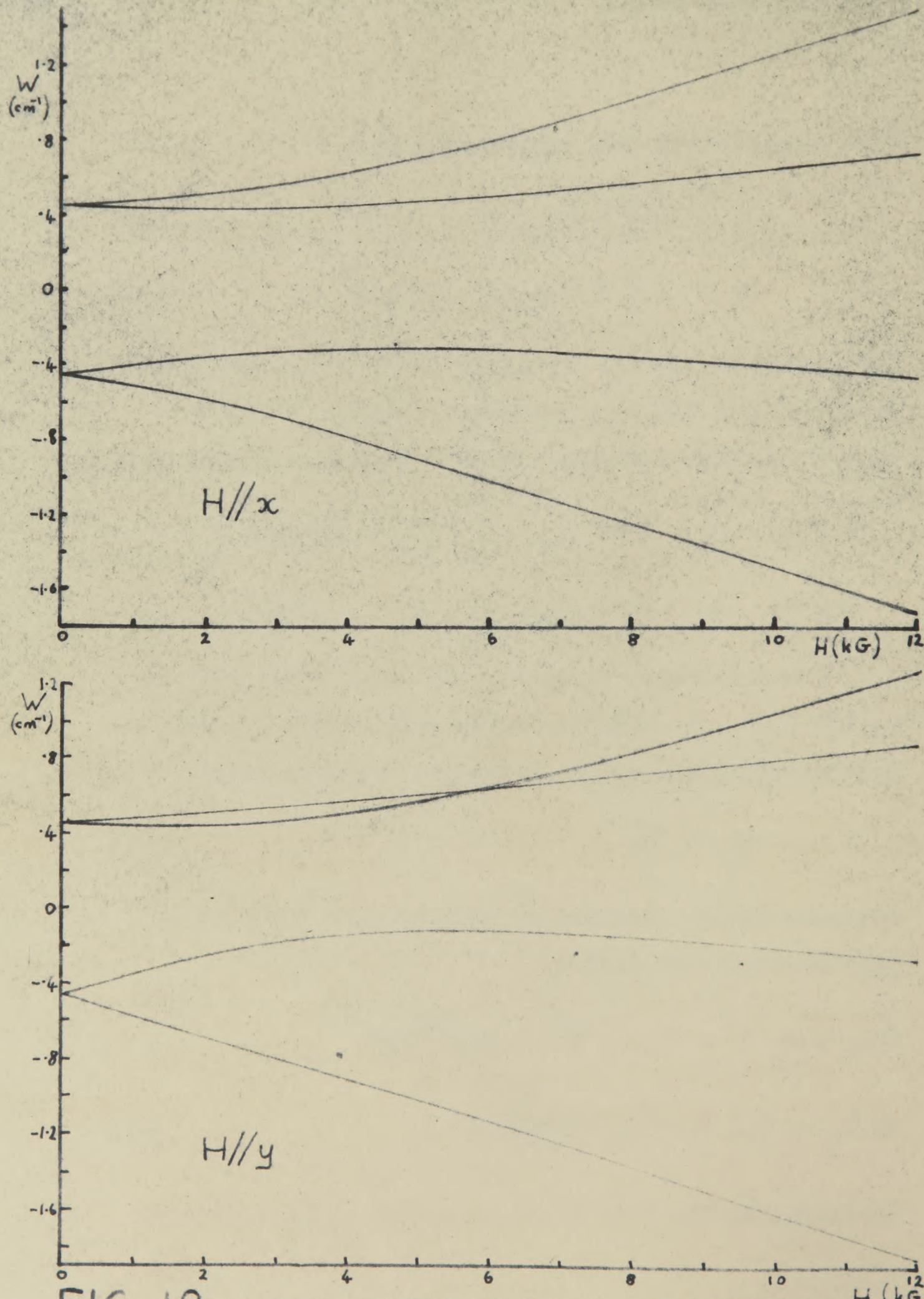
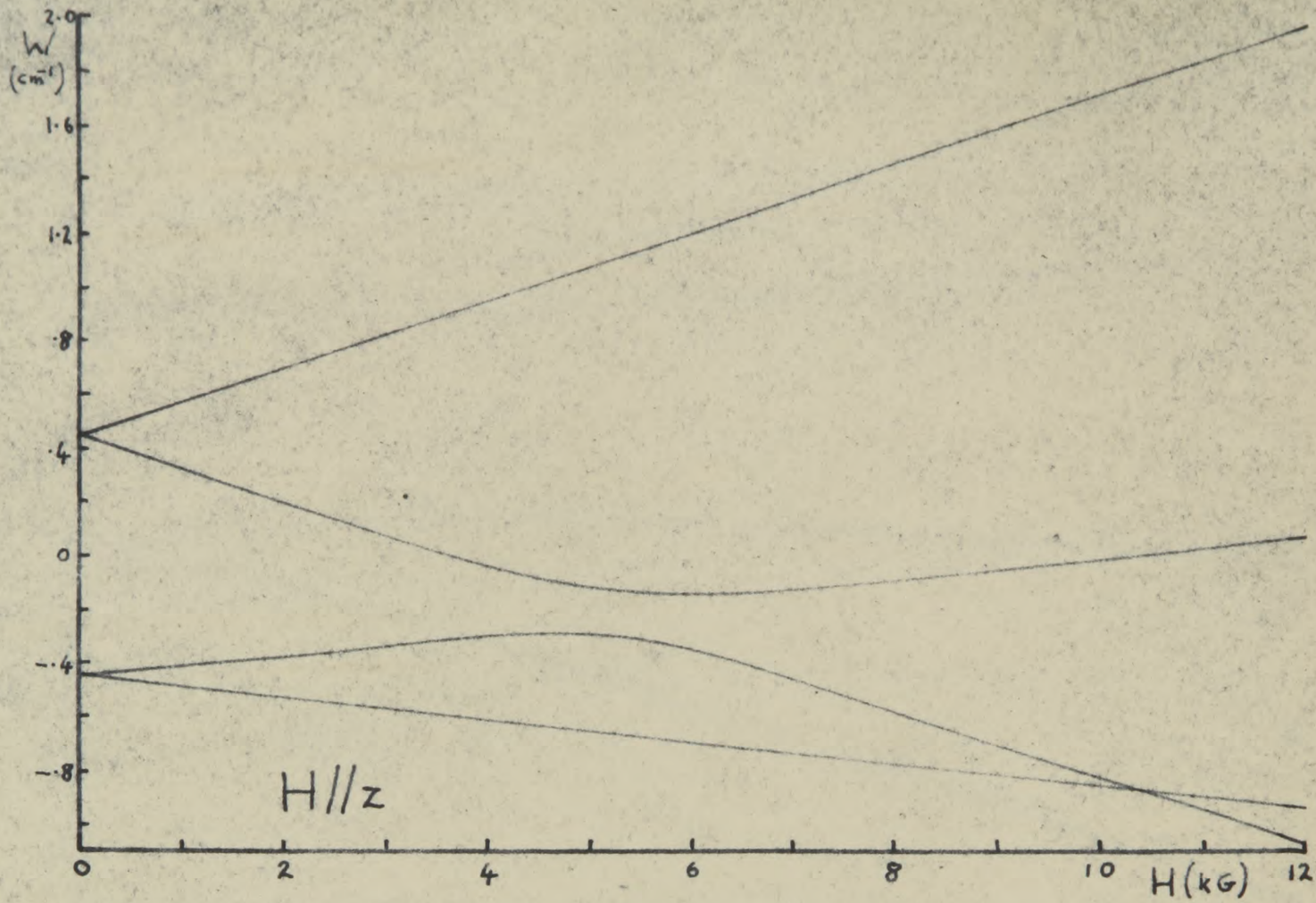


FIG. 19. LINE TRIAD ENERGY LEVELS $K_2IrPtCl_6$.



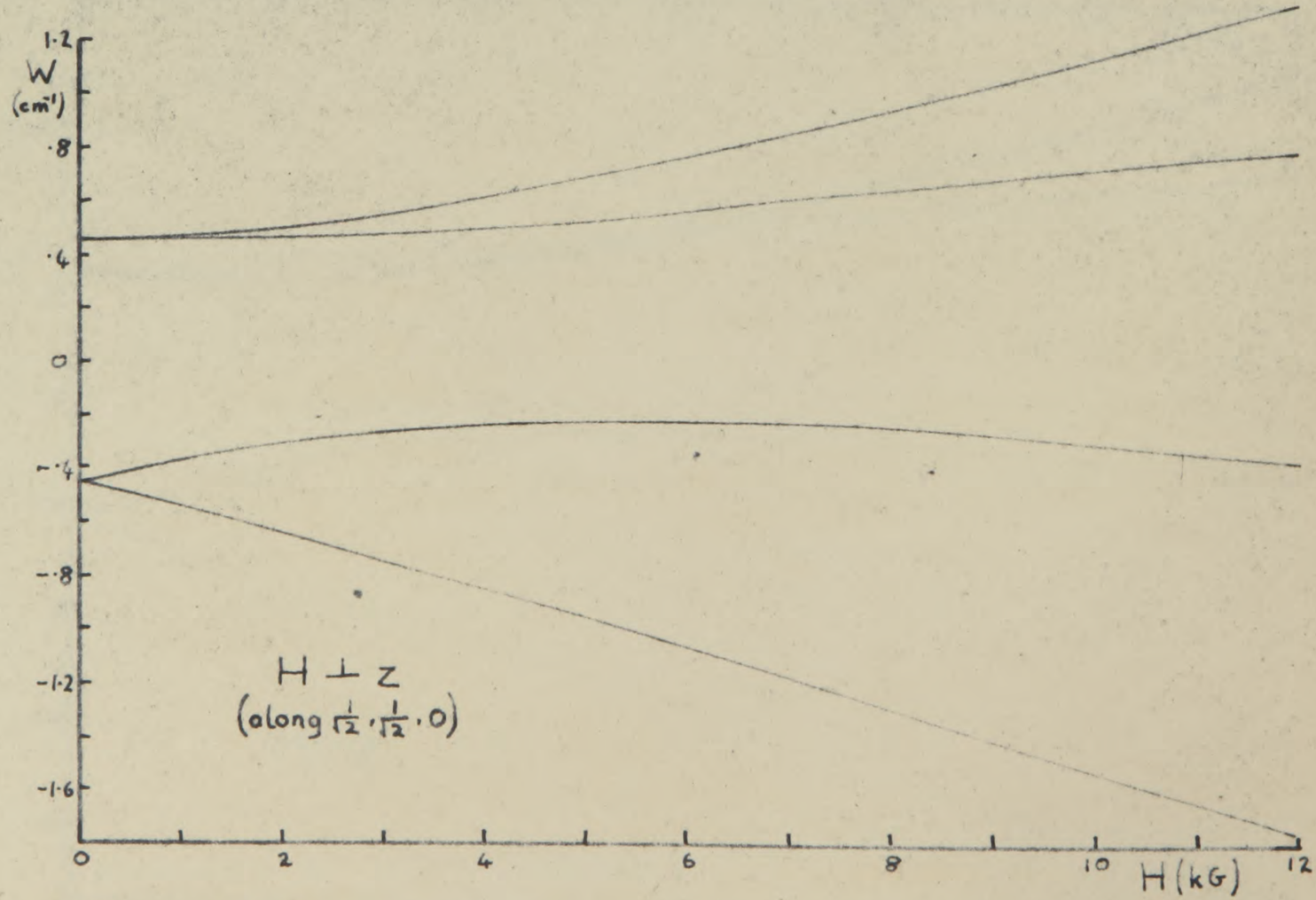


FIG. 20. LINE TRIAD ENERGY LEVELS, $K_2IrPtCl_6$.

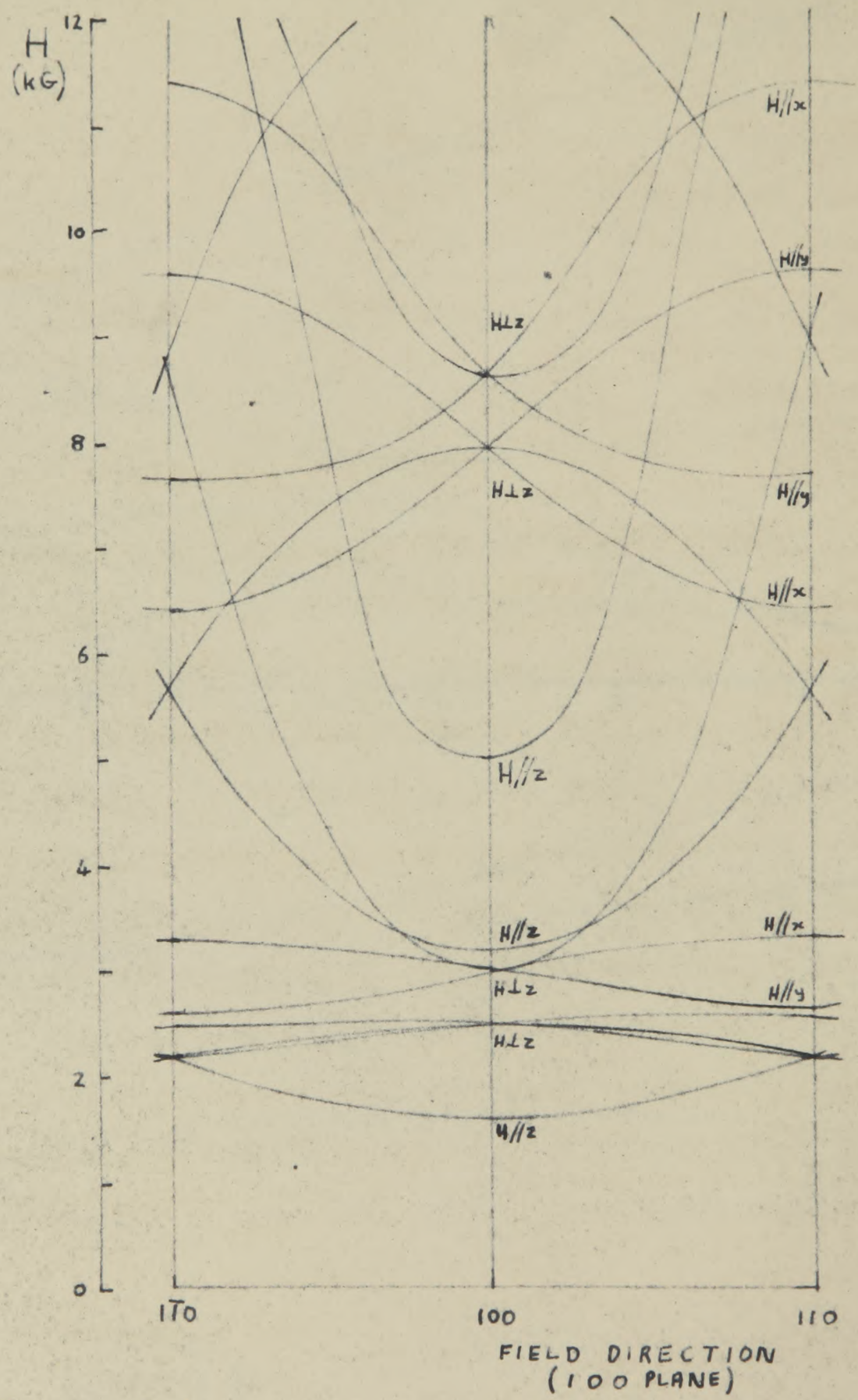


FIG. 21. LINE TRIAD, THEORETICAL SPECTRUM FOR $K_2IrPtCl_6$ AT Q BAND

measurements the parameters for the line triad are found to be as follows.

	$D_1(cm^{-1})$	$E_1(cm^{-1})$
$(NH_4)_2Ir,PtCl_6$	0.416	-0.073
$K_2Ir,PtCl_6$	0.443	-0.000

The energy levels for the line triad as a function of field are given in figs 19 and 20 for the salt $K_2Ir,PtCl_6$. They are plotted for four different field directions, with direction cosines relative to the triad axes, (100), (010), (001), and $(\frac{1}{\sqrt{2}}\ \frac{1}{\sqrt{2}}\ 0)$.

The spectrum predicted from these levels using a quantum of 1.18 cm^{-1} (Q band), and rotating the magnetic field in a (100) crystal plane, is shown in fig 21. This takes account of the fact that there are six differently oriented line triads in the crystal lattice, each of which gives its own characteristic spectrum. The spectrum for the salt $(NH_4)_2Ir,PtCl_6$ is very similar to this.

<u>The Right Angle Triad</u>

Much of the theory given in the previous section on the line triad applies also to the right angle triad.

The Hamiltonians differ in two ways.

(i) The two n.n. interactions have different x and y axes. The z axis will still be the same, normal to the plane of the triad, so this only affects the rhombic (E_o) term.

(ii) There will be a n.n.n. interaction between s_1 and s_3, given by $J_2 \underline{s}_1 \cdot \underline{s}_3$.

The full Hamiltonian is,

$$\mathcal{H} = J_1(\underline{s}_1\cdot\underline{s}_2+\underline{s}_2\cdot\underline{s}_3) + D_o(3s_{1z}s_{3z}-\underline{s}_1\cdot\underline{s}_3+3s_{2z}s_{3z}-\underline{s}_2\cdot\underline{s}_3)$$
$$+E_o(s_{1x}s_{3x}-s_{1y}s_{3y}-s_{2x}s_{3x}+s_{2y}s_{3y}) + J_2(\underline{s}_1\cdot\underline{s}_3) \qquad (22)$$

To a first approximation the states will be the same as given in table 1. Operating on these states with this Hamiltonian we get the energy matrixbelow.

	$\|a\rangle$	$\|b\rangle$	$\|c\rangle$	$\|d\rangle$
$\|a\rangle$	$\frac{J_1}{2}+\frac{J_2}{4}+D_o$	0	0	0
$\|b\rangle$	0	$\frac{J_1}{2}+\frac{J_2}{4}-D_o$	0	0
$\|c\rangle$	0	0	$\frac{J_1}{2}+\frac{J_2}{2}-D_o$	0
$\|d\rangle$	0	0	0	$\frac{J_1}{2}+\frac{J_2}{4}+D_o$

The terms in E_o have cancelled out. Since the x and

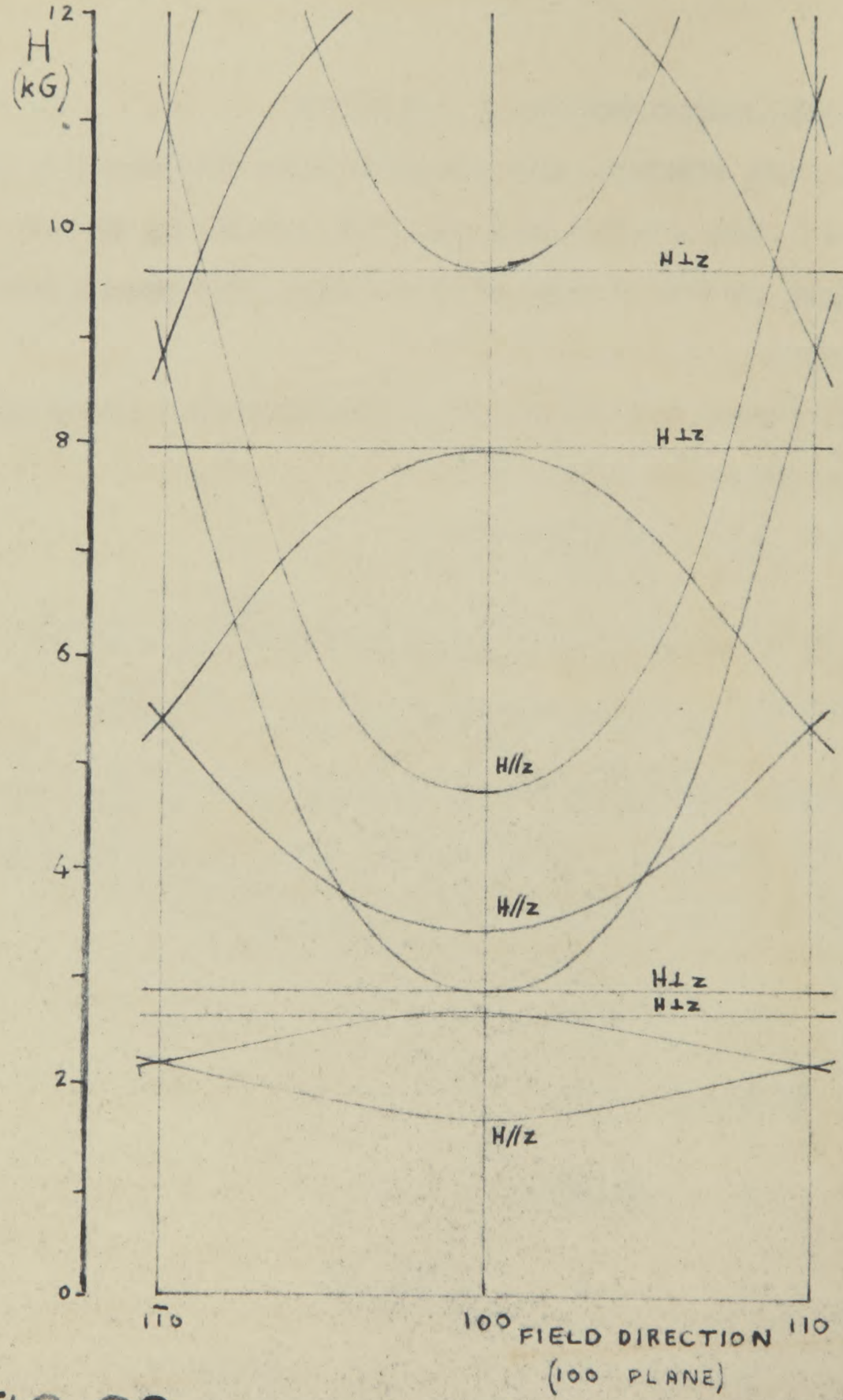


FIG. 22. RIGHT ANGLE TRIAD, THEORETICAL SPECTRUM FOR $K_2IrPtCl_6$ AT Q BAND.

y axes are equivalent for the right angle triad, this is to be expected. The n.n.n. interaction has the effect of moving all the quadruplet levels by the same amount, $\frac{J_0}{4}$, so this term will not have any observable effect on the spectrum.

In a magnetic field the quadruplet levels for the right angle triad can be described by the Hamiltonian,

$$\mathcal{H} = g\beta \mathbf{H}\cdot\mathbf{S} + D_p(S_z^2 - \tfrac{1}{3}S(S+1)) \qquad (23)$$

The total splitting in zero field will be,

$$\Delta = 2D_0 - \frac{D_0^2}{3J_1 - 2D_0} = 2D_p \qquad (24)$$

Using the values for D_0 and J_1 estimated from pair measurements we get the parameters below.

$K_2Ir_2PtCl_6$	$D_p = 0.443\ cm^{-1}$
$(NH_4)_2Ir_2PtCl_6$	$D_p = 0.416\ cm^{-1}$

The predicted spectrum for rotation in the (100) plane with a quantum of $1.18cm^{-1}$ is plotted in fig 28. Since all directions with H perpendicular to z are equivalent, some of the resonance lines will be isotropic for rotation in this plane.

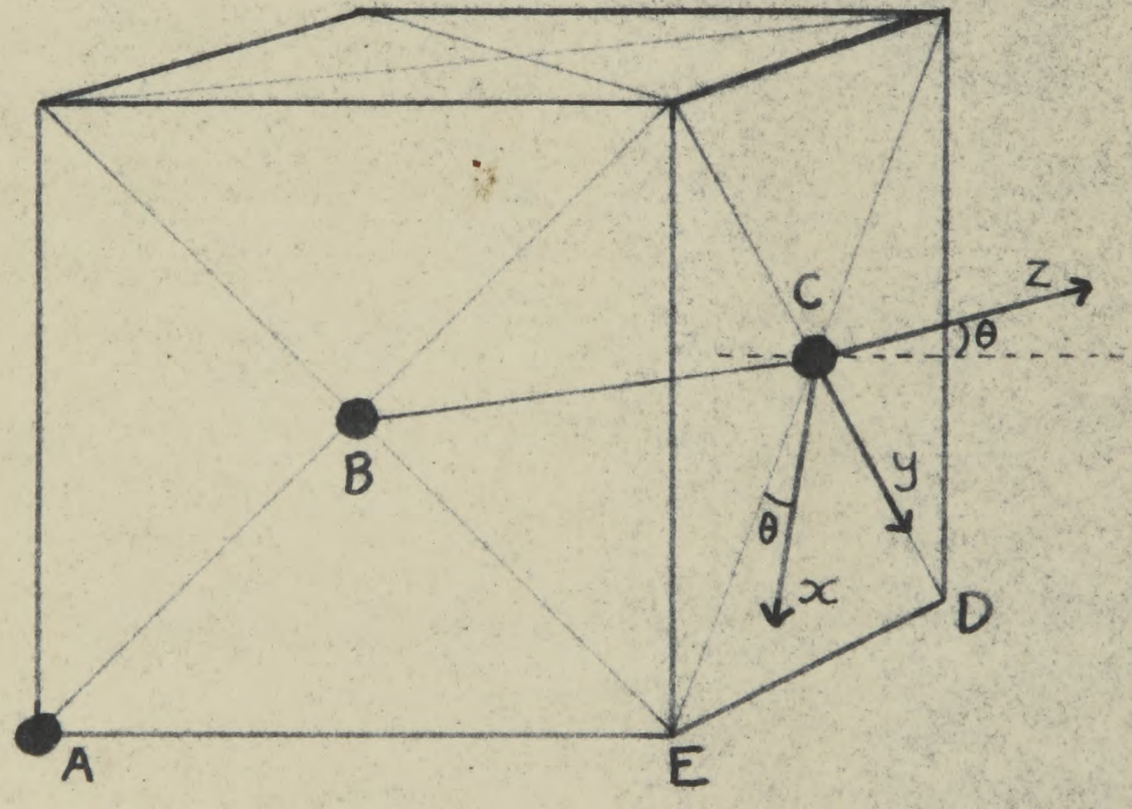


FIG. 23. THE SKEW TRIAD.

AXES OF SYMMETRY

The Skew Triad.

For this triad again, the energy levels differ from those of the line triad only in the splitting of the $S = \frac{1}{2}$ levels by the anisotropic terms in the Hamiltonian. The axes of the two n.n. interactions are quite different in this case, so the chief problem is to find the axes of symmetry for the triad. Consider the triad ABC in fig 23. If the axes for the AB interaction are x', y', z', and those for the BC interaction are $x^\circ, y^\circ, z^\circ$, then the Hamiltonian can be written,

$$\mathcal{H} = \mathcal{H}_{12} + \mathcal{H}_{23} \qquad (25)$$

where,

$$\mathcal{H}_{12} = D_o(3s_{1z'}s_{2z'} - \mathbf{s}_1 \cdot \mathbf{s}_2) + E_o(s_{1x'}s_{2x'} - s_{1y'}s_{2y'})$$

$$\mathcal{H}_{23} = D_o(3s_{2z^\circ}s_{3z^\circ} - \mathbf{s}_2 \cdot \mathbf{s}_3) + E_o(s_{2x^\circ}s_{3x^\circ} - s_{2y^\circ}s_{3y^\circ})$$

The direction BC in fig 23 is equivalent for both interactions, will be an axis of symmetry. Calling this the y axis, and taking z arbitrarily along the perpendicular 100 direction AE, and x along the CE direction, we have the transformations,

$$x' = \frac{\sqrt{2}}{2}\mathbf{k} - \frac{\sqrt{2}}{2}\mathbf{i}, \quad y' = -\frac{\sqrt{2}}{2}\mathbf{k} - \frac{\sqrt{2}}{2}\mathbf{i}, \quad z' = \frac{1}{\sqrt{2}}(x-y)$$

$$x^\circ = \frac{\sqrt{2}}{2}\mathbf{k} + \frac{\sqrt{2}}{2}\mathbf{i}, \quad y^\circ = \frac{\sqrt{2}}{2}\mathbf{k} - \frac{\sqrt{2}}{2}\mathbf{i}, \quad z^\circ = \frac{1}{\sqrt{2}}(-x-y) \qquad (26)$$

After applying these transformation, the terms in the Hamiltonian with non-zero matrix elements for the S = $\frac{3}{2}$ states are,

$$\mathcal{H} = \frac{3D_0}{2}(s_{1x}s_{2x}+s_{1y}s_{2y}+s_{2x}s_{3x}+s_{2y}s_{3y}) - D_0(\underline{s}_1\cdot\underline{s}_2 + \underline{s}_2\cdot\underline{s}_3)$$
$$+\frac{E}{\sqrt{2}}(s_{1x}s_{2z}+s_{1z}s_{2x}+s_{2x}s_{3z}+s_{2z}s_{3x}) \qquad (27)$$

The absence of any cross terms in y (e.g. $s_{1x}s_{2y}$ etc.) shows that y is an axis of symmetry. The coordinates can now be rotated about y by an angle θ, until the cross terms between x and z vanish. The new transformations are,

$$z = z\cos\theta + x\sin\theta$$
$$x = z\sin\theta - x\cos\theta \qquad (28)$$

With these substitutions, the coefficients of the cross terms are all,

$$-\frac{3D_0}{2}\sin\theta\cos\theta + \frac{E_0}{\sqrt{2}}(\cos^2\theta - \sin^2\theta)$$

This is zero when,

$$\tan\theta = \frac{2\sqrt{2}E_0}{3D_0} \qquad (29)$$

This gives the axes of symmetry shown in fig 23. With reference to the new axes, the Hamiltonian can be written,

$$\mathcal{H} = D'(3s_{1z}s_{2z} - \underline{s}_1\cdot\underline{s}_2 + 3s_{2z}s_{3z} - \underline{s}_2\cdot\underline{s}_3) + E'(s_{1x}s_{2x} - s_{1y}s_{2y} + s_{2x}s_{3x} - s_{2y}s_{3y}) \quad (30)$$

where,

$$E' = \frac{3D_o}{8}(1-\cos 2\theta) - \frac{E_o}{2\sqrt{2}}\sin 2\theta \quad (31)$$

$$D' = \frac{3D_o}{8}(1-\cos 2\theta) - \frac{E_o}{2\sqrt{2}}\sin 2\theta - \frac{D_o}{2} \quad (32)$$

This is exactly the same form as the Hamiltonian for the line triad, and the energy levels are found in the same way. In a magnetic field the triad can be described by a Hamiltonian,

$$\mathcal{H} = g\beta\underline{H}\cdot\underline{S} + D_s(S_z^2 - \tfrac{1}{3}s(s+1)) + E_s(S_x^2 - S_y^2) \quad (33)$$

where, $E_s = \frac{E'}{3}$

$$D_s = D'\left(1 - \frac{(D'^2 + E'^2/3)}{6J_1 - 4D'}\right) \quad (34)$$

Using the values found from pair measurements, we get.

	$K_2Ir_2PtCl_6$	$(NH_4)_2Ir_2PtCl_6$
θ	-10.3°	-13.2°
D'	-0.237 cm^{-1}	-0.228 cm^{-1}
E'	-0.011 cm^{-1}	-0.013 cm^{-1}
D_s	-0.235 cm^{-1}	-0.227 cm^{-1}
Z_s	-0.004 cm^{-1}	-0.006 cm^{-1}

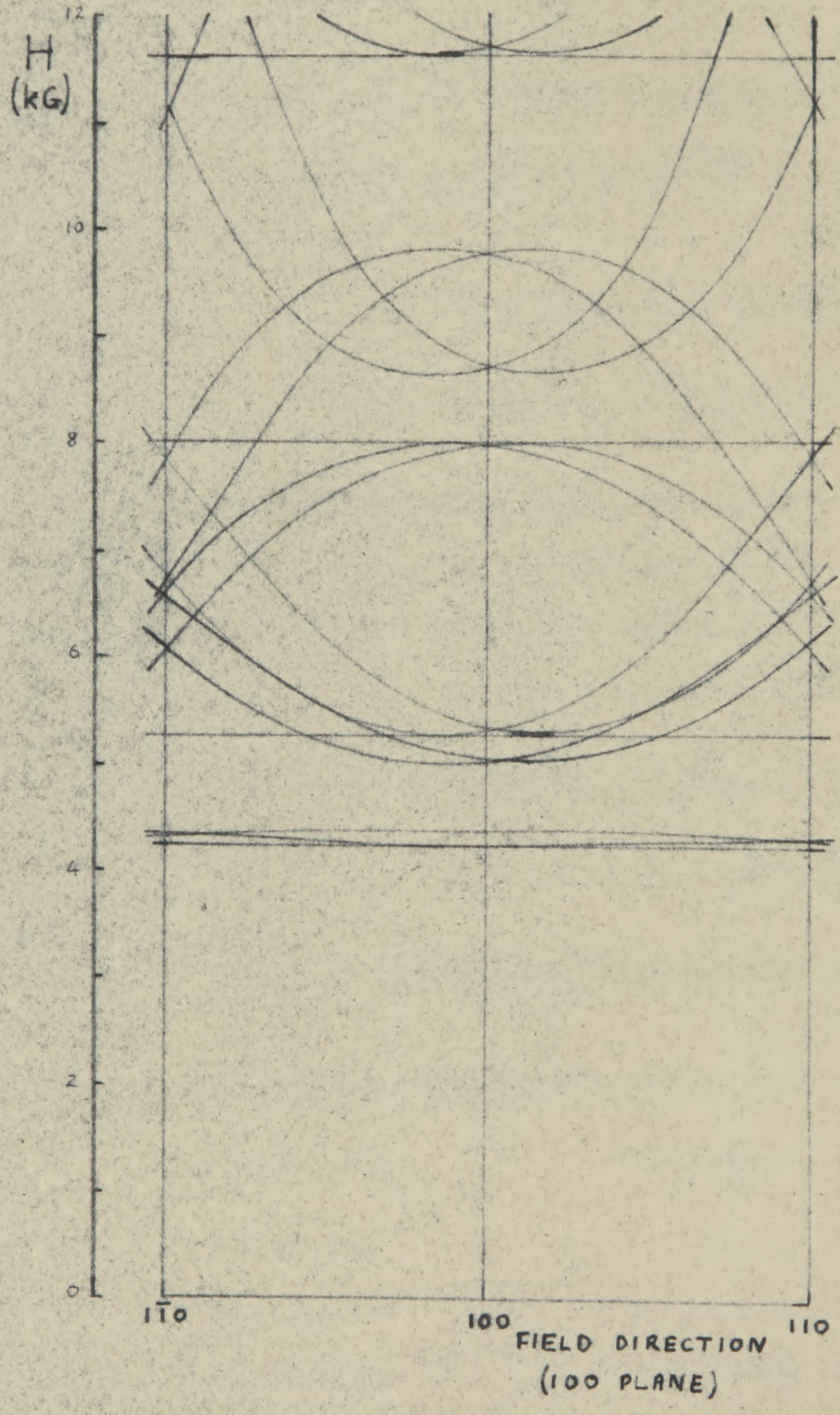


FIG. 24. SKEW TRIAD, THEORETICAL SPECTRUM FOR $K_2Ir,PtCl_6$ AT Q BAND.

If the magnetic field is rotated in the (100) plane, the anisotropic resonance lines should have turning values at angles approximately $\frac{\theta}{\sqrt{2}}$ from the 100 direction. The predicted spectrum for $K_2Ir_xPtCl_6$ at a frequency of 1.18 cm^{-1} is drawn in fig 24.

The Equilateral Triad.

For this triad, each ion is a nearest neighbour to the other two. Consider first just the isotropic interactions.

$$\mathcal{H} = J_1 (\underline{S}_1 \cdot \underline{S}_2 + \underline{S}_2 \cdot \underline{S}_3 + \underline{S}_3 \cdot \underline{S}_1) \qquad (35)$$

Putting $\underline{S} = \underline{S}_1 + \underline{S}_2 + \underline{S}_3$, this can be written,

$$\mathcal{H} = \frac{J_1}{2} (\underline{S}^2 - \underline{S}_1^2 - \underline{S}_2^2 - \underline{S}_3^2) \qquad (36)$$

This Hamiltonian has energy levels,

$$W = \frac{J_1}{2}(S(S+1) - s_1(s_1+1) - s_2(s_2+1) - s_3(s_3+1)) \qquad (37)$$

For $S = \frac{3}{2}$, $W = +\frac{3}{4}J_1$

For $S = \frac{1}{2}$, $W = -\frac{3}{4}J_1$ (twice)

The states are found in the same way as for the line triad and have exactly the same form as before (Table II). Anisotropic terms are found to have no effect at all upon the energy levels. Each interaction

has a different set of axes, the z axes being mutually perpendicular. The anisotropic components for the three interactions cancel out for all directions. This means that all transitions will fall under the main line, and no spectrum will be observed from this triad.

The N.N.N. Triad.

A n.n.n. triad consists of a pair, one ion of which also has a next nearest neighbour. There are two types of n.n.n. triad, having angles between the two interactions of 90° and 135°. However, since the n.n.n. interaction is assumed to be isotropic, these will behave in exactly the same way. The Hamiltonian is,

$$\mathcal{H} = J_1 \underline{S}_1 \cdot \underline{S}_2 + D_0(3s_{1z}S_{2z} - \underline{S}_1 \cdot \underline{S}_2) + E_0(s_{1x}S_{2x} - s_{1y}S_{2y}) + J_2 \underline{S}_2 \cdot \underline{S}_3 \qquad (38)$$

The spectrum is very similar to that of a pair because J_2 is quite small, and the Hamiltonian can be written in terms of the pair spin $\underline{S} = \underline{S}_1 + \underline{S}_2$, interacting with the third spin $\underline{s} = \underline{S}_3$. The energy levels are a doublet, $S = 0$, $s = \frac{1}{2}$, with energy $W = -\frac{1}{2}J_1$, and a sextuplet, $S = 1$, $s = \frac{1}{2}$, with energy $W = +\frac{1}{2}J_1$, corresponding to the singlet and triplet pair levels.

The S = 1 levels are split up by the anisotropic terms and by the J_o term, and transitions can be observed between these levels.

In a magnetic field the Hamiltonian can be written,

$$\mathcal{H} = g\beta\underline{H}\cdot(\underline{S}+\underline{s}) + D_p(S_z^2 - \tfrac{1}{3}s(s+1)) + E_p(S_x^2 - S_y^2) + \tfrac{1}{3}J_o\underline{S}\cdot\underline{s} \qquad (39)$$

where D_p and E_p are the parameters used to describe the pair spectrum,

$$D_p = \tfrac{3}{2} D_o \; , \qquad E_p = \tfrac{1}{3} E_o$$

In the usual notation we get with H // z,

$$\mathcal{H} = g\beta H(S_z + s_z) + D_p(S_z^2 - \tfrac{2}{3}) + \tfrac{1}{3}E_p(S_+^2 + S_-^2) + \tfrac{1}{3}J_o S_z s_z + \tfrac{1}{3}J_o(S_+ s_- + S_- s_+) \qquad (40)$$

Operating with this Hamiltonian on the various states, which will be written in the form $|M,m\rangle_{S,s}$, matrix elements are found between the three states,

$$|1,\tfrac{1}{2}\rangle_{1,\frac{1}{2}} \; , \qquad |0,-\tfrac{1}{2}\rangle_{1,\frac{1}{2}} \; , \qquad |-1,\tfrac{1}{2}\rangle_{1,\frac{1}{2}} \; ,$$

and between the three states,

$$|1,-\tfrac{1}{2}\rangle_{1,\frac{1}{2}} \; , \qquad |0,\tfrac{1}{2}\rangle_{1,\frac{1}{2}} \; , \qquad |-1,-\tfrac{1}{2}\rangle_{1,\frac{1}{2}}$$

This means that the 6 x 6 energy matrix reduces to two 3 x 3 matrices.

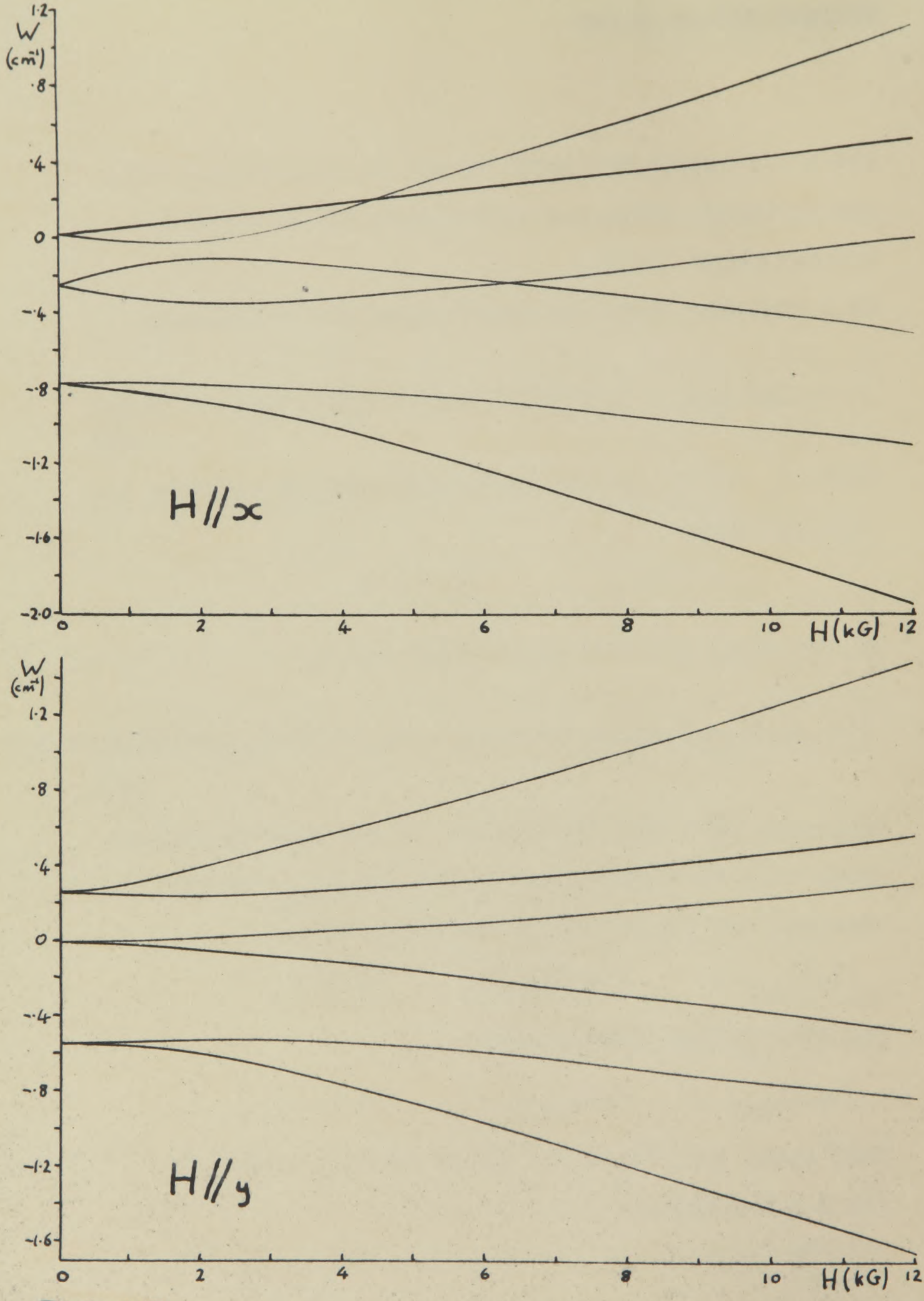


FIG. 25. N.N.N. TRIAD ENERGY LEVELS, $(NH_4)_2IrPtCl_6$, $J_2 = \cdot 03 cm^{-1}$.

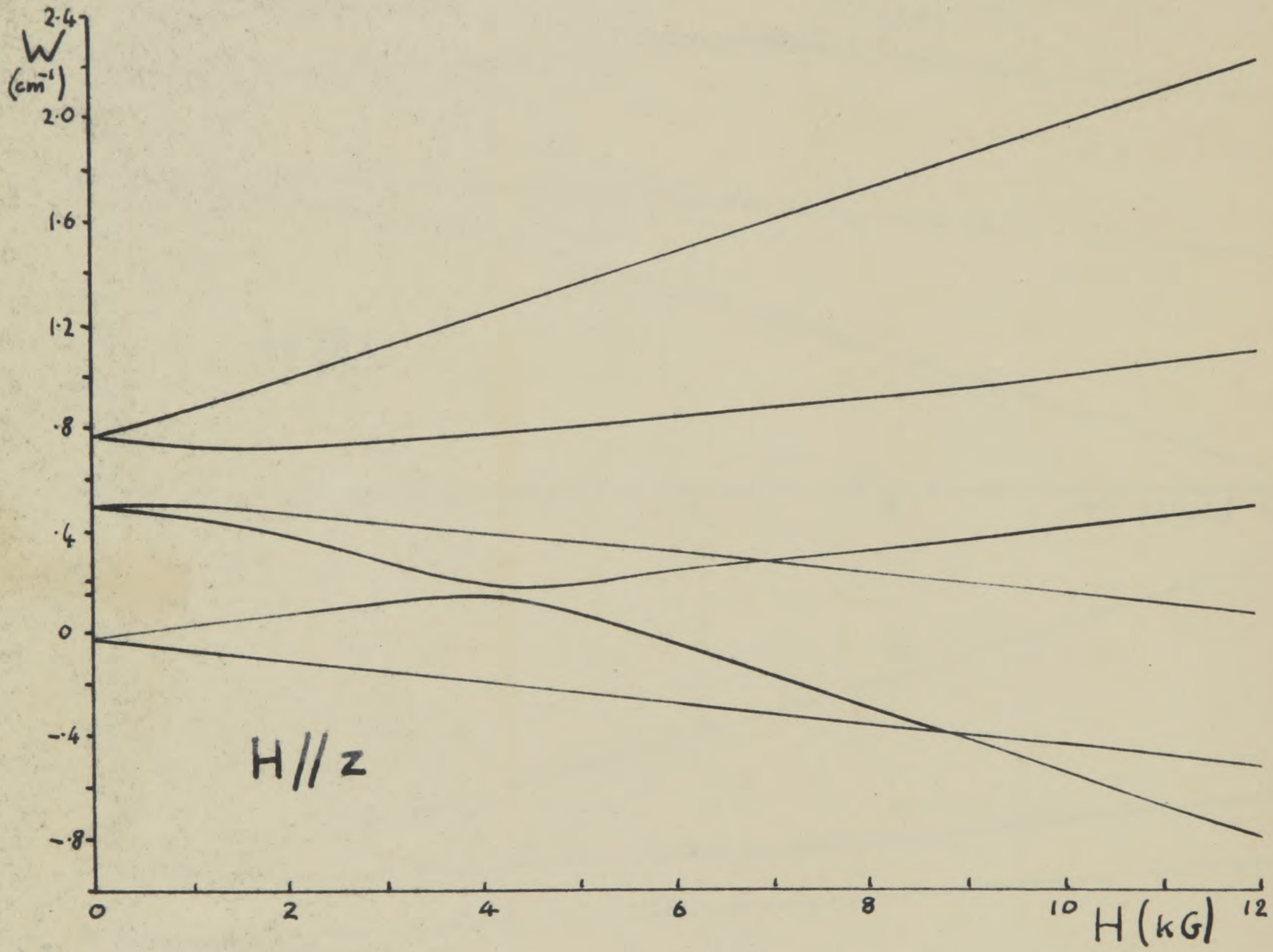


FIG. 26. N.N.N. TRIAD ENERGY LEVELS

$(NH_4)_2\, Ir, Pt\, Cl_6$, $J_2 = \cdot 03\ cm^{-1}$.

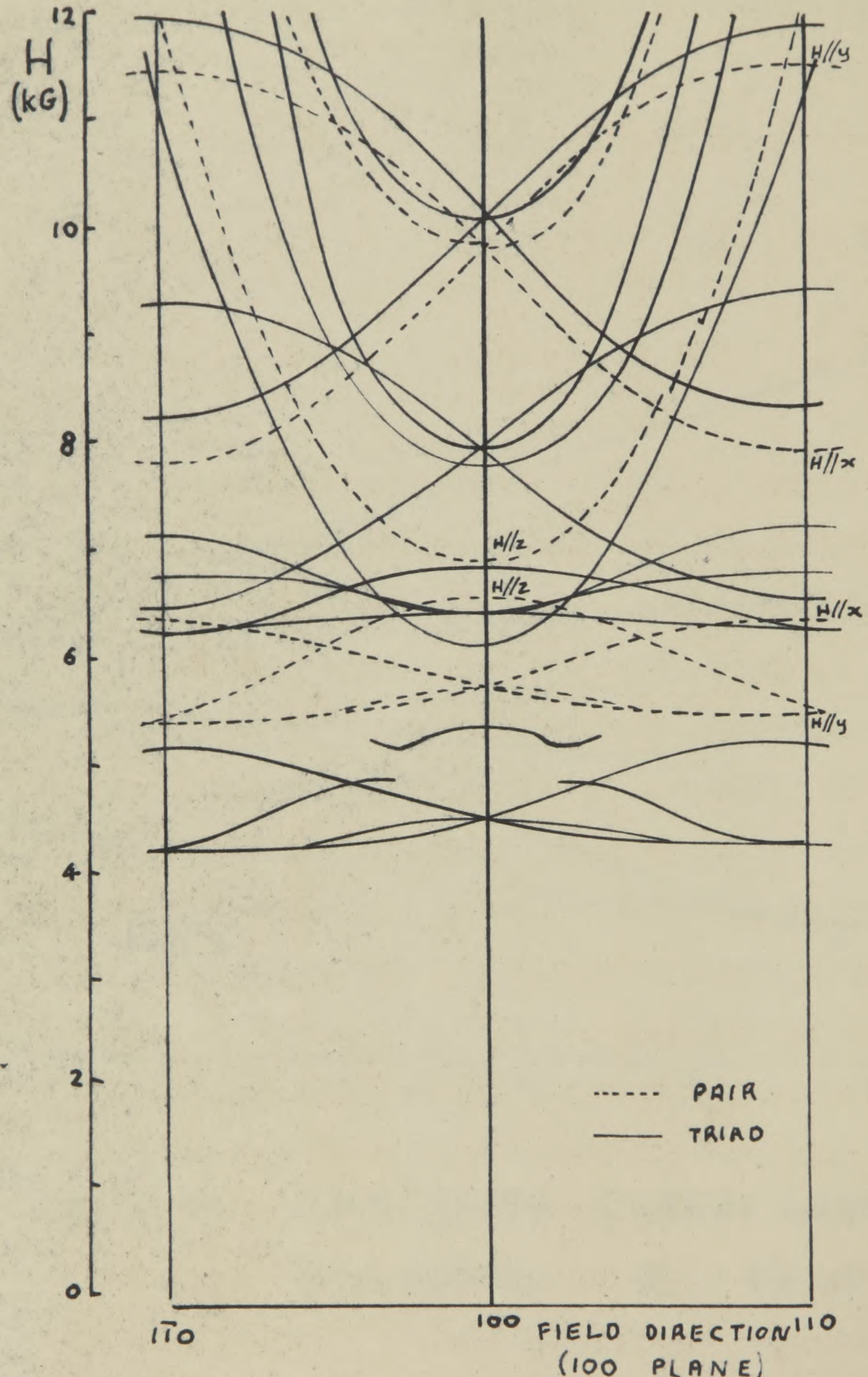


FIG. 27 N.N.N. TRIAD, AND PAIR

THEORETICAL SPECTRUM FOR $(NH_4)_2 IrPtCl_6$ AT Q BAND.
(ASSUMING $J_2 = -.03\,cm^{-1}$)

$$\begin{array}{c|ccc} & & & \\ \left|1,-\tfrac{1}{2}\right\rangle & D_p-\frac{J_s}{4}+\frac{G}{3} & E_p & \frac{J_s}{2\sqrt{3}} \\ \left|-1,-\tfrac{1}{2}\right\rangle & E_p & D_p+\frac{J_s}{4}-\frac{3G}{3} & 0 \\ \left|0,\tfrac{1}{2}\right\rangle & \frac{J_s}{2\sqrt{3}} & 0 & \frac{G}{3} \end{array}$$

The other matrix is similar, but with the sign of $G = g\beta H$ reversed. The energy levels are the roots of two cubic equations. For the field directions $H \parallel x$ and $H \parallel y$ the energy levels are again found by using the transformations for D_p and E_p given earlier (see P. 74). The energy levels were calculated over a range of values for J_s using the Oxford University Mercury Computer. The experimentally observed spectrum could then be compared with these energy levels, and a value for J_s deduced.

The energy levels for a n.n.n. triad in $(NH_4)_2IrCl_6$ with $J_s = 0.30\ cm^{-1}$ are drawn in figs 25 and 26. The predicted spectrum for a frequency of $1.18\ cm^{-1}$ is drawn in fig 27. For each pair line, there are two triad lines corresponding to the two directions of spin s. These lines are split from the pair lines by an amount $\Delta\nu = \pm \frac{J_s}{4}$ when $g\beta H \gg J_s$, but in low fields the splitting varies.

Other Triads.

All triads involving n.n. interactions have now been considered. There will be triads however consisting of an ion with two n.n.n. These will have a Hamiltonian,

$$\mathcal{H} = J_3(\underline{S}_1 \cdot \underline{S}_2 + \underline{S}_2 \cdot \underline{S}_3) \qquad (41)$$

This Hamiltonian has already been discussed with reference to the line triad, and the states were shown to be those given in Table II. In this case however, since the anisotropy is small, all transitions from the $S = \frac{3}{2}$ state will be obscured by the main line. Transitions between different S states are forbidden.

By similar reasoning, no triads involving more distant neighbours will give observable spectra either, all allowed transitions falling under the main line.

Hyperfine Structure

It has been mentioned earlier (p.64) that the main line from isolated ions has a hyperfine structure due to interactions with the Ir and Cl nuclei. In the present experiments the concentration of Ir:Pt was about 1 : 10, and all the lines were broadened so that no hyperfine structure was resolved. However, the principal

contribution to the line widths was still due to the hyperfine structure, so it is considered here.

Neglecting the effect of the Cl nuclei, the interaction of a single spin $s = \frac{1}{2}$ with an Ir nucleus with nuclear spin $I = \frac{3}{2}$, can be written,

$$\mathcal{H} = A\, \underline{s} \cdot \underline{I} \qquad (42)$$

This splits the main line into four components of equal intensity and separation A.

For a pair the interaction reduces to,

$$\mathcal{H} = \frac{A}{2}(\underline{s}_1 + \underline{s}_2)\cdot(\underline{I}_1 + \underline{I}_2) \qquad (43)$$

when $J >> A$ (see p 82). This gives a seven-line structure with intensities 1:2:3:4:3:2:1, and a spacing of $\frac{A}{2}$. The total spread of the line is the same as for a single ion, but more of the intensity will be concentrated in the middle.

For a triad the hyperfine term can be written,

$$\mathcal{H} = A(\underline{s}_1\cdot\underline{I}_1 + \underline{s}_2\cdot\underline{I}_2 + \underline{s}_3\cdot\underline{I}_3) \qquad (44)$$

This can be put in the form,

$$\mathcal{H} = \frac{A}{3}(\underline{s}_1+\underline{s}_2+\underline{s}_3)\cdot(\underline{I}_1+\underline{I}_2+\underline{I}_3) + \frac{A}{3}(\underline{s}_1-\underline{s}_2)\cdot(\underline{I}_1-\underline{I}_2)$$

$$+ \frac{A}{3}(\underline{s}_2-\underline{s}_3)\cdot(\underline{I}_2-\underline{I}_3) + \frac{A}{3}(\underline{s}_3-\underline{s}_1)\cdot(\underline{I}_3-\underline{I}_1) \qquad (45)$$

For the n.n. triads only the first term gives diagonal matrix elements for the $S = \frac{3}{2}$ states, so the effect of the other terms will be very small. The lines will be split by amounts,

$$\frac{A}{3}(I_{1z} + I_{2z} + I_{3z})$$

giving 10 equally spaced lines of separation $\frac{A}{3}$, and intensities in the ratio 1:3:6:10:12:10:6:3:1. The envelope of this hyperfine structure will have the same total spread as before, but will be even more peaked in the middle than a pair line. This is an example of the phenomenon known as exchange narrowing.

Although the hyperfine structure was not resolved in the present experiments, the line widths at low temperatures were observed to be greater for the main line than for pairs, and greater for pairs than for n.n. triads, in agreement with this.

For a n.n.n. triad, the effect of the last three terms in equn 45 will not be small. The states between which the transitions are observed are similar to the pair states, and the hyperfine structure will correspond more to a pair or single ion than to a triad of more strongly coupled spins.

The Intensity of the Resonance Lines.

Predictions can also be made concerning the intensities of the various lines, and these provide another means for identifying the various components of the spectra. The intensity of a line depends on:

(i) The number of isolated magnetic units in the crystal giving rise to the line.

(ii) The transition probability.

(iii) The populations of the particular energy levels involved in the transition at the temperature concerned. These are now treated in more detail.

(i) The number of units in the crystal

Suppose the fractional concentration of Iridium ions in the mixed crystal is c, i.e. Ir : Pt = c : (1-c). Then the probability of finding an Ir ion at any site is c, and the probability of finding Pt ions at each of the 12 n.n. sites and 6 n.n.n. sites is $(1-c)^{18}$. If the total number of lattice sites in the crystal is N, then the number of isolated ions will be $Nc(1-c)^{18}$. Similar calculations are made for pairs and triads. The number of units contributing to a line is proportional to.

(a) The probability of finding any site occupied by

a member of the unit,

(b) The reciprocal of the number of ions in the unit, to give the number of units,

(c) The reciprocal of the number of differently oriented units in the crystal, because in general only one of these contributes to any line.

These factors are listed in the table below for the various units being considered.

Type of Unit	(a)	(b)	(c)	Rel. Number n, of units in crystal	$n \times 10^4$ for c=0.1
Isolated ion	$c(1-c)^{18}$	1	1	$c(1-c)^{18}$	150.00
N.N. Pair	$18c^2(1-c)^{26}$	$\frac{1}{2}$	$\frac{1}{2}$	$c^2(1-c)^{26}$	6.40
N.N. Triads Line	$18c^3(1-c)^{34}$	$\frac{1}{2}$	$\frac{1}{2}$	$c^3(1-c)^{34}$	0.98
Rt. Angle	$36c^3(1-c)^{34}$	$\frac{1}{2}$	$\frac{1}{2}$	$4c^3(1-c)^{34}$	1.10
Skew	$72c^3(1-c)^{34}$	$\frac{1}{2}$	$\frac{1}{4}$	$2c^3(1-c)^{34}$	0.56
Equilateral	$24c^3(1-c)^{31}$	$\frac{1}{3}$	$\frac{1}{4}$	$2c^3(1-c)^{31}$	0.76
n.n.n. Triads 135°	$72c^3(1-c)^{38}$	$\frac{1}{2}$	$\frac{1}{2}$	$4c^3(1-c)^{38}$	0.72
90°	$72c^3(1-c)^{37}$	$\frac{1}{2}$	$\frac{1}{2}$	$4c^3(1-c)^{37}$	0.80

(ii) The Transition Probability

The probability for a transition between two states (a) and (b) is given by,

$$P \propto |\langle a | \underline{h}\cdot\underline{S} | b \rangle|^2 \qquad (46)$$

where h is the microwave magnetic field, and S is the total spin. In general this will be greater for the higher S states, but will vary between the different transitions.

(iii) The Population of the Levels.

The intensity of a resonance absorption between two levels with energy E and E+h is proportional to the difference in population between the levels.

$$I \propto \frac{e^{-\frac{E}{kT}} - e^{-\frac{E+h\nu}{kT}}}{Z} \qquad (47)$$

where Z is the Partition Function

$$\therefore I \propto (1 - e^{-\frac{h}{kT}}).\frac{1}{Z}.e^{-\frac{h}{kT}} \qquad (48)$$

If the energy level splittings due to the magnetic field and anisotropic terms are neglected, we have for pair lines and n.n.n. triads,

$$I_p \propto (1 - e^{-\frac{h}{kT}})\frac{e^{-\frac{J_1}{kT}}}{1 + 8e^{-\frac{J_1}{kT}}} \qquad (49)$$

For the n.n. triads the temperature variation is

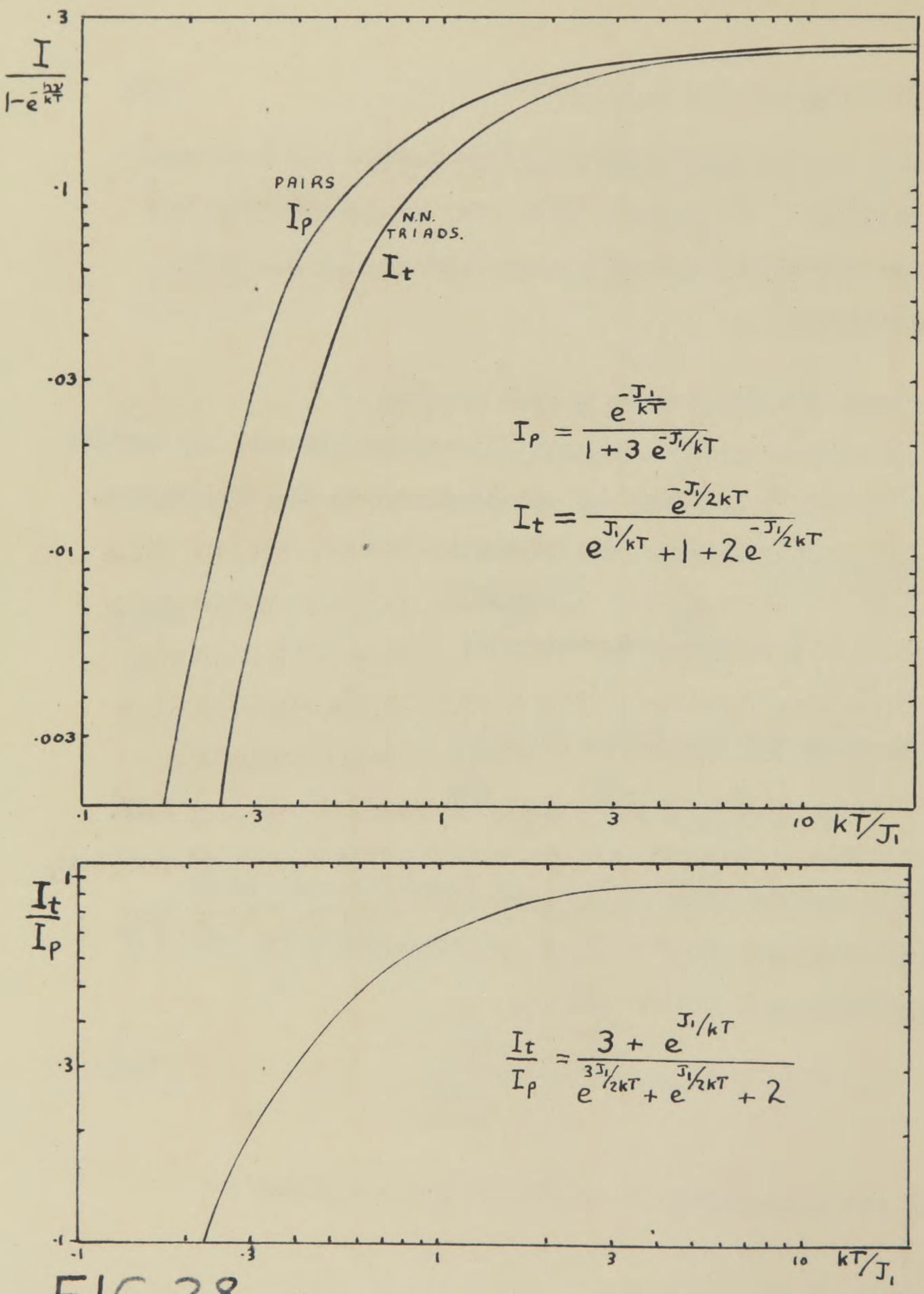


FIG. 28. INTENSITY VARIATIONS FOR PAIRS AND TRIADS.

different,

$$I_t \propto (1 - e^{-\frac{h}{kT}}) \frac{e^{-J_1/2kT}}{e^{J_1/kT} + 1 + 2e^{-J_1/2kT}} \qquad (50)$$

The relative temperature variations for pairs and n.n. triads are given by,

$$\frac{I_t}{I_p} \propto \frac{3 + e^{J_1/kT}}{2 + e^{J_1/2kT} + e^{3J_1/2kT}} \qquad (51)$$

The temperature variations given by equns 49, 50, 51, are shown in fig 28. As temperatures are lowered below $T = \frac{J}{k}$, the intensities of the n.n. triad lines decrease very quickly relative to the pair lines. Because the n.n.n. triad lines come from energy levels very similar to those of the pairs, they have a similar temperature variation. Thus by observing the spectrum at a number of different temperatures the triad lines can be identified, and by measuring the intensities accurately, values can be obtained for J_1.

4 . 5 Experimental Work.

The Crystals

Because the pair lines were found to be very intense, tending to obscure the weaker triad lines nearby, the concentration, c, of Ir:Pt was chosen so as to give the highest ratio of number of triads : number of pairs. This ratio is approximately,

$$R \propto c(1 - c)^{10} \qquad (52)$$

and this has its maximum value when $c = \frac{1}{11}$.

The crystals were grown from aqueous solutions. For both the Potassium and the Ammonium salts, the chloroplatinate is less soluble than the chloroiridate, and so the crystals may be expected to contain a smaller proportion of the chloroiridate than the solution. Saturated solutions were made containing Ir : Pt = 1 : 8 and also about 10% Hydrochloric acid, to discourage chemical decomposition. Two methods of growing the crystals were tried.

(i) Evaporation of the solution in a dessicator maintained at about 40°C for several days. This method yielded a large number of very small crystals which were used as seeds for further attempts.

(ii) Slow cooling of the solution from about 80°C to room temperature over a period of about 8 days. This method produced well shaped crystals weighing up to about 50 mg.

The crystals used in the paramagnetic resonance experiments weighed about 30 mg.

Paramagnetic Resonance Experiments

The paramagnetic resonance experiments were carried out using wavelengths of 1.2 cm (K band) and 0.85 cm (Q band). The principal features of interest have already been indicated and are,

(i) The variation of the line positions with field direction, - the anisotropy,

(ii) The variation of line intensities with temperature. While studying the latter it was found necessary to consider a third feature,

(iii) The variation of line widths with temperature.

Anisotropy Measurements.

The crystals were mounted in the cavity in such a way that the magnetic field could be rotated in the (100) plane. This plane was chosen because it includes

both the 100 and the 110 directions. The paramagnetic resonance spectrum was drawn out on the pen recorder as the magnetic field was swept from zero field up to the main line, 10 kG at K band, 14 kG at Q band. The main line is very intense at all temperatures and all other lines within about 1 kG of the main line are obscured. The pair spectrum is observed as a set of anisotropic lines with intensities about .01 of that of the main line. In addition to these there are many fainter lines with intensities about 0.1 of the pair lines, and these are attributed to the triads. These were found to be best resolved at about 20°K, and it was at this temperature that most anisotropy plots were made. Anisotropy plots of the spectra were made from pen recordings, with the magnet field direction varied in intervals as small as $\frac{1}{2}$°.

At K band, the pair spectrum extends over the whole range of available magnetic fields. It is difficult to follow some of the lines observed in high fields near to the main line, where they are very numerous and close together, and it is also difficult to follow with any confidence the anisotropy of triad lines which lie close to, or cross, the more intense pair lines. Of the weaker lines at K band, some could

certainly be identified as due to n.n. triads, because their intensities dropped relative to the pair lines at liquid Helium temperatures. A number of these were isotropic and are consistent with those predicted for the right angle triad. The positions at which these lines were observed are given below.

Salt	Frequency	Observed Position	Theoretical Position
$K_2Ir_2PtCl_6$	0.806 cm^{-1}	5.64($\pm$.03) kO.	5.68($\pm$0.1) kO.
	"	6.28	6.36
$(NH_4)_2Ir_2PtCl_6$	0.776 cm^{-1}	5.24	5.40
	"	6.40	6.32

The other n.n. triad lines also appeared to be much as predicted from the pair data, but they were too numerous to allow their anisotropy to be plotted over a wide range of angle, so it was not possible to identify them without ambiguity.

Some lines were clearly identified as n.n.n. triads. Their anisotropy was quite similar to that of the pair lines and the temperature variation was the same. One of the lines attributed to a n.n.n. triad was found to occur very near to zero field, and

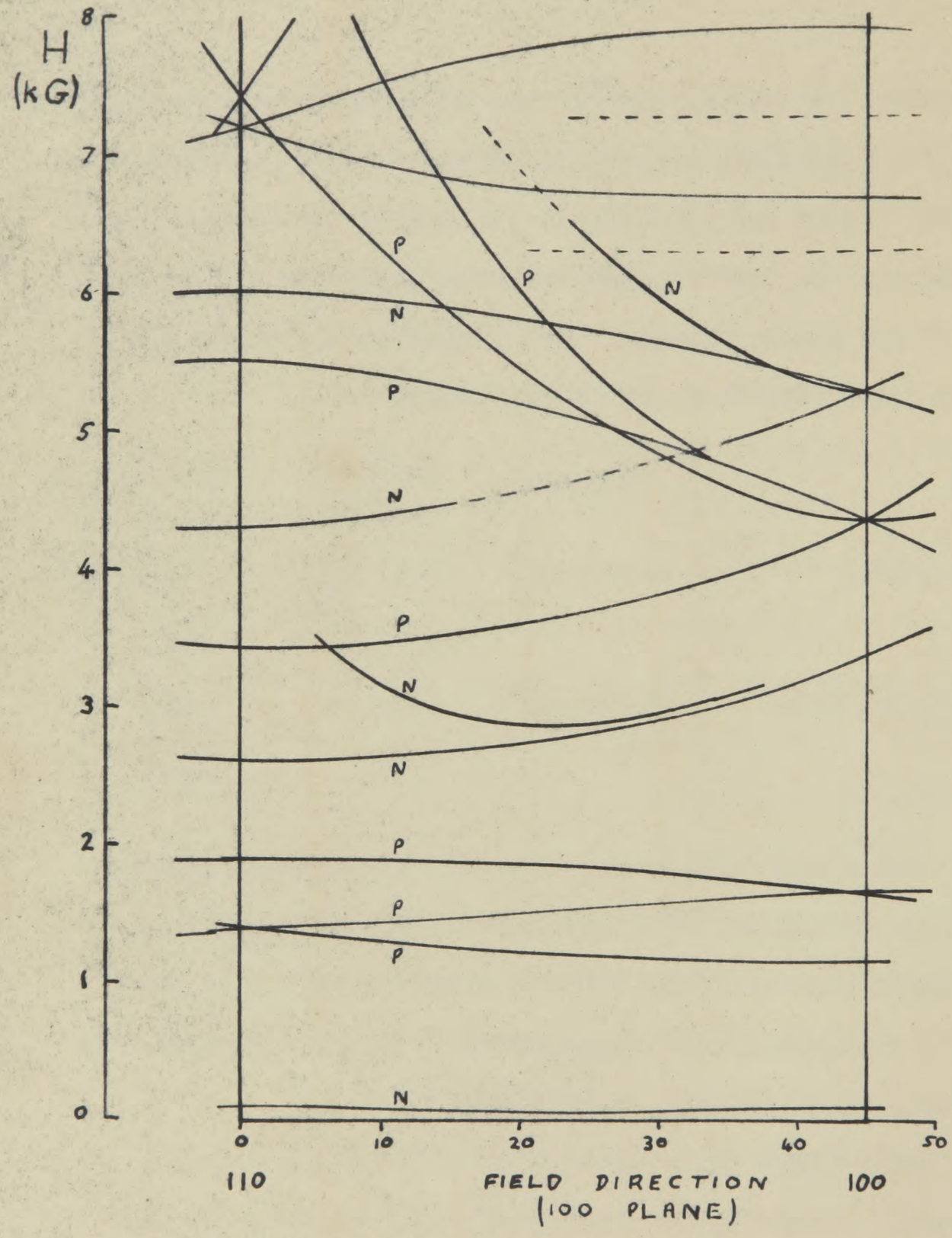


FIG. 29 ANISOTROPY PLOT, $K_2 Ir, Pt Cl_6$

MADE AT K BAND ($\nu = \cdot 807\ cm^{-1}$) AT 4·2° K.

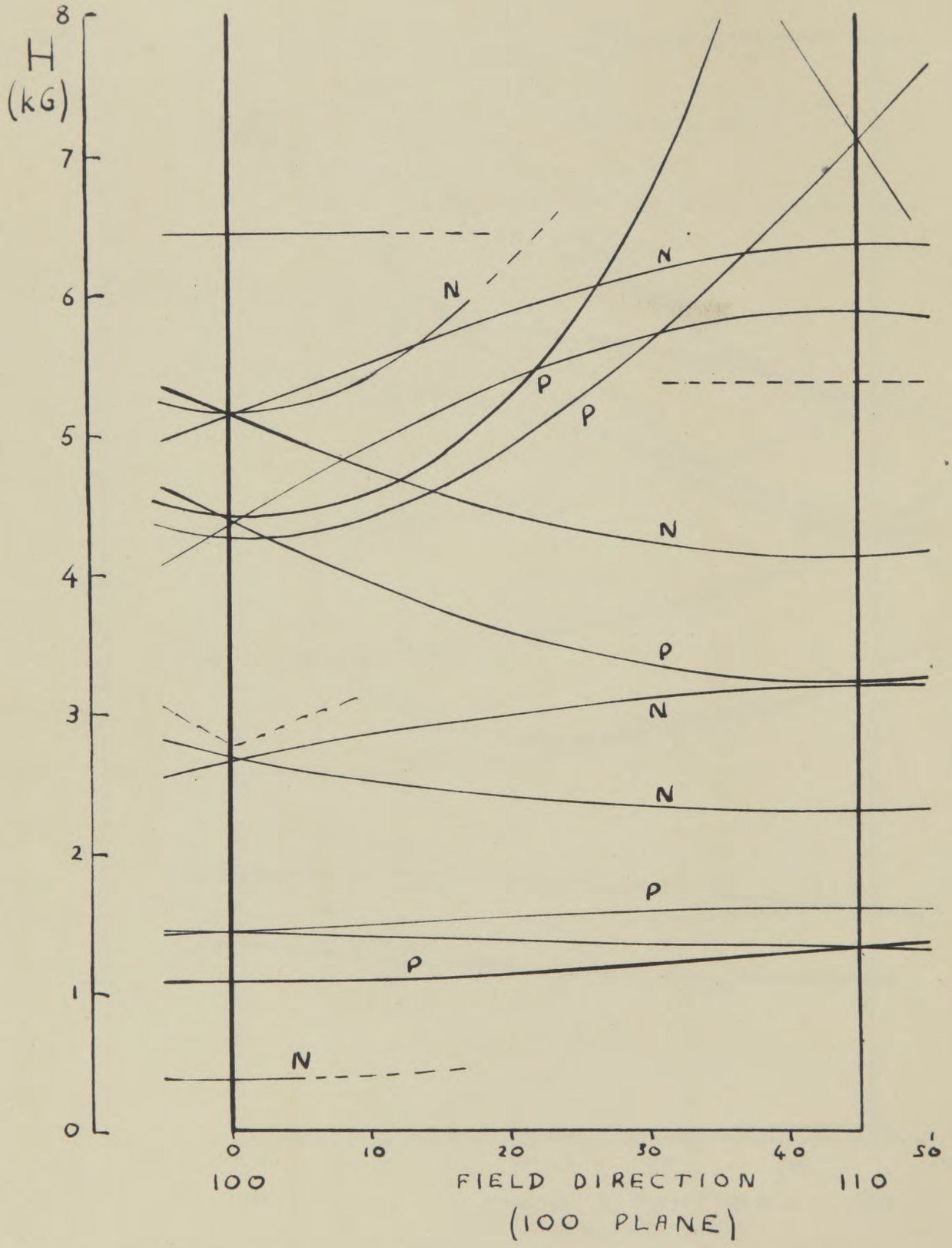


FIG. 30. ANISOTROPY PLOT, $(NH_4)_2 Ir, PtCl_6$

MADE AT K BAND ($\nu = \cdot 776\,cm^{-1}$) AT $4 \cdot 2^{\circ}$ K.

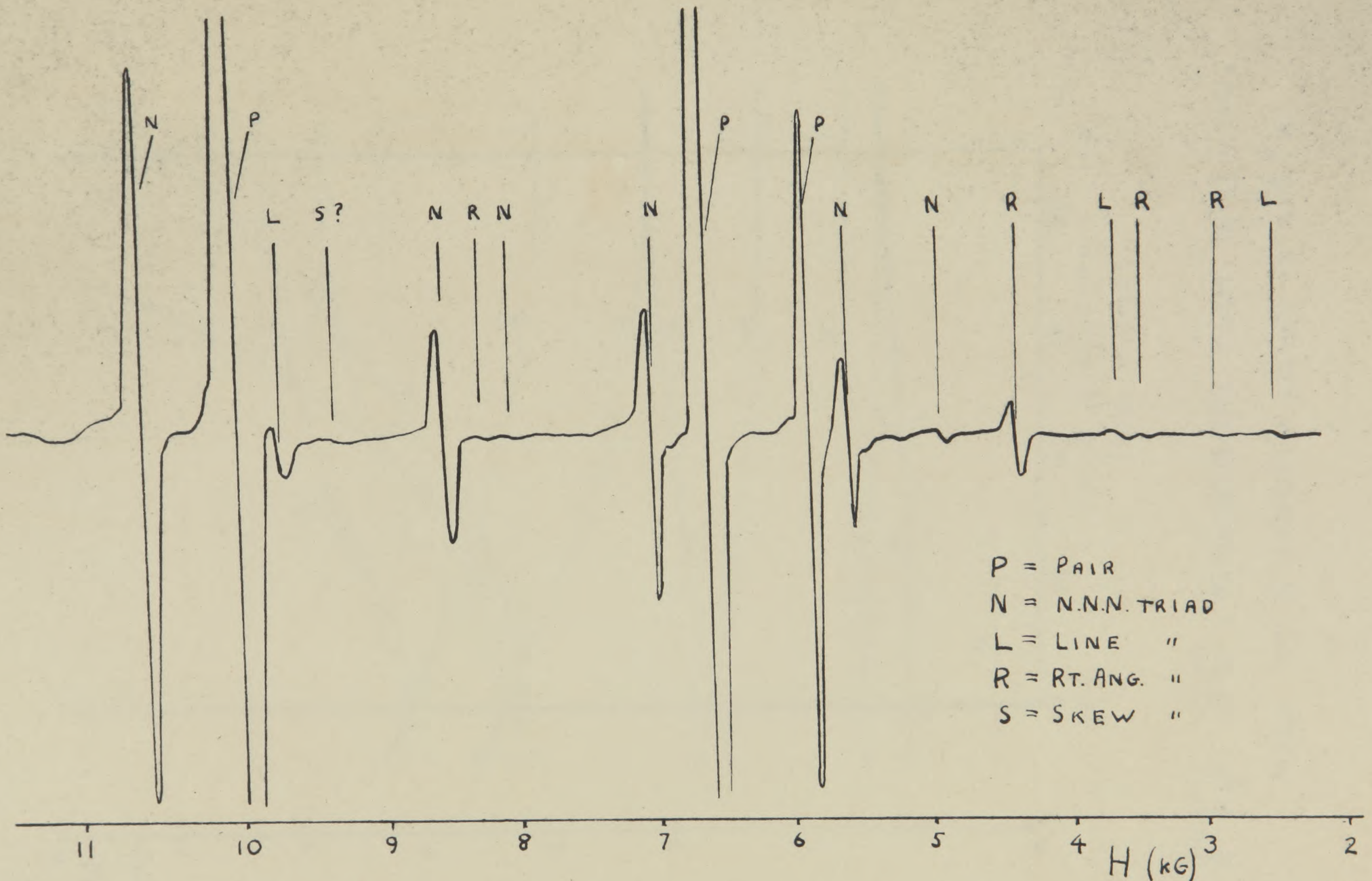


FIG. 31. PART OF THE SPECTRUM FOR $(NH_4)_2 Ir_1 Pt Cl_6$ AT Q-BAND.

[100] DIRECTION, $\nu = 1.183\ cm^{-1}$, $T = 20°K$.

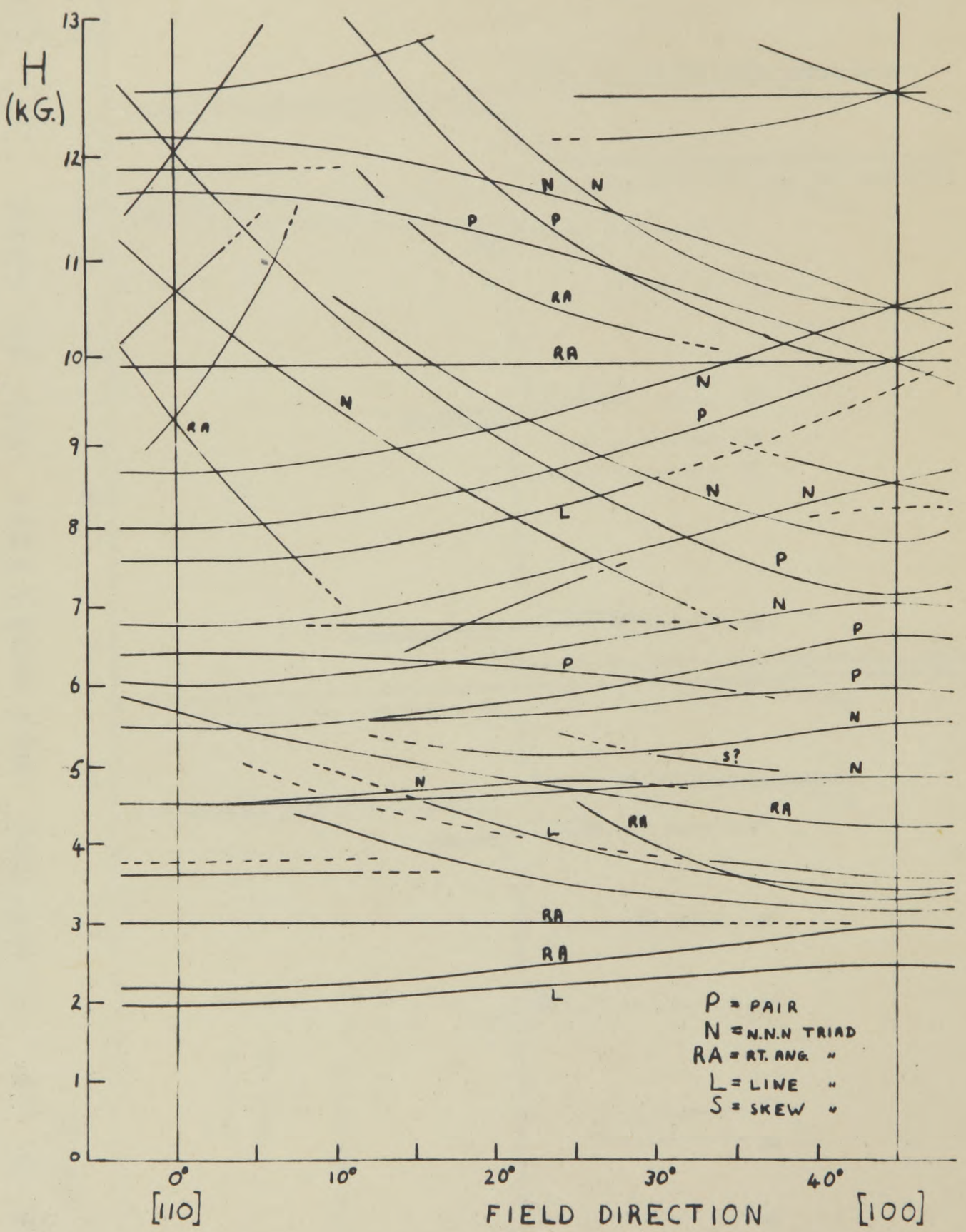


FIG. 32. $(NH_4)_2 Ir, PtCl_6$, ANISOTROPY PLOT AT Q BAND ($\nu = 1{\cdot}183\ cm^{-1}$) AT 20°K ROTATING THE FIELD IN A (100) PLANE.

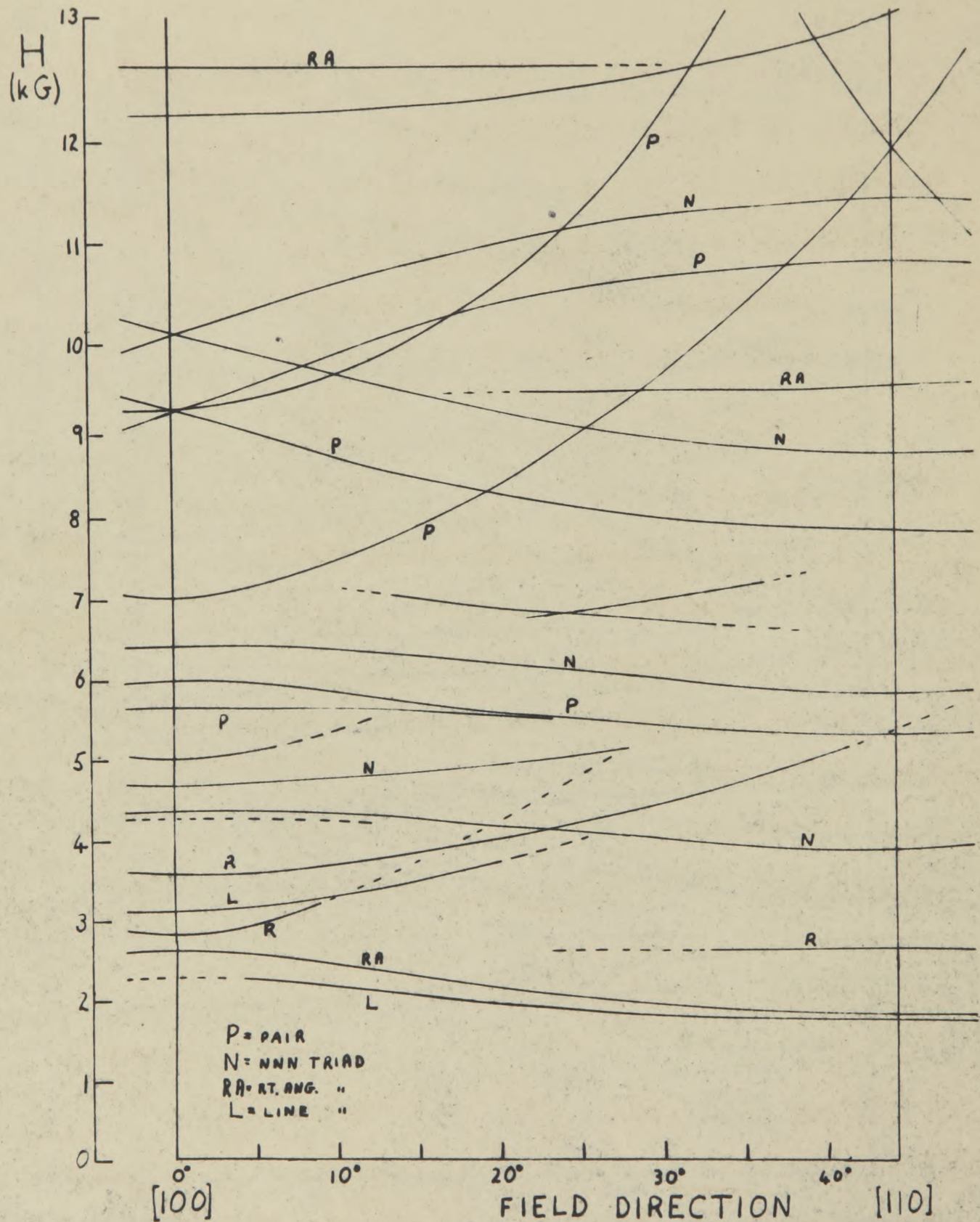


FIG. 33. ($K_2Ir,PtCl_6$), ANISOTROPY PLOT AT Q BAND ($\nu = 1.183\ cm^{-1}$) AT 20°K, ROTATING THE FIELD IN A (100) PLANE.

this enabled the zero field splitting to be measured directly by varying the frequency of the klystron and actually following the line through zero field. The frequencies at which this occured were,

$(NH_4)_2Ir_2PtCl_6$ 0.775 cm^{-1}

$K_2Ir_2PtCl_6$ 0.840 cm^{-1}.

Experimental anisotropy plots for the two salts at K band are given in figs 29 and 30. These were made at 4.2°K, at which temperature the background of n.n. triad lines has diminished in intensity, leaving just the pair and n.n.n. triad lines.

By working at a higher frequency the whole spectrum moves into higher fields. At Q band the lowest pair lines are observed at about 5 kG. The lowest lines for the Line and Right angle triads occur at about 2 kG, well separated from any larger lines. Fig 31 shows a pen recording of part of the spectrum for $(NH_4)_2Ir_2PtCl_6$ at a wavelength of 0.85 cm, with the field near to a (100 direction. The Q band anisotropy plots are reproduced in figs 32 and 33. These were made at 20°K and give some idea of the large number of lines in the spectra. Most of these lines have been identified and are labelled accordingly.

The spectrum of the skew triad does not extend much further from the main line than the pairs, and many of the lines fall under the pair lines. As a result of this it was not possible to identify positively the lines from the skew triad. However small lines were always observed in the positions where they were expected, although it was never possible to follow their anisotropy over a wide range of angles.

The right angle and line triad spectra appear almost exactly as predicted from pair data. The positions of some of the lines are compared with theory in the table below. The frequency used was 1.183 cm^{-1}.

Salt	Triad	Crystal direction	Triad direction	Exptl. Posn(kG)	Theor. Posn(kG)
$(NH_4)_2IrPtCl_6$	Rt.Ang.	100	$H \perp z$	8.95±.03	8.92±.10
	Rt.Ang.	100	$H \perp z$	8.95	8.14
	Rt.Ang	100	$H \parallel z$	4.80	4.80
	Rt.Ang.	100	$H \perp z$	9.72	9.59
	Line	100	$H \parallel z$	8.42	8.48
	Line	110	$H \parallel x$	7.48	7.45
$K_2IrPtCl_6$	Rt.Ang	100	$H \perp z$	2.64	2.59
	Rt.Ang	100	$H \perp z$	2.86	2.74
	Rt.Ang	100	$H \parallel z$	3.58	3.54
	Rt.Ang	100	$H \perp z$	9.37	9.43
	Line	100	$H \parallel z$	3.14	3.13

The spectrum for n.n.n. triads was again clearly distinguishable. Generally the anisotropy was similar to that of the pair spectrum, but in places they differed, particularly the potassium salt which has a larger J_2 value, and this was always in accordance with the theory. Where lines were identified as being due to n.n.n. triads with the field along one of the triad axes, it was possible to compare the line positions with those predicted theoretically to obtain values for J_2. This provided a number of separate determinations of J_2, and these are tabulated below.

Salt: $K_2Ir_2PtCl_8$

Crystal direction	Triad direction	Experimental position(kG)	J_2 (deduced) (cm^{-1})
Q band, 1.186 cm^{-1}			
100	H // z	4.36 ±.03	.38 ±.03
100	H // z	4.66	.38 ±.04
100	H // z	6.36	.34 ±.04
110	H // y	8.38	.39 ±.03
110	H // x	11.83	.42 ±.06
K band, 0.806 cm^{-1}			
110	H // y	3.69	.40 ±.09
110	H // x	6.10	.38 ±.03

Zero field measurement, ν = 0.840 cm^{-1} .39 ±.03

Mean Value .39 ±.03

Salt: $(NH_4)_2IrPtCl_6$

Crystal direction	Triad direction	Experimental position(kG)	J_2 (deduced) (cm^{-1})
Q band, 1.183 cm^{-1}			
100	H // z	5.44 ±.03	.29 ±.03
100	H // z	6.91	.30 ±.12
100	H // z	7.68	.25 ±.05
110	H // z	6.68	.24 ±.04
110	H // z	8.56	.34 ±.10
110	H // y	11.92	.34 ±.05
K band, 0.776 cm^{-1}			
110	H // z	2.38	.28 ±.03
110	H // z	4.33	.26 ±.05
110	H // y	5.18	.30 ±.08
110	H // y	6.30	.30 ±.10
Zero field measurement,		= 0.775 cm^{-1},	.26 ±.03
		Mean Value,	.28 ±.03

For both salts, J_2 is positive, indicating that the interactions are antiferromagnetic.

If the n.n.n. interaction is anisotropic, the spectra from the two different types of n.n.n. triad will be slightly different, and some of the lines

would be split into two components, with a separation of the order of $\frac{D_2}{2}$. No such effect was observed, indicating that D_2 must be less than the line width of about 100 g.

i.e., $D_2 \leq .015\ cm^{-1}$

Intensity measurements

The determination of J_1 was originally carried out by measuring the variation of intensity with temperature of the n.n. pair lines. The intensities were compared with lines in Neodymium Ethyl Sulphate, Lanthanum Magnesium double Nitrate (J.C.Park,1957). Some of the difficulties in making these comparisons have been discussed in chapter 2, where the advantages in using lines from similar systems in the same sample were pointed out. Such a system is provided by the pairs and triads, and so measurements on these lines do provide a useful method for measuring J_1.

The lines used were the low field lines at Q band from the right angle triad and the n.n.n. triad, occurring at 2.25 and 4.51 kG respectively, with the field in the 110 direction for $(NH_4)^2Ir,PtCl_6$, and at 3.38 and 4.36 kG, with the field in the 100 direction

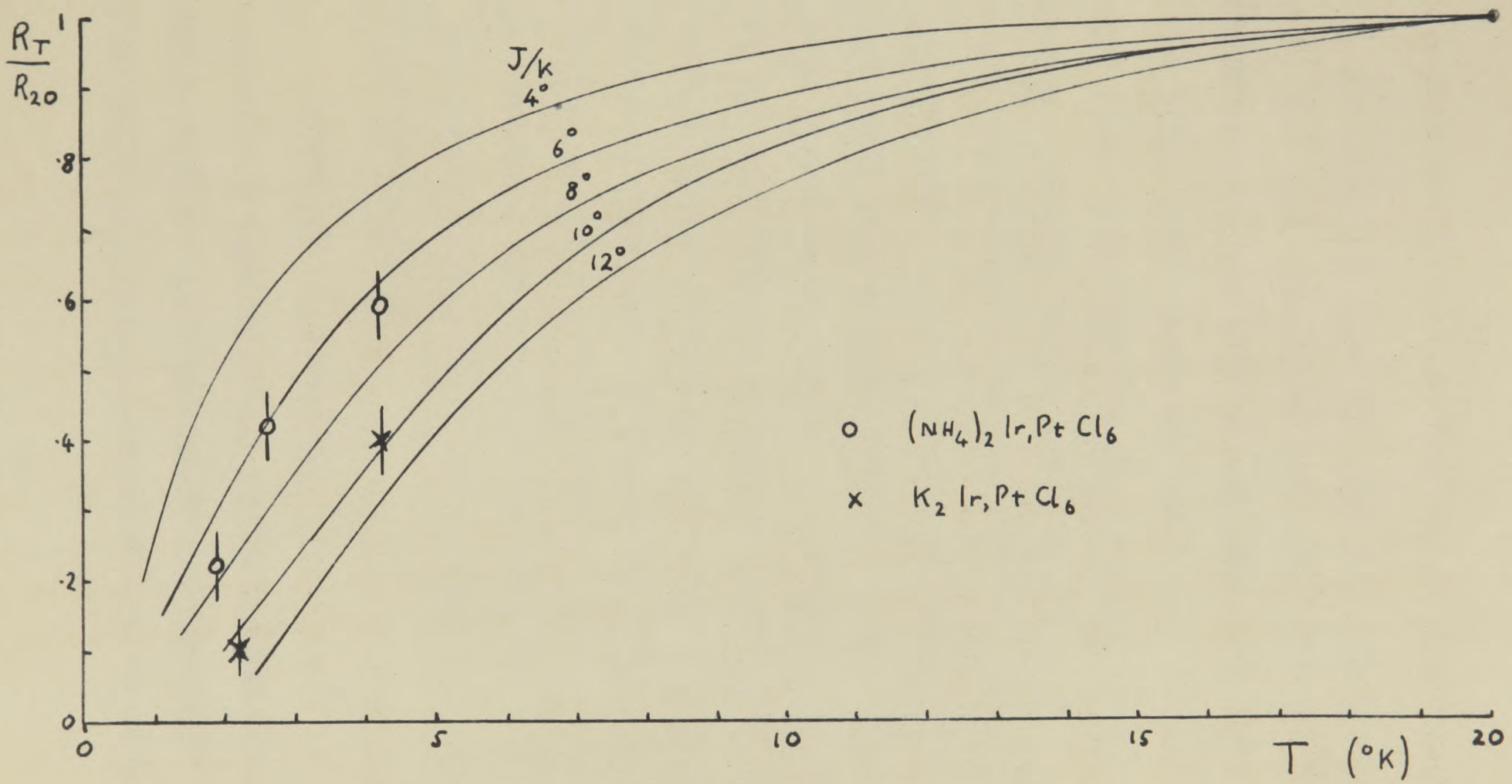


FIG. 34. EXPERIMENTAL INTENSITY VARIATIONS FOR PAIRS & TRIADS

THE OBSERVED DROP IN THE RATIO $R_T = I_t/I_p$ AT TEMPERATURES BELOW 20°K IS COMPARED WITH THEORETICAL CURVES TO ESTIMATE J_1/k.

for $K_2Ir_xPtCl_6$. The right angle triad was chosen because it was the most intense, well resolved n.n. triad line, and the n.n.n. triad was chosen because it was near to the other line and of similar intensity. By comparing lines of similar intensities, any systematic errors due to nonlinearity of the detection system are reduced

Because of the different unresolved hyperfine structures in the lines, they were found to have slightly different widths, and also the widths were found to change with temperature. In order to allow for this the pen recordings were integrated twice in order to obtain the intensities.

The results of the measurements are plotted in fig 34, where they are compared with a number of theoretical curves. The best values obtained for J_1 are given below, compared with the values obtained from pair measurements.

$K_2Ir_xPtCl_6$ $\frac{J_1}{k} = 10.5 \pm 2°K$ (Pairs: $11.5 \pm 1°K$)

$(NH_4)_2Ir_xPtCl_6$ $\frac{J_1}{k} = 6.5 \pm 1°K$ (Pairs: $7.5 \pm 1°K$)

These values are no more accurate than those originally

obtained, -they are probably worse, because the signal to noise ratio for the triads was rather small, giving a large scatter on the measurements. However they do provide good confirmation of the earlier measurements.

Direct comparisons of the relative intensity variations between the n.n.n. triads and the n.n. pairs were also made, but no significant difference was detected.

Line Widths.

All of the lines were found to broaden at high temperatures. Below about 30°K, however their widths were approximately constant. This effect was studied in some detail on $(NH_4)_2IrPtCl_6$ at Q band with respect to lines from a n.n.n. triad, a pair, and a single ion, those at 4.51 and 5.44 kG with the field in the [110] direction, and the main line.

The shapes of the lines were found to be approximately Lorentzian at high temperatures, i.e. the intensity at a distance h from the centre of the line is given by,

$$I = \frac{A}{\Delta^2 + h^2} \qquad (83)$$

At low temperatures the shape becomes more Gaussian, i.e.

$$I = Be^{-ch^2} \qquad (84)$$

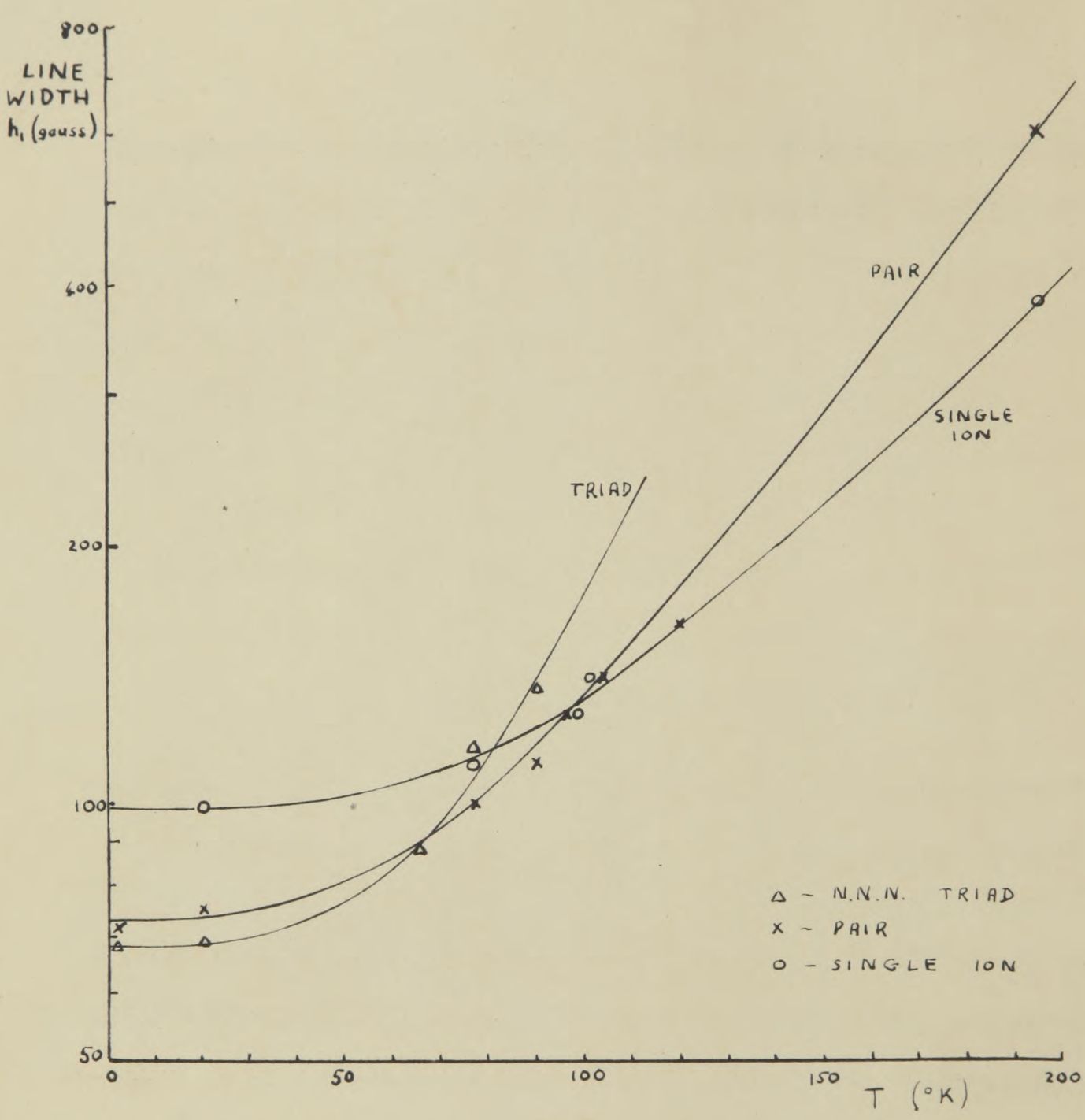
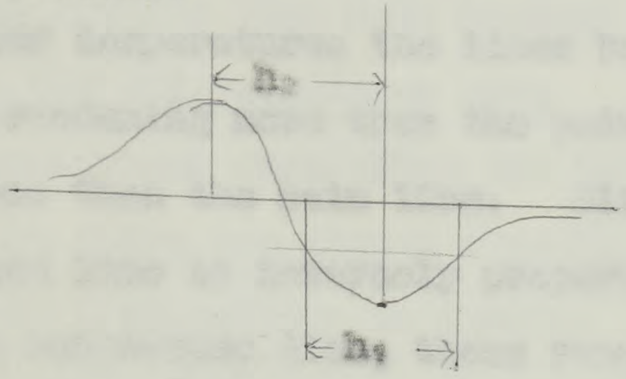


FIG. 35. VARIATION OF LINE WIDTHS WITH TEMPERATURE.

This change of shape is consistent with an unresolved hyperfine structure.



Two widths were measured, h_1, the differential half-peak width, and h_2, the peak to peak width. The ratio $\frac{h_1}{h_2}$ is an indication of the line shape.

For a Lorentzian line, $\frac{h_1}{h_2} = 1.06$

For a Gaussian line, $\frac{h_1}{h_2} = 0.78$

The observed values of this ratio varied between these limits. The variation of line width with temperature is plotted in fig38. Here the width h_1 is used because it was possible to measure it more accurately from recordings with a high noise level, and because 2 measurements were possible from each line. Each point represents the mean value for the width from about six separate recordings. At low temperatures, the width of the pair and triad lines are almost equal, but the single ion line is slightly wider. This is expected,

and is due to the different unresolved hyperfine structure on the lines.

At higher temperatures the lines broaden, the triad line broadening more than the pair line, and the pair line more than the main line. Since the width of a resonance line is inversely proportional to the spin lattice relaxation time, these results indicate that the relaxation time is shorter for the larger magnetic units. This is consistent with a relaxation process operating through magnetic interactions with neighbouring paramagnetic ions.

For the concentrated salts $(NH_4)_2IrCl_6$ and K_2IrCl_6 no resonance lines have been observed at all. This is probably because the anisotropic exchange field is very great. It is estimated that this might lead to a half width of about 20kO (Griffiths et al,1950) which could not be detected using the present apparatus.

4 . 6 Discussion of results

The main results that have emerged from this study of triads in the chloroiridates are,

(i) The parameters describing the n.n. exchange interaction in pairs are almost exactly correct for describing the interactions in triads.

(ii) The n.n.n. isotropic exchange is about .05 of the n.n. interaction, and the n.n.n. anisotropic exchange is very much smaller than this.

The importance of the first of these results is not solely the confirmation it gives for the parameters determined previously. In order that the parameters can be applied to the bulk properties of the concentrated chloroiridate crystals, one must assume that every ion can act with each of its 12 n.n. in the same way simultaneously. The present work shows that an ion does interact with two n.n. ions in the same way as with just one, and this indicates that the interaction is probably the same for all 12.

The magnitude of J_s appears to be in good agreement with other experimental work on the chloroiridate exchange. As a simple theoretical model, that part of

the interaction which acts through two chlorine ions may be compared with that given by a simple Morse curve, (see Hornberg, 1950).

$$J \propto 1 - (1 - e^{-\beta \Delta r})^2 \qquad (83)$$

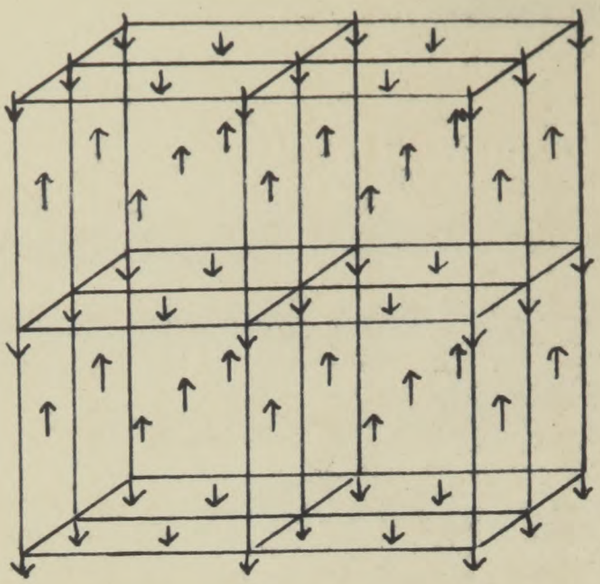
where $\beta = 2.04 \times 10^8$ cm^{-1}, and Δr is the difference in separation of the Cl ions from that in a Cl_2 molecule. From this it is predicted that $J_2 = .03\ J_1$, which compares favourably with the observed value, $J_2 = .05 J_1$.

Bulk magnetic properties for the concentrated salts K_2IrCl_6 and $(NH_4)_2IrCl_6$ have been measured by Cooke, Lazenby, McKinn, Owen, and Wolf, (1959), and by Bailey and Smith (1959). For both salts the susceptibility at high temperatures can be expressed as a sum of a temperature independent susceptibility, and one which follows a Curie-Weiss law,

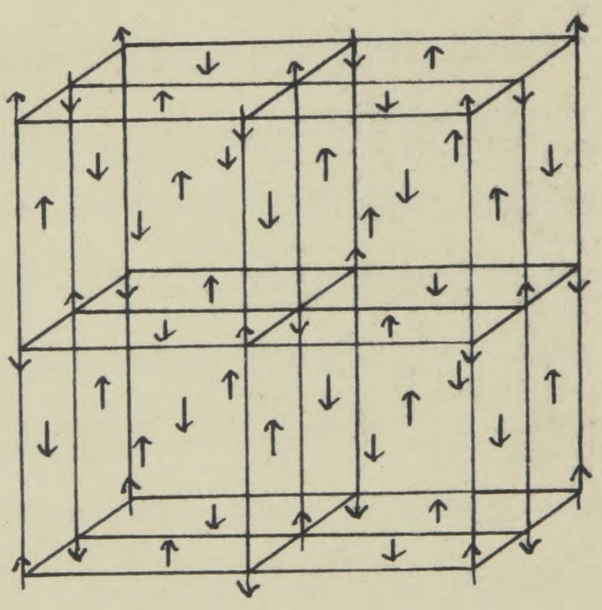
$$\chi = \frac{C}{T + \theta} + a \qquad (86)$$

At lower temperatures the susceptibility becomes less temperature dependent until it drops sharply at the antiferromagnetic transition temperature, T_N. These transitions are also marked by λ type specific heat anomalies.

TYPE. 1



TYPE. 2



TYPE 3

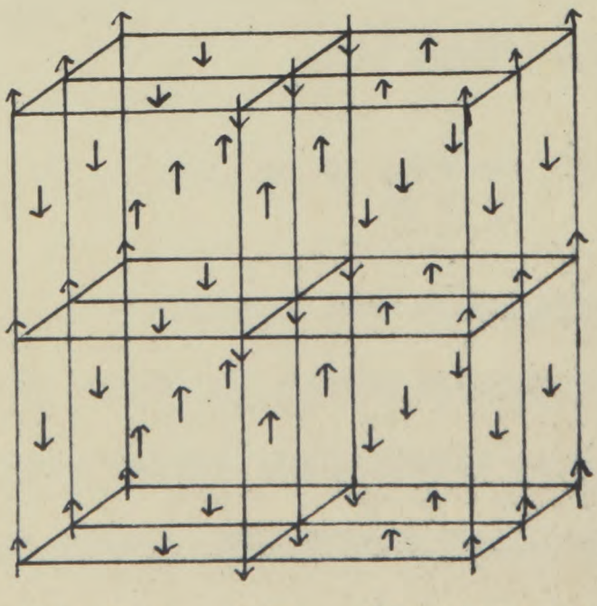


FIG. 36. TYPES OF ORDERING IN A F.C.C. LATTICE

A simple molecular field approach, which should be valid if $T \gg T_N$, gives for the Curie-Weiss constant,

$$\theta = \frac{(12J_1 + 6J_2).S(S+1)}{3k}$$

$$= \frac{2}{k}(J_1 + \tfrac{1}{2}J_2) \qquad (37)$$

Inserting the measured values for $\frac{J_1}{k}$ and $\frac{J_2}{k}$, this may be compared with the observed values for θ.

	θ(Calculated)	θ(Observed)
K_2IrCl_6	36.4 °K	32 ± 4 °K
$(NH_4)_2IrCl_6$	23.1 °K	20 ± 3 °K

Much theoretical work has been done on the antiferromagnetic transition in a face centred cubic lattice. The situation is complicated by the fact that there are several ways in which the spins may order themselves. Three of these are shown in fig 36. The ordering that occurs is that which minimises the exchange energy of each ion. This depends on the relative numbers of n.n. and n.n.n. spins which are parallel or antiparallel. These are listed below for the types of order shown in fig 36, together with the exchange energy per ion.

	n.n. spins		n.n.n. spins		Exchange energy per ion.
	p	a-p	p	a-p	
Type 1 Order	4	8	6	0	$-4J_1 + 6J_2$
Type 2 Order	6	6	0	6	$-6J_2$
Type 3 Order	4	8	4	2	$-4J_1 + 2J_2$

From the above table it appears that if J_2 is negative (ferromagnetic), then type 1 order will be the most favoured energetically. If J_2 is positive and small, then type 3 order will be favoured. If J_2 is larger than 0.5 J_1 however, type 2 ordering takes place, as in MnO.

Several authors (Anderson 1950, LI 1951, Zinan 1953) have reached these conclusions using more rigorous theory, and have shown that for a completely isotropic exchange there can be no antiferromagnetic transition unless J_2 is finite. Lines (1963) has shown that this is so even if the exchange has anisotropic components, and has applied spin wave theory to the particular case of the chloroiridates, showing how the transition temperature depends not only on J_1 and J_2, but also on n.n. anisotropic exchange. His theoretical prediction for the variation of T_N with J_1, J_2, and D_2 is shown

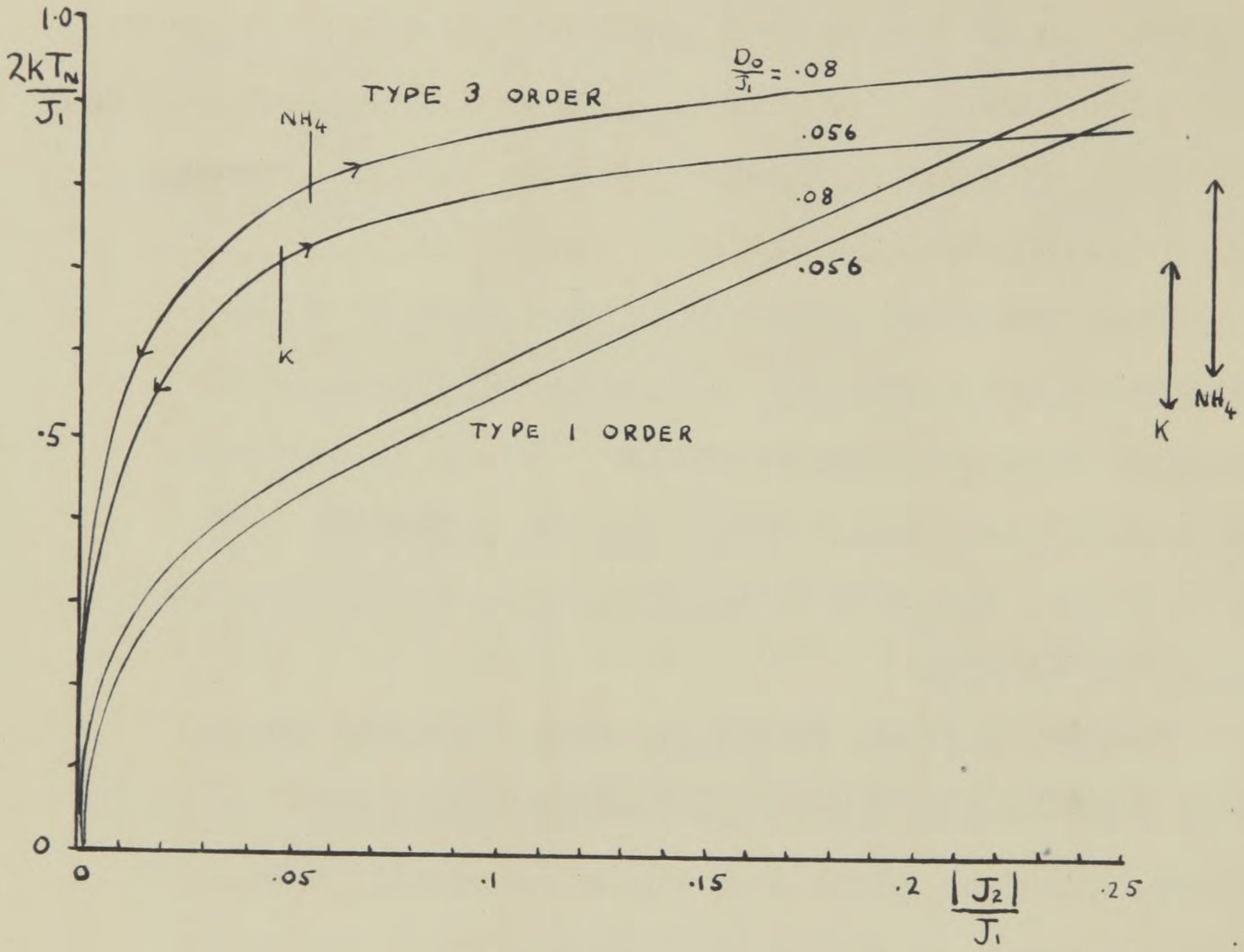


FIG. 37. DEPENDENCE OF T_N ON J_2.

THIS DIAGRAM IS TAKEN FROM THE PAPER BY LINES, (1963). IT SHOWS THE DEPENDENCE OF T_N ON THE TYPE OF ORDER, J_2, AND D_0. THE PRESENT RESULTS, INDICATED ON THE LEFT, ARE IN AGREEMENT WITH VALUES FOR T_N/J_1, ESTIMATED FROM BULK PROPERTIES, WHICH ARE INDICATED ON THE RIGHT.

in fig 37.

The present measurements of J_3 indicate that the ordering is of the third type, with the spins directed along the unique 100 axis. The transition temperatures predicted by Lines's theory using the present results are compared with the observed values below.

	T_N (Calculated)	T_N (Observed)
K_2IrCl_6	4.0 °K	3.05 °K
$(NH_4)_2IrCl_6$	2.9 °K	2.15 °K

The agreement between these figures is well within the estimated error due to approximations in the spin wave theory, and in the experimental measurements.

REFERENCES

Anderson, Phys Rev 72, 550, 1950

Phys Rev, 115, 2 1959

Solid State Physics, 14, 1963

Bailey and Smith, Phys Rev, 114, 1010, 1959

Beam and Rodbell, Phys Rev, 126, 104, 1962

Banewicz, Heidelberg and Luxon, J Phys Chem, 65, 615, 1961

Bizotte, Squire and Tsai, Comp Rend, 207, 449, 1938

Bleaney and Bowers, Proc Roy Soc, A214, 451, 1952

Bowers and Owen, Rep Prog Phys, 18, 304, 1955

Brown, Coles, Owen and Stephenson, Phys Rev Lett,

7, 246, 1961

Cipollini, Owen, Thornley and Windsor, Proc Phys Soc,

79, 1083, 1962

Coles, Oxford D.Phil. Thesis, 1959

Coles, Orton and Owen, Phys Rev Lett, 4, 116, 1960

Cooke, Lazenby, McKim, Owen and Wolf, Proc Roy Soc,

A250, 97, 1959

Dirac, Proc Roy Soc, A110, 561, 1926

Proc Roy Soc, A133, 714, 1929

Feher, Bell Syst Tech Journ, 36, 449, 1957

Foex, Comp Rend, 207, 193, 1948

Goldsborough and Handel, Rev Sci Inst, 31, 1044, 1960

Griffiths and Owen, Proc Roy Soc, A226, 96, 1954

Griffiths, Owen Park and Partridge, Proc Roy Soc, A250, 84, 1959

Harris, Lines and Owen, Israel Conference on Paramagnetic Resonance, Academic Press N.York, 1962.

Heisenberg, Zeits f Physik, 38, 411, 1926

Herzberg, Molecular Spectra and Molecular Structure, 1950

Jacobs, Rodbell, Owen and Harris, P R Lett, Submitted for publication, 1963

Kittel, Phys Rev 120, 335, 1960

Kramers, Physica, 1, 182, 1934

Li, Phys Rev 84, 721, 1951

Lines, Proc Roy Soc, A271, 105, 1963

Lines and ter Haar, Phil Trans 254, 521, 1962

Liu, Behrendt, Legvold and Good, Phys Rev, 116, 1464, 1959

Low, Phys Rev 105, 793, 1957

Moriya, Phys Rev, 120, 91, 1960

Opechowski, Physica, 4, 181, 1937

Orton, Oxford D.Phil. Thesis, 1959

Owen, J App Phys, 32S, 213. 1961

Owen, J App Phys, 33S, 385, 1962

Park, Oxford D.Phil. Thesis, 1957

Rimai, Statz, Weber, dellara and Koster, P R Lett, 4,135, 1960

Shull, Strauser and Wollan, Phys Rev, 83, 333, 1951

Sievers and Tinkham, Phys Rev, 129, 1966, 1963

Singer, Phys Rev, 104, 929, 1956

Van Kranendonk and Van Vleck, Rev Mod Phys, 30, 2, 1958

Van Vleck, Phys Rev, 52, 1195, 1937

J Chem Phys, 9, 85, 1941

Rev Mod Phys, 17, 27, 1945

J Phys Rad, 12, 114, 1951

Weiss, Phys Rev, 74, 1493, 1948

Windsor, Oxford D.Phil. Thesis, 1963

Wykoff, Crystal Structures, Interscience Publishers Inc. 1960

Ziman, Proc Phys Soc, A66, 89, 1953.

ACKNOWLEDGEMENTS

I would like to offer my thanks

to Professor B. Bleaney, for allowing me to work at the Clarendon Laboratory:

to my supervisor, Dr J. Owen, for his continued encouragement, and his invaluable advice and assistance:

to Dr J. H. E. Griffiths, for his generous advice:

to Dr M. E. Lines and Mr C. C. Windsor and my other colleagues for many useful discussions, and for help in other ways:

to the workshop staff of the Clarendon Laboratory, and in particular to Mr E. J. Jenkinson, for converting my impractical designs into apparatus that worked:

to the Director of the Oxford University Computing Laboratory:

to the Lincoln College Boat Club, for providing much-needed recreational facilities:

to H. M. Board of Admiralty, who generously supported this work:

to the Department of Scientific and Industrial Research for a research studentship.